Aus der Neurochirurgischen Klinik und Poliklinik der Universitätsmedizin
der Johannes Gutenberg-Universität Mainz

Untersuchung pathophysiologischer Mechanismen nach intrazerebralen Blutungen und deren Beitrag zur Entstehung des Sekundärschadens

Habilitationsschrift
zur Erlangung der Venia legendi
für das Fach Neurochirurgie

Universitätsmedizin der Johannes Gutenberg-Universität Mainz

vorgelegt von

Dr. med. Harald Krenzlin
Plauen, Deutschland

Mainz, 2020

Wissenschaftliche Originalpublikationen der kumulativen Habilitationsschrift

I. **Krenzlin H,** Gresser E, Jussen D, Riede N, Taylor L, Vogelaar CF, Ringel F, Kempski O, Alessandri B. The Cerebral Thrombin System Is Activated after Intracerebral Hemorrhage and Contributes to Secondary Lesion Growth and Poor Neurological Outcome in C57Bl/6 Mice. J Neurotrauma. 2020 Jun 15;37(12):1481-1490. doi: 10.1089/neu.2019.6582. Epub 2020 Mar 11. PMID: 31830857

II. **Krenzlin H,** Frenz C, Schmitt J, Masomi-Bornwasser J, Wesp D, Kerz T, Lotz J, Alessandri B, Ringel F, Keric N. High CSF thrombin concentration and activity is associated with an unfavorable outcome in patients with intracerebral hemorrhage. PLoS One. 2020 Nov 11;15(11):e0241565. doi: 10.1371/journal.pone.0241565. eCollection 2020.

III. **Krenzlin H,** Rosenthal C, Wolf S, Vierecke J, Kowski A, Hetzer R, Vajkoczy P, Czabanka M. Surgical treatment of intraparenchymal hemorrhage during mechanical circulatory support for heart-failure--a single-centre experience. Acta Neurochir (Wien). 2014 Sep;156(9):1729-34. doi: 10.1007/s00701-014-2141-6. Epub 2014 Jun 13. PMID: 24919800

IV. **Krenzlin H,** Jussen D, Plath M, Tretzel SJ, Krämer T, Kempski O, Alessandri B. Occurrence of Spontaneous Cortical Spreading Depression Is Increased by Blood Constituents and Impairs Neurological Recovery after Subdural Hematoma in Rats. J Neurotrauma. 2019 Jan 15;36(2):395-402. doi: 10.1089/neu.2018.5657. Epub 2018 Aug 10. PMID: 29756530

V. **Krenzlin H,** Behera P, Lorenz V, Passaro C, Zdioruk M, Nowicki MO, Grauwet K, Zhang H, Skubal M, Ito H, Zane R, Gutknecht M, Griessl MB, Ricklefs F, Ding L, Peled S, Rooj A, James CD, Cobbs CS, Cook CH, Chiocca EA, Lawler SE. Cytomegalovirus promotes murine glioblastoma growth via pericyte recruitment and angiogenesis. J Clin Invest. 2019 Mar 11;129(4):1671-1683. doi: 10.1172/JCI123375. eCollection 2019 Mar 11. PMID: 30855281

1 Inhaltsverzeichnis

2 Einleitung

Im auf das Jahr 1550 v. Chr. datierten *Edwin Smith Surgical Papyrus* (Breasted 1930) vertrat man die Meinung, dass alle Erkrankungen in 3 Kategorien einzuordnen sind: heilbare-, beherrschbare- und infauste Erkrankungen. Eine Schädigung des Zentralennervensystems durch Blutungen wurde der dritten Kategorie zugeschrieben- einer Tatsache, an der sich trotz großer medizinischer Fortschritte des vergangenen Jahrhunderts, wenig geändert hat.

Die Inzidenz des Schlaganfalls liegt in Deutschland bei etwa 250 pro 100.000 Einwohnern.[1] Intrazerebrale Blutungen (ICB), eine Form des Schlaganfalls, sind für 10-15% alle auftretenden Fälle weltweit verantwortlich.[2] Zwischen dem Jahr 1990 und dem Jahr 2000 kam es zu einem Anstieg der Zahl an stationär behandelten Patienten mit ICB um 18%.[3] Mögliche Erklärungen fußen auf einer Überalterung der Bevölkerungsstruktur und einer damit verbundenen Zunahme der Prävalenz der arteriellen Hypertonie und dem Einsatz anti-aggregierender und anti-koagulierender Medikamente.[4] Ältere Menschen haben ein höheres Risiko eine ICB zu erleiden, deren Inzidenz sich mit jeder Lebensdekade verdoppelt.[5] Vor dem Hintergrund der derzeitigen demographischen Entwicklung ist daher zukünftig eine Zunahme der Häufigkeit der ICB sowie eine Zunahme der resultierenden sozio-ökonomischen Belastung zu erwarten. Patienten mit ICB leiden unter der höchsten Morbidität und Mortalität aller Schlaganfallpatienten. In einer deutschen Studie mit 586 Patient lag die 30- Tage Mortalität zwischen 30-50%.[6] In anderen Studien lag die 7-Tage Mortalität bei 31%, die 1-Jahres Mortalität bei 59% und die 10-Jahres Mortalität sogar bei 89%.[5,7,8]

Abhängig von Ihrer zugrundeliegenden Ursache werden spontane Blutungen in primäre und sekundäre ICBs unterteilt.[2,9] Während den primären ICBs keine äußeren Umstände zuzuordnen sind, entstehen sekundäre ICBs durch die Einnahme gerinnungshemmender Wirkstoffe. Beiden Blutungsformen liegen jedoch ähnliche pathologische Veränderungen der zerebralen Gefäße zugrunde.[9] Die Blutungen treten zumeist (sub-)kortikal, im Bereich der Stammganglien, des Thalamus, der Pons oder des Kleinhirns auf und sind Folge durch einen arteriellen Hypertonus verursachter Veränderungen oder einer zerebralen Amyloidangiopathie.[10]

Hypertonie bedingte Blutungen treten vorwiegend im Bereich von Gefäßbifurkationen perforierender Verästelungen der vorderen-, mittleren- und hinteren Zirkulation auf.[11] Betroffen sind zumeist kleinere Gefäße mit einem Durchmesser von 50-700µm. Häufig finden sich multiple Bruchstellen, assoziiert mit Schichten aus Thrombozyten und Fibrinaggregaten. Mikroskopischen finden sich Brüche in der *Membrana elastica*, eine Atrophie der Muskulatur der *Membrana tunica media*, sowie Risse innerhalb der Wandschichten und eine zelluläre Degeneration.[9,11] Durch die Einlagerung von Cholesterinestern im Rahmen der Atherosklerose, kommt es vor allem bei älteren Patienten zu einer weiteren Schädigung der Gefäßwand, während subendotheliale Nekrosen zur Dilatation und konsekutiven Entstehung Ruptur gefährdeter Mikroaneurysmata führen.[11]

Die zerebrale Amyloidangiopathie (CAA) ist durch eine Ablagerung von β- Amyloid und degenerativer Veränderungen (Mikroaneurysmata, konzentrische Einrisse der Gefäßwand, Entzündungsinfiltrate und Fibrinoide Nekrosen) in den Kapillaren, Arteriolen und kleineren Arterien des Kortex, des Kleinhirns sowie leptomeningeal gekennzeichnet.[12] Die CAA ist mit Mutationen des für Apolipoprotein E codierenden Gens (APOE) assoziiert und führt bei vorwiegend älteren Menschen zu sporadischen ICBs. Familiäre Formen mit einer Mutation des Amyloid-Vorläuferproteins APP führen auch bei jüngeren Patienten das Risiko für das Auftreten von ICBs zu erhöhen.[13,14] Durch eine Antikoagulation ausgelöste Blutungen treten gehäuft bei Patienten mit vorbestehender Vaskulopathie aufgrund einer Hypertonie oder Amyloidangiopathie auf, wodurch eine Aggravation bestehender Risikofaktoren naheliegend erscheint.[15]

3 Pathophysiologie

Die Morbidität und Mortalität nach ICB wird durch den Primärschäden innerhalb der ersten 48h und den Sekundärschäden im Verlauf der Blutungsrekonstitution bedingt. Durch das Blutungsereignis kommt es zur physikalischen Auflösung bestehender Gewebestrukturen und eines begleitenden Masseneffektes. Der so verursachte Schaden ist einer kausalen Therapie prinzipiell nicht zugänglich. Obwohl die Blutung bei ca. 2/3 durch Hämostase und Tamponade kurz nach dem Iktus sistiert, kommt es in 73% zu einer Zunahme des Hämatoms in den ersten 3h.[16] Innerhalb von 24h nach ICB kommt es zum Auftreten eines perihämatomalen Ödems, welches nach 4-6 Tagen seine größte Ausdehnung erreicht und bis zu 14 Tagen andauert.[17-19] Ein großes perihämatomales Ödemvolumen relativ zur Blutungsgröße gilt als negativer Prädiktor eines guten klinischen Outcomes.[20] In der Literatur wird eine als *„hibernation phase“* bezeichnete, transiente, hypometabole Phase, gekennzeichnet durch mitochondriale Dysfunktion und metabolisches Versagen des perihämatomalen Gewebes, beschrieben.[21-23] Diese Phase der Hypoperfusion scheint in klinischen und präklinischen Studien allein jedoch nicht ausreichend eine Ischämie und sekundäre Zunahme des Schadenvolumens zu erklären und legt den Einfluss weiterer Mechanismen an der Schadensentstehung nach ICB nahe.[24,25]

3.1 Entstehung des primären Hirnschadens

Primärschaden beschreibt den unmittelbaren Gewebeschaden, ausgelöst durch die akut auftretende Raumforderung mit Zerreißung des physiologischen Zellgefüges. In Folge der Einblutung kommt es zu einer mechanischen Unterbrechung und Deformierung des Zellgefüges von Neuronen und Glia-Zellen mit konsekutiver Ausschüttung verschiedener Neurotransmitter, mitochondrialer Dysfunktion und Membrandepolarisation.[26-28] Abhängig vom Ausmaß dieser Dysfunktion kommt es zu transienten metabolischen Veränderungen (Hibernation), zellulärer Schwellung oder Nekrosen. Das an die Blutung grenzende Gewebe wird durch das perifokale Ödem, Apoptose, Nekrose und die Infiltration von Entzündungszellen mit beeinflusst.[29]

3.1.1 Der Einfluss des Gerinnungssystems auf das Blutungsvolumen und die Entstehung des Primärschaden

In 73% der Patienten mit ICB kommt es zu einer sekundären Blutungszunahme. Bei 1/3 dieser Patienten kommt es wiederum zu einer Zunahme des Blutungsvolumens von mehr als 33%, einer als kritisch definierten Schwelle, deren Übertritt zu einer deutlichen Mittellinienverlagerung, einer Zunahme des intrakraniellen Drucks und einer neurologischen Verschlechterung beiträgt.[16,30] Koagulation resultiert aus der Aktivierung zweier Systeme, dem intrinsischen und dem extrinsischen Gerinnungssystem, deren gemeinsame Endstrecke durch die Aktivierung des Gerinnungsfaktors X (FXa) zur Umwandlung von Prothrombin (FII) zu Thrombin (FIIa) und der Quervernetzung von Fibrin besteht.[31] Eine Beeinträchtigung des extrinsischen oder intrinsischen Gerinnungssystems führt zu einer stärkeren Zunahme des Blutungsvolumens nach Iktus.[32]

Aktivierter Faktor VII (FVIIa), ein Bestandteil der extrinsischen Gerinnungsaktivierung, vermittelt Hämostase im Bereich von Gefäßschäden und führt über diesen Mechanismus zur Prävention eines Blutungsprogress.[33,34] In einer prospektiv-randomisierten Phase III Studie (FAST; *fVIIa for Acute Hemorrhagic Stroke Treatment*) wurde die Wirksamkeit einer Gabe von 20-80 µg/kg rekombinanten fVIIa 3h nach Iktus an insgesamt 821 Patienten (263 Placebo, 265 20µg/kg und 293 80µg/kg) untersucht. In dieser Arbeit konnte die generelle Wirksamkeit von fVIIa zur Verminderung einer Blutungsexpansion bestätigt werden, jedoch fand sich kein Überlebensvorteil nach 3 Monaten (24% Placebo, 26%/29% fVIIa).[33,34] Darüber hinaus fand sich keine Verbesserung des funktionellen Befundes, bei einer Zunahme unerwünschter Arzneimitteleffekte wie arterieller Verschlüsse.[33,34] Die FAST Studie untermauert durch ihr Ergebnis die Hypothese des Einflusses weiterer, über die initiale mechanischen Verhältnisse hinausgehender pathophysiologischer Mechanismen in der Entstehung des Gewebeschadens und daraus resultierender neurologischer Beeinträchtigungen nach ICB.

3.2 Entstehung des sekundären Hirnschadens

Der Sekundärschaden addiert sich dem Primärschaden übereinen Zeitraum von mehreren Stunden bis Tagen auf und kann diesen erheblich vergrößern. Dieser umfasst die weitere neurologische Verschlechterung durch Zelluntergang in Folge anfallender Koagulationsprodukte des Blutgerinnungssystem, der Akkumulation

zytotoxischer Substanzen im Rahmen des Hämoglobinabbaus sowie Perfusionsschäden durch Vasospasmus. Einzelberichte legen eine besondere Bedeutung der Serinprotease Thrombin (FIIa) an der Schadensentstehung in der Akut- und Spätphase nach ICB nahe.[35-37] Innerhalb der ersten 4h nach ICB kommt es durch FIIa zu einer Aktivierung der Mikroglia. Diese führen durch die Ausschüttung von Tumornekrosefaktor alpha (TNF-a) sowie dem Auftreten von Zytokinen und reaktiver Sauerstoffspezies (ROS) den ultimativen Zusammenbruch der Bluthirnschranke (*blood brain barrier, BBB*). Es entsteht ein vasogenes Ödem, dass die Apoptose von Neuronen und Gliazellen induziert.[38-40] Der Einfluss von Thrombin auf die Ausbildung des Sekundärschadens ist hierbei von besonderer Bedeutung, da der Nachweis von Prothrombin m-RNA in Zellen neuronalen und glialen Ursprungs die Existenz eines zerebralen Thrombinsystems, nahelegt.[41-43]

3.2.1 Der Einfluss von Thrombin auf die Schadensentstehung nach ICB

Thrombin wird aus dem inaktiven Vorläufer Prothrombin abgespalten, welcher vornehmlich in der Leber synthetisiert und ins Plasma ausgeschwemmt wird. Die Hauptaufgabe von Thrombin besteht in der Spaltung von Fibrin zu Fibrinogen. Darüber hinaus besitzt Thrombin eine wichtige Rolle bei der Aktivierung der p44/42 *mitogen-activated kinase* (MAPK). Die Wirkung von Thrombin wird durch verschiedene Rezeptoren gesteuert. Diese Rezeptoren sind G-Protein gekoppelte, transmembranöse Rezeptoren, welche durch proteolytische Spaltung, nicht durch Ligandenbindung, aktiviert werden. Zurzeit sind drei solcher Protease aktivierter Rezeptoren (*protease-activated receptors*, PARs), PAR1, PAR-3 und PAR-4, bekannt. Das Vorkommen von PAR-1 erstreckt sich von Neuronen über Astrozyten, Oligodendro-Gliazellen bis zu mikroglialen Zellen. [41,44] Es kommt hierdurch zur Aktivierung intrazerebraler Signalwege wie MAPK, Phosphoinositol und p70. Die Folge ist ein Anstieg der DNA Synthese, Zellmigration und schließlich Neurogenese. PAR-1 führt zu einer möglichen Regulation von Rho, Inositol-1,4,5-trisphosphate, Diacylglycerol, Adenylat-Zyklase und anderer Signalkaskaden. [45,46]

Durch den Nachweis von Prothrombin m-RNA in Zellen neuronalen und glialen Ursprungs legt darüber hinaus die Existenz eines zerebralen/zellulären Thrombinsystems nahe. [41-43] Zerebral wirkt Thrombin als multivalentes Signalmolekül und vermittelt den morphologischen Wandel von Neuronen und Astrozyten. Es hat dabei Auswirkungen auf die Angiogenese (vermittelt durch PAR-1 induziertes

Angiopoietin, *hypoxia inducble factor-1* und *vascular endothelial growth factor*), Neurogenese (Stimulation endothelialer Progenitor-Zellen des Knochenmarkes und Stimulation der Sekretion des *nerve growth factor* aus Gliazellen) sowie der neuronalen Plastizität (vermittelt durch synaptische Re-Modulation). Die Bedeutung von Thrombin für die Veränderung des Zytoskeletts stellt einen Mechanismus der Regulation des zellulärem Re-Arrangement und der neuronalen Proliferation dar. [47,48] Astrozyten besitzen eine wichtige Bedeutung in der Aufrechterhaltung der BBB. Über eine Modifikation astrozytärer Strukturen besitzt Thrombin eine direkte Bedeutung für die Integrität der BBB und mögliche pathologische Konsequenzen bei der Entstehung des interstitiellen Hirnödems. Über eine *N-Methyl-D-Aspartat* (NMDA) Rezeptorbindung wird ein potentiell zytotoxischer Effekt des Thrombins nach ICB vermittelt. [46] Die Aktivierung von PAR-Rezeptoren auf Astrozyten führt zur Entstehung von Stickstoffmonoxid (NO) und konsekutiv zum Auftreten einer lokalen Entzündungsreaktion. In der Literatur finden sich Hinweise auf eine dosisabhängige Regulation des perifokalen Ödems, eine Limitation der Blutungsgröße und Prävention einer sekundären Blutungszunahme innerhalb von 24h, die Aufhebung der BBB sowie die Aktivierung des Komplement-Systems und TNF-α mit konsekutiver Entstehung von Gewebsnekrosen [46,49-51].

Eine direkte Beteiligung von Thrombin an der Entstehung des Sekundärschadens scheint daher naheliegend.

3.2.2 Komponenten des *Liquor cerebrospinales* und deren Einfluss auf die Entstehung des Sekundärschadens nach ICB

Eine intraventrikuläre Einblutung korreliert mit schwerwiegenderen neurologischen Defiziten nach ICB.[52] Experimentelle und klinische Studien belegen eine Entzündungsreaktion im Liquor als Folge einer Einblutung.[53,54] Diese aseptische Entzündungsreaktion umfasst Veränderungen der Zellzahl, des Eiweißgehaltes und der Glucosespiegel.[53] In einer prospektiven Beobachtungsstudie bei 464 Patienten konnte ein direkter Zusammenhang zwischen intraventrikulärer Blutungsmenge, Degradierung der Blutbestandteile und einer Zunahme der Entzündungsparameter (Leukozyten, Zellzahl, Glucose) bestätigt werden.[55] Es bestand jedoch kein Zusammenhang zwischen den gemessenen Parametern und dem funktionellen Neurostatus. Im Rahmen der *Clot Lysis Evaluation of Accelerated Resolution of Intraventricular Hemorrhage* (CLEAR) III Studie konnte bei 500 Patienten keine

Verbesserung eines funktionell guten Überlebens (mRS0-3) nach intraventrikulärer Lysetherapie mit Alteplase gefunden werden. Die Mortalität bei Patienten, die eine intraventrikuläre Lysetherapie erhielten, war nach 6 Monaten mit 18% geringer, als die der Patienten mit Placebo-Gabe (29%).[56]

3.2.3 *Cortical spreading depressions* und Blutabbauprodukte

Als *cortical spreading depolarization* (CSD) bezeichnet man Depolarisationswellen der grauen Substanz, welche sich langsam mit einer Geschwindigkeit von 2 bis 5 mm/min ausbreiten.[57] Im gesunden lassen sich CSDs nur nach Provokation mittels mechanischer oder elektrischer Stimuli beobachten und führen in der Folge zu einer Unterdrückung der synaptischen Aktivität für 5 – 15min.[58] Durch Hypoxie, Ischämie oder Hypoglykämie kommt es zu einem spontanen Auftreten dieser Depolarisationswellen, wobei es meisten zu einer protrahierten Rekonstitution kommt.[58] CSDs führen klinisch zu einer Suppression im Elektroencephalogramm (EEG). Im Rahmen von CSDs kommt es zu einem Anstieg des extrazellulären K+ bis 60 mmol/L und einem Abfall von Ca2+ auf bis zu 0.1 mmol/L, und einer Reduktion von Na+ auf 50 bis 70 mmol/L.[58] Dieser Zusammenbruch der Ionenhomöostase führt zu einem neuronalen Flüssigkeitsinflux mit konsekutiver Schwellung vor allem der Dendriten und stellt einen Mechanismus der neuronalen Beteiligung im Rahmen der CSDs dar.[59] Während der Phase der Depolarisation kommt es darüber hinaus zu einer Freisetzung der exzitatorischer Neurotransmitter Glutamat und Aspartat.[60] In Studien der *Co-Operative Study on Brain Injury Depolarizations* (COSBID; see http://www.COSBID.org) konnte gezeigt werden, dass es bei Patienten mit einer traumatischen Hirnschädigung innerhalb des geschädigt sowie des läsionsfreien Hirnparanchyms zum Auftreten von CSDs kommt und diese zur Ausbreitung des Schadens beitragen.[61] Die Existenz einer perihämatomalen Penumbra im Rahmen intrazerebraler Blutungen ist noch immer umstritten. Es wird jedoch spekuliert, dass die durch CSDs angestoßene Neuroinflammation und Entstehung eines perifokalen Ödems zu einer Rekrutierung gesunder Bereiche in den periläsionalen Schaden vermittelt.[38] Ein Einfluss von CSDs wird in der Pathophysiologie und Schadensentstehung verschiedener intrakranieller Blutungen diskutiert. So kommt es nach aneurysmatischen Subarachnoidalblutungen zu einer Umkehr der neurovaskulären Rückkopplung in Folge von CSDs und damit zu einer lokalen Vasokonstriktion und konsekutiven Minderperfusion.[62] In einem porcinen ICB Modell

wurde das Auftreten CSDs nach intrazerebralen Blutungen beschrieben.[63] Auch nach TBI und subduralen Hämatomen wurde das Auftreten sich ausbreitender Depolarisationswellen beobachtet. [61] Trotz des zunehmenden Verständnisses über die Entstehung und Auswirkung von CSDs, bleibt das Kausalitätsprinzip- führt neuronaler Schaden zur Entstehung der Depolarisation oder ist er die Folge derselben, ein Gegenstand der wissenschaftlichen Diskussion.

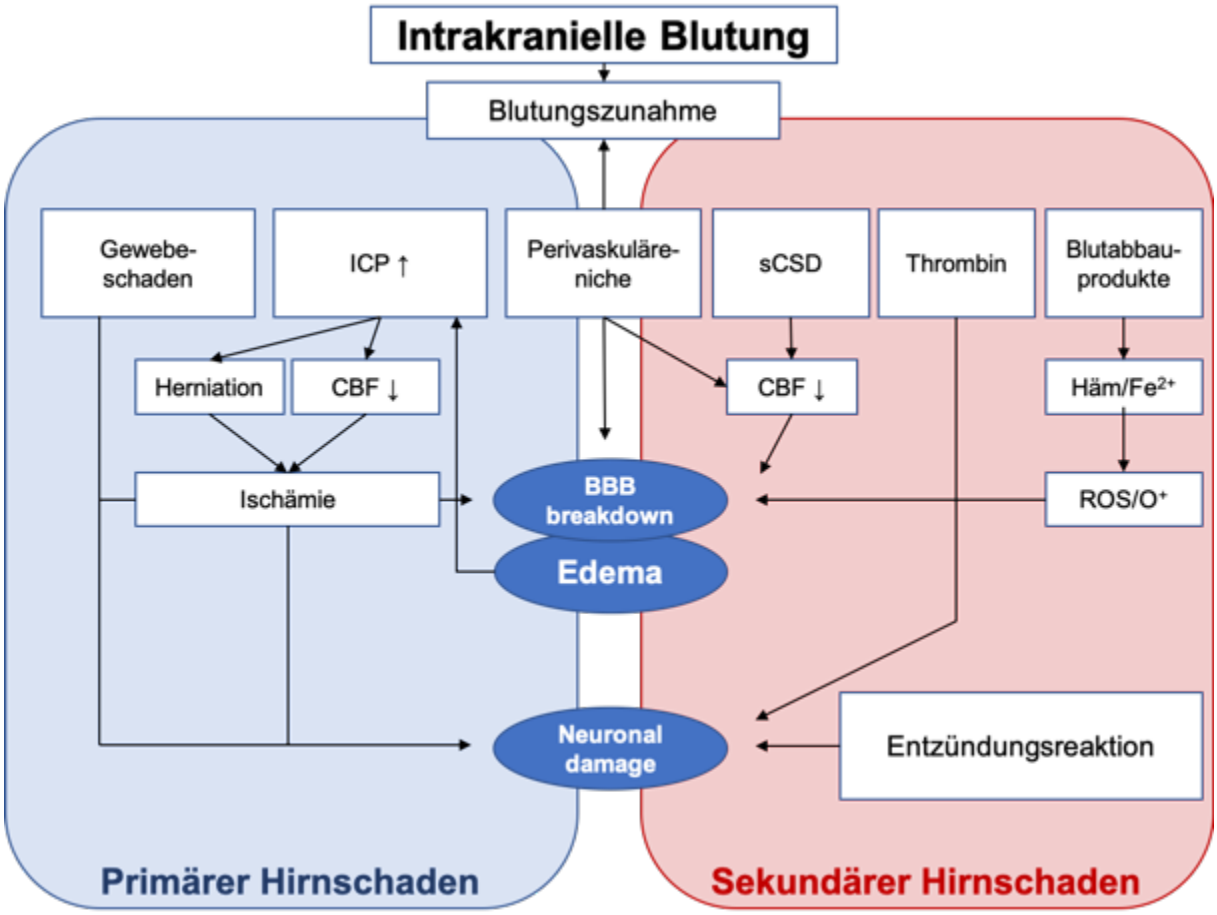

Abb. 1: Mechanismen der Entstehung des primären und sekundären Hirnschaden nach intrakraniellen Blutungen (nach Mracsko et. al. Front. Cell. Neurosci. 2014)

3.2.4 Bedeutung von Perizyten und einer aberranten Gefäßarchitektur für die Entstehung und Rekonstitution nach ICB

Perizyten sind perivaskuläre, multipotente Zellen der abluminalen Seite der Kapillaren. Im Bereich des zentralen Nervensystems treten Perizyten zu Endothelzellen in einem Verhältnis von bis zu 1:1 auf.[64] Eine derartig hohe Dichte von Perizyten ist dabei für

die Aufrechterhaltung der BBB notwendig.[65] Im ZNS erfüllen Perizyten weiterhin eine Vielzahl unterschiedlichster Aufgaben; der Regulation des zerebralen Blutfluss, Stammzellreservoir sowie Modulation von Angiogenese und Entzündungsreaktionen.[66] Perizyten stehen über eine Vielzahl unterschiedlicher Signalkaskaden inklusive *platelet derived growth factor* (PDGF), *vascular endothelial growth factor* (VEGF), *transforming growth factor beta* (TGF-ß) und Wnt mit den Endothelzellen der assoziierten Gefäße in Verbindung. Eine Störung einer dieser Regelkreise führt zu pathophysiologischen Phänomenen wie Tumorangiogenese oder diabetische Retinopathie.[65-67] Ein Mangel an Perizyten führt zu einer Zunehmenden Schrankenstörung über die BBB und eine Ausbildung von Mikroaneurysmata.[68] In verschiedenen Arbeiten konnte ein Zusammenhang zwischen einem Verlust von Perizyten und dem Auftreten intraventrikulärer-, aneurysmatischer- und Tumor assoziierter Blutungen nachgewiesen werden.[69,70] Eine aberrante Angiogenese, wie zum Beispiel im Rahmen des Tumorwachstums auftritt, führt über eine Unterdrückung des TGF- β1 Signalweges zur Gefäßdysplasien und konsekutiver Einblutung.[71,72] Solche Einblutungen sind ein Charakteristikum hirneigener Tumore wie dem Glioblastom.[73] Das Glioblastom zählt zu den am stärksten vaskularisierten Tumoren, vermittelt durch die Expression von VEGF in Folge einer lokalen Hypoperfusion. Die Überexpression von VEGF in Glioblastomzellen führt zu einer konsekutiven Zunahme der für diese Tumorentität pathognomonischen intrazerebralen Blutungen im Mausmodell.[73] Da es ausgelöst durch VEGF zu einer Ablation von gefäßumgebenden Perizyten kommt, sind diese oft unreif und fragil; einer möglichen Erklärung der Häufung von ICBs beim Glioblastom.[74] Im Rahmen einer Gewebsminderperfusion kommt es außerdem zu einer Ischämie bedingten Konstriktion der Kapillaren, ausgelöst durch Kontraktion der umgebenden Perizyten und einem damit verbundenen Gewebsuntergang.[75]

Trotz einer stitigen Zunahme neuer Hinweise über die Rolle von Perizyten im Rahmen der ICB, ist bisher wenig über die zugrundliegenden molekularen Mechanismen und der Beteiligung im Rahmen der Entstehung des Sekundärschadens bekannt.

4 Behandlung intrazerebraler Blutungen

Ein einheitliches Behandlungskonzept für ICBs existiert aktuell nicht. Die Therapie umfasst konservative und invasive Ansätze. Die operativen Verfahren sind breit gefächert und beinhalten die stereotaktische oder navigierte Aspiration, Lyseverfahren, die mikrochirurgische Evakuation sowie die dekompressive Hemikraniektomie. In einem Review von 1421 Patienten mit ICB war das Begrenzen und Einstellen therapeutischer Bemühungen der führende Grund der hohen Mortalität.[76] Die Behandlung auf einer neurologisch-/neurochirurgischen Intensivstation führte in einer prospektiven Studie zu einem deutlichen Rückgang der Mortalität.[77]

4.1 Konservatives Management

Gängige Maßnahmen der konservativen Therapie umfassen die Sicherung der Atemwege, Aufhebung etwaiger Antikoagulation, sowie eine enge Einstellung des intrakraniellen Drucks (ICP) und Normalisierung des Blutdrucks.[78] Die Senkung des Blutdrucks auf Zielwerte von 140mHg konnte im Rahmen multizentrischer Phase II (ATACH, *Antihypertensive Treatment of Acute Cerebral Hemorrhage*) und III (INTERACT, *Intensive Blood Pressure Reduction in Acute Cerebral Haemorrhage*) Studien als sicher und empfehlenswert identifiziert werden.[79] In einer Subgruppenanalyse der INTERACT Studie konnte gezeigt werden, dass Patienten mit einem initialen Blutdruck von mehr als 181mmHg am meisten von einer konsequenten Senkung des Blutdrucks profitieren, wenn diese innerhalb der ersten 3h nach Iktus eingeleitet wird. [79,80]

Mehr als 17% aller intrazerebrale Blutungen stehen in Zusammenhang mit der Einnahme einer oraler Antikoagulation (oAK).[9] Bei der Hälfte aller Patienten mit ICB unter oAK kommt es zu einer neurologischen Verschlechterung innerhalb der ersten 48h und einer Mortalität innerhalb der ersten 6 Monaten von 64%.[81] Es wird daher eine Gerinnungsnormalisierung durch Gabe von Vitamin-K und Prothrombinkomplex (PPSB) bei Vitamin-K-Antagonisten, Protaminsulfat bei Heparin und Fresh-Frozen Plasma (FFP) innerhalb von 2h nach Iktus empfohlen.[9,82] Eine Reduktion der *International normalized ratio* (INR) auf unter 1,4 innerhalb von 2h nach Iktus trägt zu einer Reduktion der sekundären Blutungszunahme bei.[83]

Die Daten der FAST Studie lassen keinen generellen Vorteil der Gabe von rFVIIa für das Gesamtüberleben und das neurologische Outcome erkennen.[84] Die Wirkung der neuen oralen Antikoagulanzien (NOAKs) lässt sich mit den Standard-Gerinnungstest nur unzureichend beurteilen, so dass Ihre Wirkung anhand der Halbwertszeit und Elimination abgeschätzt werden muss.[85] Spezifische Antidote wie Idarucizumab für den direkten Thrombininhibitor Dabigatran oder Andexanet Alfa für die Faktor-Xa-Hemmer Rivaroxaban und Apixaban sind in Ihrer Bedeutung zur Behandlung mit diesen Antikoagulanzien assoziierten Blutungen bisher nicht hinreichend erforscht.[86,87] Uneinigkeit besteht über den Einfluss der Thrombozytenfunktion auf ICBs. Die Hemmung der Thrombozyten-Aggregation führte in zwei Beobachtungs-Studien zu einem häufigeren Auftreten von intraventrikulären Blutungsanteilen, frühen Nachblutungen, einer Zunahme der Mortalität und schlechtem neurologischen Outcome, während die CHANT (*Cerebral Hemorrhage and NXY-059 Treatment*) Studie keine dieser Auswirkungen belegen konnte.[88-90]

Durch den raumfordernden Effekt der ICB selbst, sowie des begleitenden perifokalen Ödems, kann es zu einer Beeinträchtigung des zerebralen Blutflusses (CBF) und einer Erhöhung des intrakraniellen Drucks (ICP) kommen. Aus arteriellem Blutdruck und ICP lässt sich der zerebrale Perfusionsdruck berechnen. Konzeptuell stellt der CPP den arteriellen Blutdruck dar, mit dem das Hirn effektiv perfundiert wird. Somit kann der CPP in Näherung als indirekter und globaler Indikator für den regionalen CBF angesehen werden. Es gibt Hinweise, dass die Aufrechterhaltung eines CPP von 50-70 mm HG zu einer Verbesserung des neurologischen Outcomes beiträgt. Trotz fehlender Beweise der Überlegenheit eines kontinuierlichen Hirndruckmonitorings wird dies durch die Europäische Schlaganfallgesellschaft empfohlen.[91,92] Ziel der Therapie ist die Senkung des ICP auf Werte < 20 mmHg wobei lediglich ein längerer Hirndruckanstieg (>15 min) zu einer spezifischen Behandlung führen sollte. Allgemeine Maßnahmen (Stufe 1) zur Senkung des intrakraniellen Drucks beinhalten die Verbesserung des venösen Abstroms durch Oberkörperhochlagerung um 30°, der Vermeidung von Fieber, Hypo- und Hyperglykämie, Hypo- und Hyperkapnie, einer adäquaten Analgosedierung sowie, wenn möglich, der Drainage von Liquor über eine externe Ventrikeldrainage.

Bei Versagen der allgemeinen Maßnahmen, kann die spezifische Therapie (Stufe 2) durch Gabe von Osmotherapeutika (Mannitol (20%), hypertone Kochsalzlösung (3.2-23.4%) oder Glycerol (10%)) und Barbituraten eskaliert werden. Hypertones Kochsalz

führt in einer Konzentration von 3,2 % - 23,4 % zu einer effektiveren ICP – Senkung als Mannitol in 20 %iger Lösung, während Mannitol der alleinigen Nutzung von Pentobarbital zu Senkung des ICP überlegen ist.[93] Die Anwendung der kontrollierten Hyperventilation, auf einen pCO2 < 32mmHg, sollte zur Vermeidung sekundärer ischämischer Komplikationen nur unter kontinuierlichem Monitoring der interstitiellen Sauerstoffpartialdruckes (ptiO2) erfolgen.[94]

4.2 Operatives Management

4.2.1 Mikrochirurgische Evakuation supratentorieller ICBs

Durch die chirurgische (offene) Evakuation intrazerebraler Blutungen kann die raumfordernde Wirkung und die sekundäre Freisetzung von Blutabbauprodukten reduziert werden. In der international, prospektiv durchgeführten STICH-Studie (*Surgical Trial in Intracerebral Haemorrhage*) wurden 1033 Patienten mit ICB eingeschlossen und innerhalb von 24h in einer der beiden Studienarme: Initial konservative Therapie (530 Patienten) oder frühe Hämatomevakuation (503 Patienten), randomisiert. Im Verlauf kam es bei sekundärer Verschlechterung der Vigilanz zu einem Wechsel von 1/4 der Patienten aus der konservativen in die chirurgische Behandlungsgruppe. Innerhalb der operativen Gruppe kam es in 26% zu einem funktionell guten Outcome, in der konservativen Behandlungsgruppe in 24% (*odds ratio* 0.89 [95% CI 0.66-1.19], p=0.414). Auch in der Mortalität bestand kein signifikanter Unterschied.[95] Eine Subgruppenanalyse der Kohorte ergab, dass die frühe chirurgische Therapie für nicht komatöse Patienten mit oberflächlich gelegenen Blutungen einen positiven Effekt haben könnte.[95] Die klinische Bedeutung dieser Subgruppe wurde in einer Nachfolgestudie (STICH-II) untersucht. In dieser ebenfalls international, prospektiv an 78 Zentren in 27 Ländern durchgeführten Studien, wurden insgesamt 601 Patienten mit oberflächlichen, nicht tiefer als 1cm von der Kortexoberfläche gelegenen Blutungen ohne Ventrikeleinbruch und mit einem Volumen zwischen 10-100ml für frühe Evakuation (307) oder konservative Therapie (294) randomisiert. Von den eingeschlossenen Patienten hatten 174 (59%) von 297 der chirurgischen Gruppe und 178 (62%) von 286 Patienten der konservativen Gruppe ein schlechtes Outcome (*odds ratio* 0,86 [0,62 to 1,20]; p=0,367). Die 6-Monats-Mortalitätsrate lag bei 18% (Evakuation) und 24% (konservative Behandlung) (odds ratio 0,71; [0,48-1,06]; p=0,095).[96] Eine Subgruppenanalyse zeigte, dass Patienten mit einem initialen *Glascow Coma Scale* (GCS) zwischen 10-12 von einer chirurgischen

Therapie profitierten.[96] Die STICH-Studien konnten somit keinen eindeutigen Vorteil der chirurgischen Therapie gegenüber einem konservativen Vorgehen belegen. Lediglich ein kleiner eng umgrenzten Teil der Patienten, profitiert eindeutig von einer frühen, operativen Evakuation. Die mikrochirurgische Evakuation kann als Einzelfallentscheidung jedoch als lebensrettende Maßnahme bei neurologischer Verschlechterung erwogen werden.[96]

4.2.2 Mikrochirurgische Evakuation infatentorieller ICBs

Eine rechtzeitige Evakuation infratentorieller Blutungen vermag die mit einer Kompression des Hirnstamms verbundene Morbidität und Mortalität zu senken. In einer Analyse des amerikanischen Schlaganfallregisters kam es bei Patienten mit einer chirurgischen Evakuation der Blutung zu einem besseren funktionellen Outcome, unabhängig des Alters und der initialen Beeinträchtigung.[97] Eine neurologische Verschlechterung der Patienten ist als Indikation zur Evakuation akzeptiert. Bei Auftreten einer Liquorzirkulationsstörung durch Kompression des 4. Ventrikels scheint eine Evakuation vor Eintreten einer Verschlechterung vorteilhaft.[98] Die Leitlinien der amerikanischen und europäischen Schlaganfallgesellschaft empfehlen die Evakuation infratentorieller Blutungen mit einem Durchmesser größer 3 cm oder mehr als 20 ml Volumen.[99,100]

4.2.3 Dekompressive Hemikraniektomie

Die Wirksamkeit der Hemikraniektomie beruht auf der Senkung des ICP durch Entfernung des äußeren Wiederlagers des Neurokraniums. Hierdurch wird eine Schwellung des geschädigten Hirngewebes nach außen ermöglicht und eine Herniation durch Kaudalverlagerung verhindert.[101] Patienten mit großen, tief unter der Kortexoberfläche gelegenen Blutungen, eintretender Mittellinienverlagerung und einem GCS < 8 können von einer dekompressiven Hemikraniektomie profitieren.[101-103] Die internationale multizentrische SWITCH-Studie (*Swiss Trial of Decompressive Craniectomy versus Best Medical Treatment of Spontaneous Supratentorial Intracerebral Hemorrhage)* untersucht prospektiv den Nutzen der frühen dekompressiven Hemikraniektomie im Vergleich zur konservativen Behandlung bei ICBs im Bereich der Stammganglien mit einem Volumen > 30 ml (www.switch-trial.ch).

4.2.4 Minimal-invasive Hämatomevakuation

Minimal-invasive Therapieverfahren stellen eine Möglichkeit zur Hämtomevakuation unter Schonung des perihämatomalen Gewebes dar. Hierbei werden Katheter stereotaktisch oder unter Zuhilfenahme einer Neuronavigation in die Blutungshöhle eingelegt.[104] Anschließend erfolgt die Aspiration und lokale Fibrinolyse des Blutclots. In Studien von Keric et al konnten die Wirksamkeit dieser Technik durch Untersuchungen in einem neuartigen *in vitro* Modell nachgewiesen werden.[105-107] Eine Sonderform, die endoskopische Blutungsevakuation, wurde bereits in den achtziger Jahren beschrieben.[108,109] In der multizentrische Phase II MISTIE-Studie (*Minimal Invasive Surgery Plus rt-PA for Intracerebral Hemorrhage Evacuation*) wurden 69 Patienten mittels rtPA-Lyse und 42 konservativ behandelt. In der Gruppe mit rtPA konnte eine signifikante Reduktion des Hämatomvolumens und des perihämatomalen Ödems ohne Auftreten neurotoxischer Effekte, erreicht werden.[110] In der nachfolgenden, internationalen Multizenterstudie MISTIE III wurde der klinische Nutzen der Katheter-basierten rtPA Lysetherapie gegenüber der konservativen Therapie untersucht. Insgesamt wurden 506 Patienten mit supratentorieller Blutung >30ml in einem Zeitraum zwischen dem 30.12.2013 und 15.08.2017 rekrutiert und die Studienarme MISTIE (255) und konservative Therapie (251) randomisiert. Die Studie konnte die Sicherheit des Verfahrens, jedoch keine Überlegenheit von MISTIE gegenüber der Standardtherapie für das funktionelle Outcome 365 Tage nach Iktus bestätigen.[111] Die Optimierung der als sicher etablierten Fibrinolyse zur Behandlung der ICB durch neue Fibrinolytika bietet Hoffnung auf eine zukünftige, positive Beeinflussung des funktionellen Outcomes.[112]

5 Zielstellung der Arbeit

Wie nie zuvor in der Geschichte der Behandlung intrakranieller Blutungen, stehen heute eine Plethora technischer- und pharmakologischer Möglichkeiten, sowie eine Vielzahl unterschiedlicher Behandlungskonzepte zur Verfügung. Gleiwohl des immensen Forschungsaufwands der letzten Jahrzehnte, ist es dennoch bisher nicht gelungen, einen für die Patienten bedeutsamen Fortschritt in der Therapie dieser Erkrankung zu erzielen.
Mehr denn je besteht daher der Bedarf, die Mechanismen der Schadensentstehung nach ICBs zu verstehen und in moderne, multimodale Behandlungskonzepte zu integrieren. Die Untersuchung dieser Abläufe während der Schadensentwicklung steht im Mittelpunkt der vorgelegten Schrift.

Im Einzelnen wurden folgende Fragestellungen untersucht:

1. Existiert ein zerebrales Thrombinsystem und welche Rolle spielt Thrombin in der Entstehung des neuronalen Schadens nach intrakraniellen Blutungen im Maus-ICB-Modell?
2. Führt eine Zunahme der zerebralen Thrombinkonzentration im Liquor von Patienten ICB zu einem schlechteren neurologischen Outcome?
3. Welche Bedeutung hat die Optimierung des Gerinnungssystem für die Zunahme der Blutung, dass neurologische Outcome sowie das Gesamtüberleben bei Patienten mit intrakraniellen Blutungen?
4. Welche weiteren Faktoren üben einen Einfluss auf die Entstehung des Gewebeschadens nach ICBs aus: Untersuchung des Einflusses spontaner kortikaler Depolarisationswellen im Rattenmodell.
5. Welche Rolle spielt die Gefäßarchitektur und die Zellen der perivaskulären Nische für das Auftreten tumorassozierter ICBs und die Entstehung des neuronalen Schadens?

6 Orginalarbeiten

6.1 The Cerebral Thrombin System Is Activated after Intracerebral Hemorrhage and Contributes to Secondary Lesion Growth and Poor Neurological Outcome in C57Bl/6 Mice.

Krenzlin H, Gresser E, Jussen D, Riede N, Taylor L, Vogelaar CF, Ringel F, Kempski O, Alessandri B. J Neurotrauma. 2020 Jun 15;37(12):1481-1490. doi: 10.1089/neu.2019.6582. Epub 2020 Mar 11. PMID: 31830857

Hintergrund: Langezeit galt die Leber als einziger Entstehungsort der Serinprotease Thrombin. In der aktuellen Literatur häufen sich jedoch die Hinweise auf die Existenz eines zerebralen Thrombinsystems. In einer dosisabhängigen Wirkungsbeziehung vermittelt Thrombin Entwicklungsprozesse des zentralen Nervensystems, Neuroprotektion sowie, in hohen Konzentrationen, neurodegenerative und toxische Wirkungen. Bisher ist wenig über die Rolle von Thrombin bei intrazerebralen Blutungen bekannt. Es wird angenommen, dass Thrombin die Entstehung des Sekundärschadens beeinflusst. In der Vorliegenden Arbeit wird die Rolle physikalischer Veränderungen durch Volumenexpansion sowie der Einfluss von Blutabbauprodukten auf die Aktivierung des zerebralen Thrombinsystems nach ICB und dessen Einfluss auf die Entstehung des Sekundärschadens untersucht.

Methoden: Um den Einfluss des Auftretens einer ICB auf die Aktivierung des zerebralen Thrombinsystem zu untersuchen, wurden entweder 30 µl autologes Blut oder Silikonöl in das Striatum von 20 C57Bl/6N-Mäusen (Charles River, Sulzfeld, Deutschland) injiziert. Silikonöl, eine synthetische Substanz, die aus sich wiederholenden Einheiten von Siloxan besteht, wird üblicherweise in Versuchsumgebungen und als Tamponade in der vitreoretinalen Chirurgie verwendet, da es chemisch inert ist. Bei einem Teil der Tiere wurde ein periprozedurales Neuromoitoring zur kontinuierlichen Aufzeichnung des RR, ICP und CBF durchgeführt (5 Blut, 5 Silikonöl, 2 Schein operierte Tiere). Die intrakranielle Blutung wurde unter Verwendung eines 2-Stufen-Modells erzeugt. Hierbei wurde eine stumpfe 26 G-Kanüle bis zu einer Tiefe von 3 mm unter Duraniveau eingeführt. In einem ersten Schritt wurden 5 µl autologes Blut oder Silikonöl unter Verwendung einer Spritzenpumpe mit 10 µl / min injiziert. Die Nadel wurde dann auf 4 mm Tiefe vorgeschoben und weitere

25 µl injiziert. Zur Beurteilung der Auswirkungen der CB auf das zerebrale Thrombinsystem wurden coronare Kryoschnitte mit Hämatoxylin und Eosin gefärbt, um die Lokalisierung und Zusammensetzung der Läsion sichtbar zu machen. Weiterhin wurden Färbungen für Prothrombin, Thrombin, PAR-1, neuronales Kernantigen, fibrilläres saures Glia-Protein (GFAP, Marker für Astrozyten) und ionisiertes Calcium-bindendes Adaptermolekül 1 (Iba-1, Marker von Mikroglia / Makrophagen) gefärbt. Die Gewebeverletzung wurde durch Färben und Zählen von NeuN-positiven Neuronen analysiert und als Prozent der kontralateralen (nicht injizierten) Seite ausgedrückt.
Verursachte Defizite wurden mit Hilfe von sensomotorischen Funktionstests wie Rotarod-, Griffstärke-, Beam-Walk- und Beam-Balance-Tests bewertet werden. Die sensorische und motorische Integrität wurde unter Verwendung eines Neuroscores getestet

Ergebnisse: Der ICP stieg während der ICB auf 54,0 ± 10 mmHg in der Gruppe mit autologem Blut und 40,8 ± 9 mmHg in der Silikongruppe an (p = 0,34). In beiden Gruppen normalisierte sich der ICP innerhalb von 30 Minuten. Umgekehrt fiel der CBF auf 32,0% ± 8,1% nach Injektion von Blut und auf 37,6% ± 10,3% bei Tieren, denen Silikonöl injiziert worden war. Der CBF erholte sich nach dem Ende der Injektion teilweise, blieb jedoch während des gesamten Überwachungszeitraums vermindert. Der mittlere arterielle Blutdruck (MAP) stieg während der Injektionsperiode reflexartig an (Cushing-Reflex). Statistisch signifikante Unterschiede im ICP-, MAP- und CBF-Verlauf zwischen Blut- und Silikonöl fand sich nicht. Im perihämatomalen Gewebe war die Anzahl der Neuronen bei Tieren, denen Blut injiziert wurde, auf 53,96 ± 4,40% (p = <0,05) und bei Tieren, denen Silikonöl injiziert wurde, auf 61,82 ± 7,39% (p = 0,02) verringert. Der neuronale Verlust nahm mit zunehmender Entfernung von der Läsion ab. Die Analyse ergab keine statistisch signifikanten Unterschiede zwischen Blut- und Silikonläsionen. 24 h nach ICB konnte ein signifikanter periläsionaler Anstieg der Thrombinexpession in beiden Läsionsgruppen festgestellt werden. (Abb. 3B) Die Höhe der Thrombinkonzentration korrelierte hierbei mit dem Verlust an Neuronen periläsional (spearman co-efficient ρ = -0.679; p < .001). (Abb. 3C) Um zwischen lokaler Thrombinexpression und zirkulatorischem Zustrom zu unterscheiden, wurde eine Immunfluoreszenz-Co-Färbung durchgeführt. Hierbei fand sich eine starke Ko-Lokalisation von Thrombin und NeuN. (Abb. 3A) Thrombin wurde überwiegend in

reifen Neuronen und der extrazellulären Matrix nachgewiesen, nicht jedoch in Gliazellen. Die Bewertung von Gleichgewicht, Griffstärke und motorischer Koordination erfolgte mit dem Rotarod®-Leistungstest. Hierbei konnten keine statistisch signifikanten Unterschiede zwischen Blut- und Silikontieren gefunden werden, während sich beide von Scheinkontrollen unterscheiden ($p < 0{,}0001$).

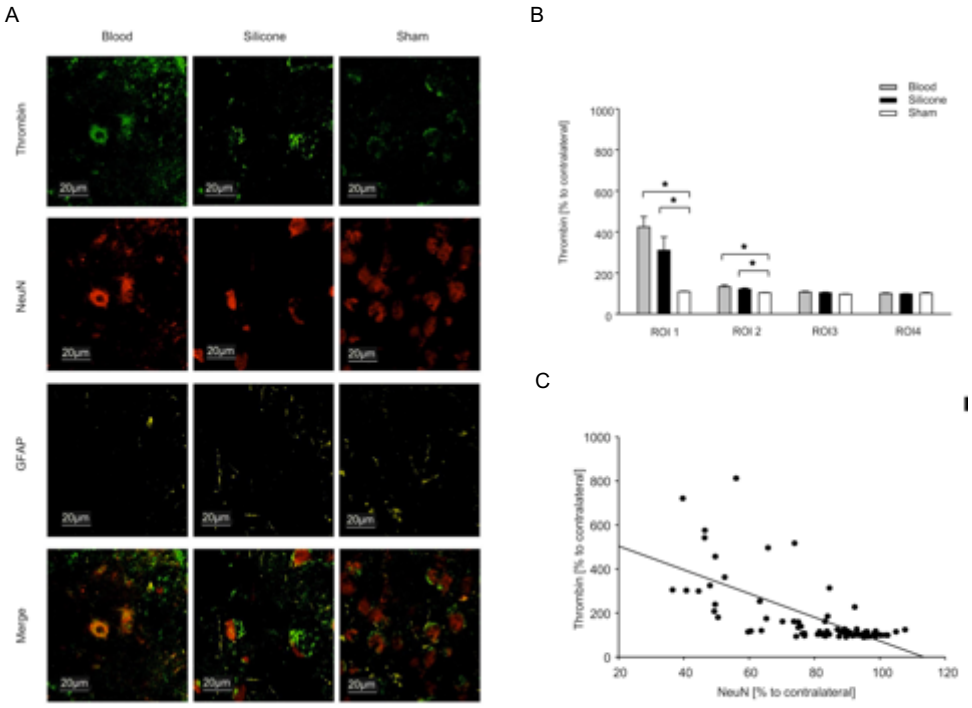

Abb. 3: (A) Ko-Lokalisation von Thrombin mit Neuronen (NuN) mittels immunfluoreszenz in der perihämatomalen Zone nach ICB bei der Maus. **(B)** Die Konzentration von perihämatomalen Thrombin nimmt mit wachsender Entfernung von der Läsion ab. **(C)** Die Konzentration von Thrombin korreliert negativ mit der Anzahl an Neuronen in der PHZ. (Krenzlin et. al. Neurotrauma. 2020)

Diskussion: In der vorgestellten Arbeit konnte erstmal die Aktivierbarkeit des zerebrale Thrombinsystem nach ICB nachgewiesen werden. Bisher gibt es nur begrenzte Daten zum lokalen zerebralen Thrombinsystem. Es wird noch immer kontrovers diskutiert, ob Thrombin infolge von Blutextravasation und Schädigung der Blut-Hirn-Schranke einströmt oder lokal produziert wird. Die Ko-Lokalisation von Thrombin mit Neuronen der perihämatomalen Zone belegt das Vorhandensein und Aktivierung eines zerebralen Thrombinsystems in der Folge einer ICB. Darüber hinaus konnte gezeigt werden, dass diese Aktivierung unabhängig vom Vorhandensein von Vollblutbestandteilen ist und zu einer konzentrationsabhängigen neuronalen Schädigung mit konsekutiv schlechterem klinischem Outcome führt. Die Ergebnisse

der Studie stimmen mit zuvor veröffentlichten Daten überein, die eine Vergleichbarkeit von subduralen Hämatomen in An- und Abwesenheit von Blutabbauprodukten nahelegt.

Hauptaussage:
In unserer Arbeit konnte die Aktivierung eines zerebralen Thrombinsystem unabhängig vom Vorhandensein von Blutabbauprodukten nach ICB nachgewiesen werden. Die Entstehung des neuronalen Schadens und der Ausbildung neurologischer Defizite in der Frühphase nach ICB korreliert mit dem Auftreten von Thrombin. Unsere Ergebnisse untermauern somit die Existenz eines zerebralen Thrombinsystems und unterstreichen dessen Bedeutung als potentieller Angriffspunkt einer gezielten ICB Therapie.

6.2 High CSF thrombin concentration and activity is associated with an unfavorable outcome in patients with intracerebral hemorrhage

Krenzlin H, Frenz C, Schmitt J, Masomi-Bornwasser J, Wesp D, Kerz T, Lotz J, Alessandri B, Ringel F, Keric N.

Hintergrund: Durch intrazerebrale Blutungen kommt es zu einer Aktivierung des zerebralen Thrombinsystems im perihämatomalen Gewebe. Durch die Expression von Thrombin kommt es in einer konzentrationsabhängigen Dosis-Wirkungsbeziehung zu einer Zunahme des Sekundärschadens und einem schlechteren neurologischen Outcome. In dieser Arbeit wurde der Einfluss der Thrombinkonzentration und der Thrombinaktivität im Liquor auf das neurologische Outcome bei Patienten mit ICB untersucht.

Methoden: Von Februar 2017 bis Februar 2019 wurden 20 konsekutive Patienten (9 Frauen und 11 Männer), welche aufgrund einer supratentoriellen ICB eine extraventrikuläre Drainage benötigten, in die vorliegende Studie eingeschlossen. Das Patientenalter lag zwischen 40 und 80 Jahren (66 ± 12 Jahre). Alle Patienten hatten mindestens eine oder mehrere Grunderkrankungen, wobei arterielle Hypertonie mit 75% am häufigsten auftrat, chronische Herzerkrankungen (35%) und maligne

Erkrankungen (30%) am zweit- und dritthäufigsten auftrat. Alle Patienten wurden standardmäßig auf Intensivstation gemäß den aktuellen klinischen Richtlinien behandelt. Die Liquorkonzentration von Thrombin, seinem Vorläufer Prothrombin und dem Thrombin-Antithrombin-Komplex (TAT) wurden mittels enzymgebundenen Immunsorbens-Assays (ELISA) gemessen. Darüber hinaus wurde die Konzentration der Superoxiddismutase (SOD), als Marker von oxidativem Stress, im Liquor bestimmt. Das initiale Blutungsvolumen und der intraventrikuläre Blutungsanteil wurden basierend auf einer bei Aufnahme angefertigten Computertomographie (CT) bestimmt. Das neurologische Ergebnis wurde unter Verwendung der erweiterten mRS- und Glasgow-Ergebnisskala (GOSE) 6 Wochen und 6 Monate nach Auftreten der ICB erhoben.

Ergebnisse: Die Konzentrationen von Prothrombin (p <0,005), Thrombin (p = 0,005) und TAT (p = 0,046) im Liquor von Patienten mit ICB zeigt eine statistisch signifikante Erhöhung im Vergleich zum Liquor von Patienten ohne ICB. Die Liquor-Konzentrationen von Thrombin 24 Stunden nach ICB korrelierten mit dem mRS-Index als Surrogat-Marker des neurologischen Outcome, 6 Wochen (r2 = 0,73; <0,005) und 6 Monaten (r2 = 0,63; <0,005) nach Entlassung aus dem Krankenhaus. (Abb. 2) Die Thrombinaktivität7TAT korrelierte ebenfalls mit dem mRS nach 6 Wochen (r^2 = 0,54; <0,01) und 6 Monaten (r^2 = 0,66; <0,04). Hohe Thrombinkonzentrationen 24 Stunden nach ICB treten gemeinsam mit höheren SOD-Spiegeln auf (p = 0,01). Im Gegensatz dazu hatten Prothrombin, Thrombin und TAT weder zum anfänglichen ICB-Volumen noch zum IVH-Volumen eine statistisch signifikante Korrelation. Ebenso korrelierten die Plasmaspiegel von FII, FIIa und TAT nicht mit dem klinischen Ergebnis. Die Korrelation der Liquorkonzentrationen von FII, FIIa und TAT mit dem klinischen Outcome war unabhängig von der Art der gewählten chirurgischen Intervention. Unsere Daten zeigen keine Überlegenheit einer Blutungsevakuation oder -lyse im Vergleich zur konservativen medizinischen Behandlung bezogen auf das neurologische Outcome (p = 0,71). Hohe Konzentrationen von FII, FIIa oder TAT im Liquor führten nicht zu einer erhöhten Notwendigkeit chirurgischer Eingriffe während der akuten Phase nach ICB.

Diskussion: In dieser Studie konnten wir zeigen, dass die anfängliche Thrombinkonzentration und -aktivität im Liquor von Patienten mit ICB nicht mit dem

ICH- und IVH-Volumen korreliert und dennoch mit einem schlechteren funktionellen neurologischen Outcome verbunden ist. Diese Ergebnisse stützen somit einen vom Primärschaden unabhängigen Beitrag von Thrombin zur Entstehung des Sekundärschadens. Die Ko-Inzidenz von Thrombin und ROS legt eine zumindest partielle Involvierung freie Sauerstoffspezies in der Pathophysiologie der Thrombin

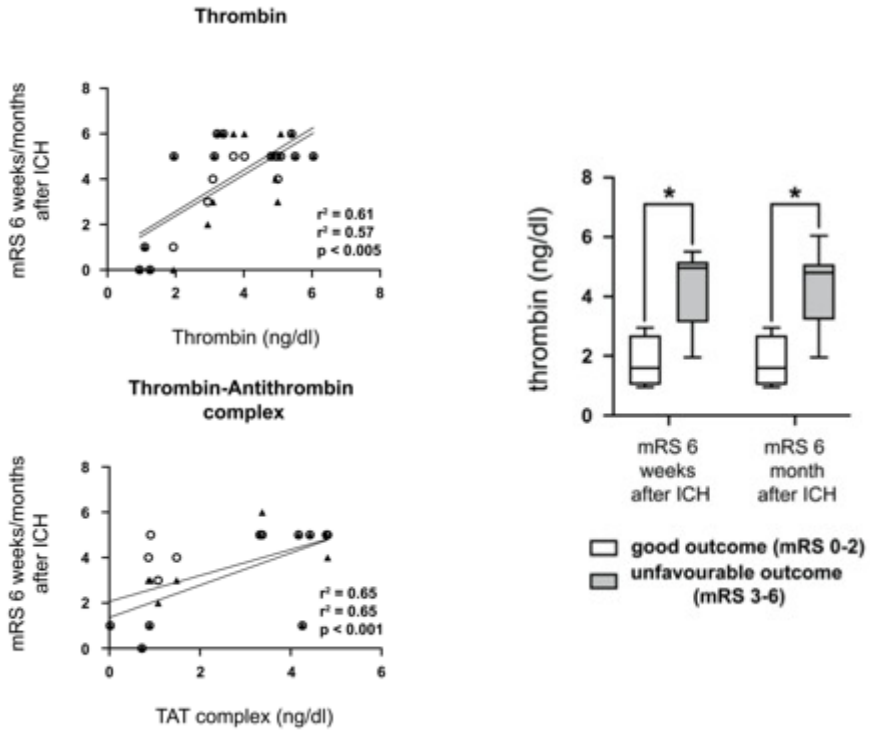

Abb. 2: (A) Die Konzentration von Thrombin und dem TAT Komplex korrelieren mit dem neurologischen Outcome (mRS) 6 Wochen und 6 Monate nach ICB. **(B)** Patienten mit niedrigeren Thrombinkonzentrationen im Liquor haben eine statistisch signifikant höhere Wahrscheinlichkeit eines günstigen Outcome. (nach Krenzlin et. al. Plos ONE. 2020)

vermittelten Schadensentstehung nahe.

Hauptaussage: Die Serin-Protease Thrombin stellt, im zentralen Nervensystem, einen multivalenten Einflussfaktor vieler, über seine Funktion im Gerinnungssystem hinausgehender, physiologischer und pathophysiologischer Prozesse dar. Wie auch im Rahmen eines ischämischen Insultes, besteht ein Zusammenhang zwischen hohen Konzentrationen von Thrombin im Liquor und einem schlechten Outcome nach intrazerebralen Blutungen. Die Unabhängigkeit der Thrombinkonzentration im Liquor von der im Blutplasma, der Größe der Blutung und der intraventrikulären Blutungsanteile liefert weitere Hinweise auf die Bedeutung des intrazerebralen Thrombinsystems für die Pathophysiologie der ICB.

6.3 Surgical treatment of intraparenchymal hemorrhage during mechanical circulatory support for heart-failure- a single-center experience.

Krenzlin H, Rosenthal C, Wolf S, Vierecke J, Kowski A, Hetzer R, Vajkoczy P, Czabanka M. Acta Neurochir (Wien). 2014 Sep;156(9):1729-34. doi: 10.1007/s00701-014-2141-6. Epub 2014 Jun 13. PMID: 24919800

Hintergrund: Intrazerebrale Blutungen stellen eine schwerwiegende Komplikation bei Patienten mit Ventricular assist devices (VAD) dar, da diese eine ständige Antikoagulation erfordern. Es ist bekannt, dass eine Beeinträchtigung des ex- oder intrinsischen Gerinnungssystem zu einer stärkeren Zunahme des Blutungsvolumens nach Iktus führt.[32] Die Operation und das post-operative Management der ICB unter Antikoagulation stellt eine besondere Herausforderung die Behandler dar, und birgt erhebliche Risiken für den Patienten.[113] Bei Patienten, bei denen eine obligate Indikation zur Antikoagulation aufgrund mechanischer Implantate oder im Rahmen einer vorliegenden Erkrankung besteht, existieren nur wenige klinische Entscheidungshilfen, eine eindeutige Evidenz für ein bestimmtes Vorgehen fehlt.[114] Ziel der vorgelegten Arbeit war es, dass chirurgische und klinische Outcome von Patienten mit Behandlungsbedürftiger ICB und VAD zu analysieren. Im Mittelpunkt der Arbeit steht das zentrale Management der Antikoagulation und sein Einfluss auf den sekundären Blutungsprogress, post-operative Nachblutung und Funktion des VAD, sowie das funktionelle Outcome.

Methoden: Im Zeitraum vom 1. Januar 2009 bis zum 1. Januar 2014 wurden 12 konsekutive Patienten mit VAD und raumfordernder supra- oder infratentorieller ICB in die Studie eingeschlossen. Die Datenerhebung erfolgte anonymisiert, retrospektiv. Die Nachbeobachtung erfolgte bis 3 Monate nach der Operation oder bis zum Tod der Patienten. In der Analyse wurden zwei primäre Outcome Parameter, das Ausmaß der Hämatomevakuation und das klinische Outcome anhand der modified Rankin Scale (mRS), definiert. Sekundäre Outcome Parameter waren die Häufigkeit einer Nachblutung, die Rate der Revisionseingriffe und die Mortalität im Krankenhaus. Das

Gerinnungsmanagement wurde anhand der präoperativen INR-Werte (International Normalized Ratio) sowie der prä- und postoperativen Antikoagulation erfasst.

Ergebnisse: Insgesamt wurden zwölf Patienten (Durchschnittsalter 44 ± 18 Jahre, 9 supratentorielle und 3 infratentorielle Blutungen) in die Auswertung eingeschlossen. Bei 10 Patienten bestand die Behandlung mit einem LVAD mit kontinuierlichem Fluss, 1 Patient wurde mit LVAD und pulsatilem Fluss und ein Patient mit extrakorporaler Membranoxigenierung behandelt. Eine chirurgische Evakuierung des Hämatoms wurde bei 11 Patienten durchgeführt, ein Patient erhielt eine dekompressive Hemikraniektomie. Bei allen Patienten bestand eine Antiaggregation mit Acetylsalicylsäure und eine Antikoagulation mit Marcumar oder Heparin. Der INR zum Zeitpunkt der ICB war 2,7 ± 1,6, die Partielle Thromboplastinzeit (PTT) 63,3 ± 40 s. Präoperativ erfolgte bei allen Patienten die Gerinnungsoptimierung durch Gabe von Blut- und Thrombozytenkonzentraten, Fresh Frozen Plasma und Fibrinogen oder PPSB. Eine intraoperative Normalisierung der Gerinnung gelang bei 50% der Patienten. Post operativ erfolgte die PTT gesteuerte Antikoagulation mit Heparin (Ziel 60-80s) bei 8 Patienten, bei 4 Patienten wurde eine vollständige Normalisierung der Gerinnung angestrebt. 7 der 8 Patienten mit PTT gesteuerter Antikoagulation verstarb während des Aufenthaltes im Krankenhaus, 4 Patienten verstarben innerhalb der ersten 24h. Der einzige Überlebende konnte mit einem mRS von 5 Punkten entlassen werden. Bei Patienten mit einer Normalisierung der Gerinnung betrug die Mortalität 50%, 2 Patienten überlebten mit einem mRS von 5 bzw 4 Punkten.
Bei allen Patienten konnte durch die Operation eine Teilevakuation der Blutung erreicht werden. Eine Vollständige oder insuffiziente Evakuation fand sich bei keinem der Patienten. Die Nachblutungsrate betrug 75%. Bei drei Patienten wurde eine Revision durchgeführt, bei zwei Patienten wurde eine partielle Hämatomevakuation und bei einem Patienten eine vollständige Evakuierung erreicht.

Diskussion: Unserer Studie belegt die Schwierigkeit einer suffizienten chirurgischen Intervention und das schlechte Outcome bei Patienten mit ICB und mechanischer Kreislaufunterstützung. Die präoperative und intraoperative Substitution von Gerinnungsfaktoren und Blutbestandteilen zeigte keinen ausreichenden Schutz zur Verhinderung von Nachblutungen und einer deutlich erhöhten Mortalität. Die

postoperative Normalisierung der Gerinnung scheint jedoch zu einer Verbesserung des Outcomes beizutragen, ohne die Kreislaufunterstützungssysteme zu behindern.

Hauptaussage: Bei den Patienten mit LVAD handelt es sich um eine kleine und schwer vorerkrankte Gruppe von Patienten. Trotz maximaler therapeutischer Anstrengung ist die Mortalität nach ICB in dieser Gruppe deutlich erhöht. Die Arbeit verdeutlicht die übergeordnete Bedeutung des Gerinnungssystems und eine stringente Optimierung desselben, für das Überleben und funktionelle Outcome bei Patienten mit intrazerebralen Blutungen.

6.4 Occurrence of Spontaneous Cortical Spreading Depression Is Increased by Blood Constituents and Impairs Neurological Recovery after Subdural Hematoma in Rats.

Krenzlin H, Jussen D, Plath M, Tretzel SJ, Krämer T, Kempski O, Alessandri B. J Neurotrauma. 2019 Jan 15;36(2):395-402. doi: 10.1089/neu.2018.5657. Epub 2018 Aug 10. PMID: 29756530

Hintergrund: Akute subdurale Blutungen (ASDH) sind häufig und mit schwerer Morbidität und Mortalität verbunden. Im Jahr 1944 entdeckte Leão eine Unterbrechung der Elektroenzephalogrammaktivität, die mehrere Minuten andauerte, während seiner Forschung zur Epilepsie bei Kaninchen. sCSDs sind ein elektrophysiologisches Phänomen mit allenfalls geringen Auswirkungen auf gesundes Gewebe. Es wird jedoch angenommen, dass diese spontanen kortikalen Depolarisationen (sCSD) in der Entstehung des Sekundärschadens bei ICBs und ASDH eine Rolle spielen. Die wellenartigen Depolarisationen sind mit Veränderungen des zerebralen Blutflusses, der Perfusion sowie einer Schwellung der Neuronen und der Dendriten verbunden. Über die Entstehung von sCSD und der durch sie ausgelösten Pathomechanismen ist bisher nur wenig bekannt. Die vorliegende Arbeit beschäftigt sich mit allgemeinen Mechanismen der Auswirkung sCSD im Rattenmodell des ASDHs.

Methoden: Die vorliegende Studie enthält zwei experimentelle Gruppen: Zunächst untersuchten und charakterisierten wir das Auftreten von sCSD nach subduraler

Blutinfusion (300 µl) mittels Gewebeimpedanzmessung (IMP) in einem Rattenmodell. Zweitens verglichen wir das Auftreten und den Einfluss von sCSD auf das Läsionswachstum und das neurologische Defizit in Gegenwart und Abwesenheit von Vollblutbestandteilen. Neurologische Ausfällen wurden mit Hilfe es 10 Punkte umfassenden ‚Neuroscores', dem Beam-Balance- und Beam-Walk-Test quantifiziert. Die Ausdehnung des neuronalen Schadens wurde an konsekutiven Coronarschnitten durch die Läsion der in Paraffin fixierten Hirne, mit Hilfe der Haematoxylin-Eosin Färbung ausgewertet.

Ergebnisse: Durch die subdurale Blutinfusion kam es zu einen ko-linearen Anstieg des IMP und ICP. Kein Unterschied im anfänglichen IMP-Anstieg (p = 0,685) oder in der Dauer (p = 0,084) bestand zwischen Tieren mit und ohne weitere sCSDs. In der ersten Versuchsgruppe konnten nach Blutung drei IMP-Merkmale unterschieden werden: kein sCSD, rezidivierende sCSD und konstant erhöhtes IMP (anoxische Depolarisation, AD). Bei 8 Tieren traten die Ersten sCSDs 53,86 ± 1,73 min nach Iktus auf, während bei 7 Tieren keine sCSDs beobachtet wurden. Im Durchschnitt wurden 6 ± 0,58 sCSDs beobachtet. Jeder sCSD dauerte 2,66 ± 0,31 min, während der Erste am längsten (3,43 ± 0,34 min) und die Letzte am kürzesten (2,47 ± 0,28 min) anhielt. Wenn sCSDs nachgewiesen wurden, war die Läsionsgröße statistisch signifikant größer war (56,7 ± 10,7 mm3), verglichen mit Tieren ohne sCSDs (27,7 ± 10,4 mm3; p = 0,01). Zwei als AD klassifizierte Tiere hatten eine mittlere Läsionsgröße von 55,8 ± 3,7 mm3. In der zweiten Versuchsgruppe trat sCSD nach autologem Blut im Vergleich zur Paraffinölinfusion häufiger auf. Das Läsionsvolumen nach 7 Tage Betrug in der Blutgruppe 27,3 ± 6,8 mm^3 und 3,4 ± 2,1 mm^3 in der Gruppe mit Paraffinöl. Die Subgruppenanalyse zeigte bei Tieren mit sCSD eine größere Läsionsgröße als bei Tieren ohne. Darüber hinaus führte das Auftreten von sCSD in beiden Gruppen zu schlechteren neurologischen Ergebnissen.

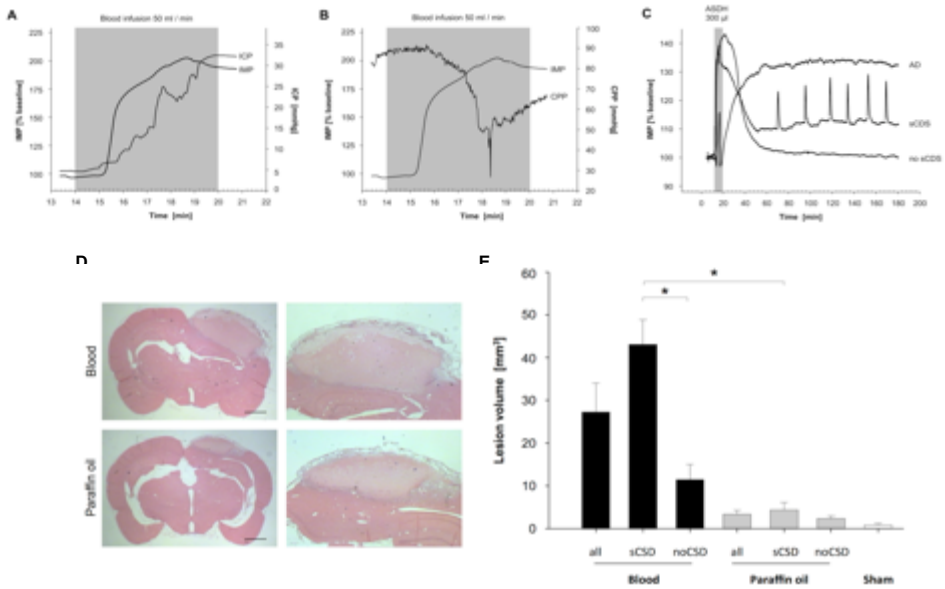

Abb. 4: (A+B) Nach Eintreten einer ICB kommt es zum gleichsinnigen Anstieg des ICP und der GEwebeimpendanz und Abfall des CBF. (C) In der Folge kommt es zum Auftreten 3 verschiedener Formen von verläufen mit unterschiedlichem Outcome: anoxischen Depolarisation, sCDS oder dem Ausbleiben von sCDS. (D) ASDHs mit Blutbestandteilen führen zu einem ähnlichen neuronalen Schaden wie solche ausgelöst durch eine inerte Volumensubstanz (D), zeigen jedoch deutlich häufiger auftretende sCDS (Krenzlin et. al. Neurotrauma 2019)

Diskussion: Unsere Experimente zeigen, sCSDs häufiger, aber nicht ausschließlich, in Gegenwart von Blutabbauprodukten beobachtet werden können. Obwohl das Auftreten von sCSDs in allen Fällen mit einem größeren Läsionsvolumen und schwereren neurologischen Defiziten verbunden war, wurde statistische Signifikanz nur bei den Tieren erreicht, die eine subdurale Infusion von autologem Blut erhielten. AD war mit einem vorzeitigen Tod des Tieres verbunden. Die Ergebnisse einer kürzlich von der COSBID-Forschungsgruppe durchgeführten multizentrischen Studie konnte zeigen, dass sCSD ein kritischer Faktor für das Outcome bei Patienten mit verschiedenen traumatischen und spontanen intrakraniellen Pathologien darstellt. Unsere Daten bestätigen das angenommene Paradigma, des sCSD zur Entwicklung des Sekundärschadens beitragen. Wir konnten zeigen, dass sCSD früh nach intrakraniellen Blutungen auftreten und nicht vom Vorhandensein von Vollblutbestandteilen abhängen. Anzahl und Grad der sCSD sind jedoch nach autologer Blutinfusion häufiger und schwerer als bei einer Substanz mit inertem

Volumen. Das Auftreten von sCSD führt zu einem Läsionswachstum und konsekutiv einem schlechteren neurologischen Outcome. Die Ergebnisse sprechen für eine Überwachung und gezielte Behandlung von sCSD nach intrakraniellen Blutungen.

Hauptaussagen: Zusammenfassend liefern wir Hinweise darauf, dass die Akkumulation von autologem Blut die Wahrscheinlichkeit des Auftretens von sCSD im Ratten-Modell erhöht. sCSDs korrelieren mit einem beeinträchtigten neurologischen Outcome in der An- und Abwesenheit von Blutabbauprodukten. Die Ergebnisse bestätigen sCSDs als wichtigen, aber nicht einzige Faktor der Entstehung des Sekundärschadens nach intrakraniellen Blutungen.

6.5 Cytomegalovirus promotes murine glioblastoma growth via pericyte recruitment and angiogenesis.

Krenzlin H, Behera P, Lorenz V, Passaro C, Zdioruk M, Nowicki MO, Grauwet K, Zhang H, Skubal M, Ito H, Zane R, Gutknecht M, Griessl MB, Ricklefs F, Ding L, Peled S, Rooj A, James CD, Cobbs CS, Cook CH, Chiocca EA, Lawler SE. J Clin Invest. 2019 Mar 11;129(4):1671-1683. doi: 10.1172/JCI123375. eCollection 2019 Mar 11. PMID: 30855281

Hintergrund: Das Glioblastom (GBM) ist der häufigste bösartige Hirntumor mit etwa 10.000 Neuerkrankungen pro Jahr. Intrakranielle Blutungen treten bei Patienten mit primären Hirntumoren wie dem Glioblastom gehäuft auf, auch wenn keine Antikoagulation vorliegt.[115] Während der Tumorangiogenese kommt es zum aussprossen von Endothelzellen, gefolgt von eine Perizytenmigration. Die Gefäßarchitektur erreicht jedoch keine vollständige Reifung, was zu mehreren strukturellen und funktionellen Anomalien wie einer starken Desorganisation, unregelmäßig geformten und undichten Gefäßen führt.[116] Diese Form der Tumorangiogenese mit konsekutiven Einblutungen läßt sich auch beim Glioblastom nachvollziehen. Ziel der Arbeit war die Untersuchung der Auswirkung des Cytomegalievirus (CMV) auf die Tumorangiogenese durch Beeinflussung tumorassozierter Perizyten und deren Bedeutung für den Krankheitsverlauf im Mausmodell zu untersuchen.

Methoden: Mittels Transwell-Migration Assays wurde der Einfluss einer Infektion von Tumorstammzellen und Zellen der perivaskulären Nische auf die Migration von Endothelzellen untersucht. Mittels Matrigel Assay konnten die Auswirkungen der von CMV infizierten Zellen sezernierten pro-angiogenetischen Faktoren auf Ihr Potential zur Induktion einer Neoangiogenese untersucht werden. Die *in vitro* gewonnen Erkenntnisse wurden im Glioblastom-Mausmodell bei CMV infizierten Mäusen überprüft. Veränderungen auf der Ebene des Transkriptoms wurden mittels RNA Sequenzierung identifiziert und im Folgenden durch knock-down mittels CRISPR/cas9 Genomeditierung verifiziert.

Ergebnisse: Zur Beantwortung der Fragen wurden zunächst ein neues, syngenes Glioblastom-Mausmodell, in perinatal mit CMV infizierten Mäusen, etabliert. In diesem Modell konnte ein schnelleres Tumorwachstum und kürzeres Gesamtüberleben in Abhängigkeit einer latenten CMV Infektion nachgewiesen werden (P <0,001). Als eine

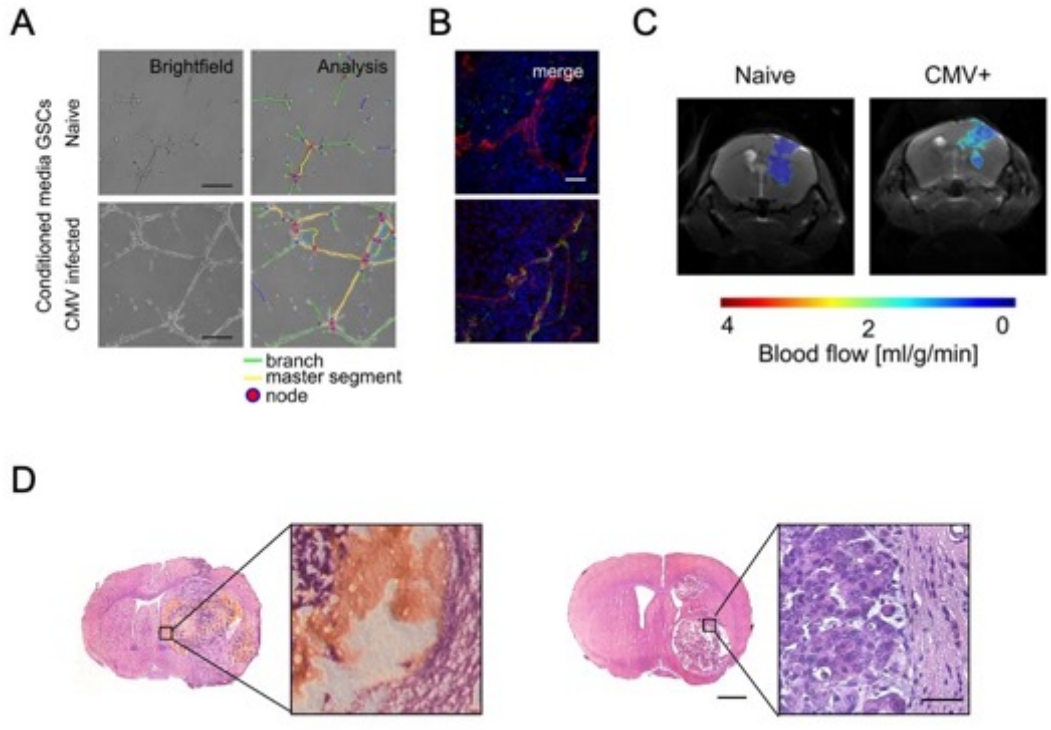

Abb.5 Tumorbedingte Veränderungen der Geffäßarchitektur führt zum Auftreten intrazerebraler Blutungen beim Glioblastom (A) Die Infektion mit CMV führt zur Freisetzung von Zytokinen und dadurch zu einer Steigerung der Angiogenese im Matri-Gel Assay *in vitro*. **(B)** Tumorgefäße in CMV postiven Mäusen mit Glioblastom zeigen eine höhre Gefäßreife und besatz mit perivaskulären Perizyten. **(C)** Hierdurch kommt es zu einer Steigerung des CBF und Tumordurchblutung in vivo. **(D)** Unreife Gefäße und ein Mangel an die Gefäße umgebende Perizyten führt zu einer Zunahme tumorassozierter Blutungen (linkes Bild).

Ursache konnten Veränderungen in der Tumorangiogenese identifiziert werden. Bei CMV positiven Tieren fand sich ein deutlich reifere Gefäßarchitektur mit einer Vielzahl perivasculärer Periyten, einem höheren intratumoralen Blutfluss, weniger thrombotischen Verschlüssen und einer Verringerung intratumoraler Einblutungen. Mittels RNAseq konnte erstmals der platelet-derived growth factor-D (PDGF-D, „Wachstumsfaktor aus Thrombozyten“) als ein führender Mechanismus hinter der CMV vermittelten Angiogenese und Ausreifung der Gefäßarchitektur identifiziert werden. Durch den knock-down von PDGF-D mittels CRISPR/cas9 kam es zu einem Rückgang der Angiogenese *in vitro* und *in vivo.* In der Abwesenheit von PDGF-D fand sich eine deutlich unreifere Tumorgefäßarchitektur mit
weniger pervaskulären Perizyten und eine Zunahme assoziierter Einblutung. Weiterhin kam es zu einem Rückgang des Tumorwachstums und Verlängerung des mittleren Überlebens.

Diskussion: Die in der vorliegenden Arbeit gewonnenen Erkenntnisse ermöglichen ein besseres Verständnis des Tumorwachstuns und gewähren Einblicke in die Bedeutung der Gefäßarchitektur und Bedeutung von Perizyten für die Entstehung von intrazerebralen Blutungen. Es konnte gezeigt werden, dass es durch Perizyten zu einer Veränderung des zerebralen Blutflusses und Verbesserung der Perfusion kommt. In Gefäßen mit niedrigem Besatz an Perizyten kommt es stärkt zum Auftreten von thrombotischen Ereignissen und Einblutungen kommt. Es ist anzunehmen das Perizyten einer ähnlichen Funktion auch im perihämatomalen Gewebe wahrnehmen und hier zur Blutungsexpansion oder der sekundären Rekrutierung nicht betroffenen Gewebes in das Schadensareal um ICB beeinflussen.

Hauptaussagen:
Im beschriebenen Tumormodell fanden wir Hinweise, dass ein Verlust perivaskulärer Perizyten zu einer Zunahme unreifer Tumorgefäße, einem verminderten Blutfluss und einer höheren Rate intratumoraler Einblutungen führt. Beim Glioblastom wird dieser Umstand durch den Einfluss des Cytomegalievirus über die Signaltransduktion mittels PDGF-D kompensiert und bewirkt so eine onkomodulatorische Wirkung auf das Tumorwachstum.

7 Fazit

Im Rahmen intrakranieller Blutungen kommt es zu zeitlich versetzt ablaufenden Mechanismen, welche summativ den entstehenden Schaden bedingen. Es lassen sich grob solche der primären Schadensentstehung und solche, welche nach der eigentlichen Blutung, zur Entwicklung des sekundären Schadens beitragen, unterscheiden. Zugrundeliegende Faktoren wie eine unreife oder abnorme Gefäßarchitektur, das Vorliegen einer Mikroangiopathie, eine Blutgerinnungsstörung sowie durch Ischämie oder Tumor veränderten Gewebes begünstigen das Auftreten von Blutungen und prägen den entstehenden Primärschaden mit. Im Rahmen der Blutung kommt es dann zunächst zu einer Unterbrechung des Gewebeverbandes und damit verbundenen Zerreißung von Zellstrukturen. Durch den Austritt und extravasale Akkumulation von Blut kommt es, entsprechend der Monro-Kelly Doktrin zunächst zu einer Kompensation durch Verdrängung intrakranieller Kompartimente und, nach dem Aufbrauchen des Kompensationsraumes, zu einem exponentiellen Anstieg des ICP. Hierdurch kommt es zu einem Abfall der Perfusion, verbunden mit Ischämie und der Schädigung von weiterem, initial nicht geschädigtem Gewebe- dem Übergang zur Entstehung des sekundären Blutungsschadens. Durch die mechanischen Veränderungen von Druck und Perfusion, dem Auftreten von Abbauprodukten der Blutbestandteile und des Gerinnungssystems, einer eintretenden Entzündungsreaktion und Aktivierung verschiedener Systeme zum Schutz und Rekonstitution, kommt es zu Formation und Konsolidierung des Sekundärschadens.

Die in dieser Schrift vorgelegten Originalarbeiten beschäftigen sich mit den unterschiedlichen Voraussetzungen und Mechanismen, die den Prozessen der Schadensentstehung nach intrakranieller und insbesondere intrazerebraler Blutung zugrunde liegen. Es konnte gezeigt werden, dass die Gefäßarchitektur und Komposition der perivaskulären Nische das Auftreten einer ICB begünstigt und direkte Auswirkung auf den zerebralen Blutfluss und die Perfusion nimmt. Darüber hinaus konnte die Bedeutung eines intakten Gerinnungssystems für die Therapie und das klinische Outcome nach ICB gegenüber der Indikation zur Antikoagulation bei Patienten mit VAD gezeigt werden. Es scheint naheliegend, dass dieses Prinzip auch auf andere Situationen, in denen eine ICB unter Antikoagulation auftritt, erweitert werden kann. Ein Bestandteil des Gerinnungssystems, Thrombin, konnte in Abhängigkeit von seiner Konzentration im Liquor als negativer Prädiktor einer guten

Erholung nach ICB identifiziert werden. Des Weiteren konnte ein bisher nicht publizierter Faktor, die Aktivierung einer zerebralen Thrombinexpression neuronaler Strukturen im perihämatomalen Gewebe und dessen Einfluss auf die Entstehung der sekundären Hirnschädigung im Mausmodel nachgewiesen werden. Abschließend konnten die Erkenntnisse der COSBID Study Group über das Auftreten und Auswirkungen sCSD in Folge von Blutbestandteilen auf die Entstehung des Schadens in einem ASDH Modell bei Ratten untersucht werden. Diese Erkenntnisse sind universell, da Form und Folgen der sCSD unabhängig der zugrundeliegenden Erkrankung zu einer Potenzierung des initialen Schadens führen.

8 Abkürzungsverzeichnis

AD	Anoxische Depolarisation
ASDH	Akutes Subduralhämatom
ATACH	Antihypertensive Treatment of Acute Cerebral Hemorrhage
BBB	Bluthirnschranke (blood brain barrier)
CAA	Zerebrale Amyloidangiopathie
CBF	Zerebraler Blutfluss
CHANT	Cerebral Hemorrhage and NXY-059 Treatment
CLEAR III	Clot Lysis Evaluation of Accelerated Resolution
CMV	Cytomegalievirus
COSBID	Co-Operative Study on Brain Injury Depolarizations
CPP	Zerebraler Perfusionsdruck
CRISPR	Clustered Regularly Interspaced Short Palindromic Repeats
CSD	Cortical Spreading Depolarization
EEG	Elektroencephalogramm
ELISA	Enzyme-linked Immunosorbent Assay
FAST	fVIIa for Acute Hemorrhagic Stroke Treatment
FFP	Fresh-Frozen Plasma
FII	Prothrombin
FIIa	Thrombin
GCS	Glasgow Coma Scale
GFAP	Saures Glia-Protein
GOSE	Glasgow Outcome Scale
IBA1	Calcium-bindendes Adaptermolekül 1
ICB	Intrazerebrale Blutungen
ICP	Intracranial pressure
IMP	Gewebeimpedanz
INR	International normalized ratio
INTERACT	Intensive Blood Pressure Reduction in Acute Cerebral Haemorrhage
m-RNA	Messenger Ribonucleic Acid
MAPK	Mitogen-Activated Kinase
MISTIE	Minimal Invasive Surgery Plus rt-PA for Intracerebral Hemorrhage Evacuation

mRS	Modified Rankin Scale
NMDA	N-Methyl-D-Aspartat
NOAKs	Neue orale Antikoagulanzien
oAK	Oraler Antikoagulation
PARs	Protease-Activated Receptors
PDGF	Platelet-derived growth factor
PPSB	Prothrombinkomplex
ROS	Reaktiver Sauerstoffspezies
SOD	Superoxiddismutase
STICH	Surgical Trial in Intracerebral Haemorrhage
SWITCH	Swiss Trial of Decompressive Craniectomy versus Best Medical Treatment of Spontaneous Supratentorial Intracerebral Hemorrhage)
TAT	Thrombin-Antithrombin-Komplex
TNF-a	Tumornekrosefaktor alpha
VAD	Ventricular assist devices
VEGF	Vascular Endothelial Growth Factor

Literaturverzeichnis

1 Abdu, E., Hanley, D. F. & Newell, D. W. Minimally invasive treatment for intracerebral hemorrhage. *Neurosurg Focus* **32**, E3, doi:10.3171/2012.1.FOCUS11362 (2012).

2 Qureshi, A. I., Mendelow, A. D. & Hanley, D. F. Intracerebral haemorrhage. *Lancet* **373**, 1632-1644, doi:10.1016/S0140-6736(09)60371-8 (2009).

3 Qureshi, A. I. *et al.* Changes in cost and outcome among US patients with stroke hospitalized in 1990 to 1991 and those hospitalized in 2000 to 2001. *Stroke* **38**, 2180-2184, doi:10.1161/STROKEAHA.106.467506 (2007).

4 Feigin, V. L., Lawes, C. M., Bennett, D. A. & Anderson, C. S. Stroke epidemiology: a review of population-based studies of incidence, prevalence, and case-fatality in the late 20th century. *Lancet Neurol* **2**, 43-53, doi:10.1016/s1474-4422(03)00266-7 (2003).

5 van Asch, C. J. *et al.* Incidence, case fatality, and functional outcome of intracerebral haemorrhage over time, according to age, sex, and ethnic origin: a systematic review and meta-analysis. *Lancet Neurol* **9**, 167-176, doi:10.1016/S1474-4422(09)70340-0 (2010).

6 Weimar, C. *et al.* Management patterns and health care use after intracerebral hemorrhage. a cost-of-illness study from a societal perspective in Germany. *Cerebrovasc Dis* **15**, 29-36, doi:10.1159/000067119 (2003).

7 Dennis, M. S. Outcome after brain haemorrhage. *Cerebrovasc Dis* **16 Suppl 1**, 9-13, doi:10.1159/000069935 (2003).

8 Flaherty, M. L. *et al.* Long-term mortality after intracerebral hemorrhage. *Neurology* **66**, 1182-1186, doi:10.1212/01.wnl.0000208400.08722.7c (2006).

9 Steiner, T., Rosand, J. & Diringer, M. Intracerebral hemorrhage associated with oral anticoagulant therapy: current practices and unresolved questions. *Stroke* **37**, 256-262, doi:10.1161/01.STR.0000196989.09900.f8 (2006).

10 Qureshi, A. I. *et al.* Spontaneous intracerebral hemorrhage. *N Engl J Med* **344**, 1450-1460, doi:10.1056/NEJM200105103441907 (2001).

11 Takebayashi, S. & Kaneko, M. Electron microscopic studies of ruptured arteries in hypertensive intracerebral hemorrhage. *Stroke* **14**, 28-36, doi:10.1161/01.str.14.1.28 (1983).

12 Rosand, J., Hylek, E. M., O'Donnell, H. C. & Greenberg, S. M. Warfarin-associated hemorrhage and cerebral amyloid angiopathy: a genetic and pathologic study. *Neurology* **55**, 947-951, doi:10.1212/wnl.55.7.947 (2000).

13 Rost, N. S., Greenberg, S. M. & Rosand, J. The genetic architecture of intracerebral hemorrhage. *Stroke* **39**, 2166-2173, doi:10.1161/STROKEAHA.107.501650 (2008).

14 Rost, N. S. Clinical neurogenetics: stroke. *Neurol Clin* **31**, 915-928, doi:10.1016/j.ncl.2013.05.001 (2013).

15 Hart, R. G. What causes intracerebral hemorrhage during warfarin therapy? *Neurology* **55**, 907-908, doi:10.1212/wnl.55.7.907 (2000).

16 Davis, S. M. *et al.* Hematoma growth is a determinant of mortality and poor outcome after intracerebral hemorrhage. *Neurology* **66**, 1175-1181, doi:10.1212/01.wnl.0000208408.98482.99 (2006).

17 Gebel, J. M., Jr. *et al.* Natural history of perihematomal edema in patients with hyperacute spontaneous intracerebral hemorrhage. *Stroke* **33**, 2631-2635, doi:10.1161/01.str.0000035284.12699.84 (2002).

18 Inaji, M. *et al.* Chronological changes of perihematomal edema of human intracerebral hematoma. *Acta Neurochir Suppl* **86**, 445-448, doi:10.1007/978-3-7091-0651-8_91 (2003).
19 Butcher, K. S. *et al.* Perihematomal edema in primary intracerebral hemorrhage is plasma derived. *Stroke* **35**, 1879-1885, doi:10.1161/01.STR.0000131807.54742.1a (2004).
20 Gebel, J. M., Jr. *et al.* Relative edema volume is a predictor of outcome in patients with hyperacute spontaneous intracerebral hemorrhage. *Stroke* **33**, 2636-2641, doi:10.1161/01.str.0000035283.34109.ea (2002).
21 Qureshi, A. I., Hanel, R. A., Kirmani, J. F., Yahia, A. M. & Hopkins, L. N. Cerebral blood flow changes associated with intracerebral hemorrhage. *Neurosurg Clin N Am* **13**, 355-370, doi:10.1016/s1042-3680(02)00012-8 (2002).
22 Siddique, M. S. *et al.* Reversible ischemia around intracerebral hemorrhage: a single-photon emission computerized tomography study. *J Neurosurg* **96**, 736-741, doi:10.3171/jns.2002.96.4.0736 (2002).
23 Kim-Han, J. S., Kopp, S. J., Dugan, L. L. & Diringer, M. N. Perihematomal mitochondrial dysfunction after intracerebral hemorrhage. *Stroke* **37**, 2457-2462, doi:10.1161/01.STR.0000240674.99945.4e (2006).
24 Schellinger, P. D. *et al.* Stroke MRI in intracerebral hemorrhage: is there a perihemorrhagic penumbra? *Stroke* **34**, 1674-1679, doi:10.1161/01.STR.0000076010.10696.55 (2003).
25 Zazulia, A. R. *et al.* Hypoperfusion without ischemia surrounding acute intracerebral hemorrhage. *J Cereb Blood Flow Metab* **21**, 804-810, doi:10.1097/00004647-200107000-00005 (2001).
26 Qureshi, A. I. *et al.* Extracellular glutamate and other amino acids in experimental intracerebral hemorrhage: an in vivo microdialysis study. *Crit Care Med* **31**, 1482-1489, doi:10.1097/01.CCM.0000063047.63862.99 (2003).
27 Lusardi, T. A., Wolf, J. A., Putt, M. E., Smith, D. H. & Meaney, D. F. Effect of acute calcium influx after mechanical stretch injury in vitro on the viability of hippocampal neurons. *J Neurotrauma* **21**, 61-72, doi:10.1089/089771504772695959 (2004).
28 Graham, D. I., McIntosh, T. K., Maxwell, W. L. & Nicoll, J. A. Recent advances in neurotrauma. *J Neuropathol Exp Neurol* **59**, 641-651, doi:10.1093/jnen/59.8.641 (2000).
29 Qureshi, A. I. *et al.* Apoptosis as a form of cell death in intracerebral hemorrhage. *Neurosurgery* **52**, 1041-1047; discussion 1047-1048 (2003).
30 Brott, T. *et al.* Early hemorrhage growth in patients with intracerebral hemorrhage. *Stroke* **28**, 1-5, doi:10.1161/01.str.28.1.1 (1997).
31 Burchell, S. R., Tang, J. & Zhang, J. H. Hematoma Expansion Following Intracerebral Hemorrhage: Mechanisms Targeting the Coagulation Cascade and Platelet Activation. *Curr Drug Targets* **18**, 1329-1344, doi:10.2174/1389450118666170329152305 (2017).
32 Takahashi, H., Urano, T., Nagai, N., Takada, Y. & Takada, A. Progressive expansion of hypertensive intracerebral hemorrhage by coagulopathy. *Am J Hematol* **59**, 110-114, doi:10.1002/(sici)1096-8652(199810)59:2<110::aid-ajh2>3.0.co;2-0 (1998).
33 Mayer, S. A. *et al.* Recombinant activated factor VII for acute intracerebral hemorrhage. *N Engl J Med* **352**, 777-785, doi:10.1056/NEJMoa042991 (2005).
34 Mayer, S. A. & Rincon, F. Treatment of intracerebral haemorrhage. *Lancet Neurol* **4**, 662-672, doi:10.1016/S1474-4422(05)70195-2 (2005).

35 Gong, Y. *et al.* Increase in brain thrombin activity after experimental intracerebral hemorrhage. *Acta Neurochir Suppl* **105**, 47-50, doi:10.1007/978-3-211-09469-3_10 (2008).
36 Hua, Y., Keep, R. F., Gu, Y. & Xi, G. Thrombin and brain recovery after intracerebral hemorrhage. *Stroke* **40**, S88-89, doi:10.1161/STROKEAHA.108.533281 (2009).
37 Garton, T., Keep, R. F., Hua, Y. & Xi, G. Brain iron overload following intracranial haemorrhage. *Stroke Vasc Neurol* **1**, 172-184, doi:10.1136/svn-2016-000042 (2016).
38 Xi, G., Keep, R. F. & Hoff, J. T. Mechanisms of brain injury after intracerebral haemorrhage. *Lancet Neurol* **5**, 53-63, doi:10.1016/S1474-4422(05)70283-0 (2006).
39 Nakamura, T. *et al.* Holo-transferrin and thrombin can interact to cause brain damage. *Stroke* **36**, 348-352, doi:10.1161/01.STR.0000153044.60858.1b (2005).
40 Wagner, K. R. *et al.* Protein oxidation and heme oxygenase-1 induction in porcine white matter following intracerebral infusions of whole blood or plasma. *Dev Neurosci* **24**, 154-160, doi:10.1159/000065703 (2002).
41 Dihanich, M., Kaser, M., Reinhard, E., Cunningham, D. & Monard, D. Prothrombin mRNA is expressed by cells of the nervous system. *Neuron* **6**, 575-581, doi:10.1016/0896-6273(91)90060-d (1991).
42 Weinstein, J. R., Gold, S. J., Cunningham, D. D. & Gall, C. M. Cellular localization of thrombin receptor mRNA in rat brain: expression by mesencephalic dopaminergic neurons and codistribution with prothrombin mRNA. *J Neurosci* **15**, 2906-2919 (1995).
43 Deschepper, C. F., Bigornia, V., Berens, M. E. & Lapointe, M. C. Production of thrombin and antithrombin III by brain and astroglial cell cultures. *Brain Res Mol Brain Res* **11**, 355-358, doi:10.1016/0169-328x(91)90045-y (1991).
44 Debeir, T., Gueugnon, J., Vige, X. & Benavides, J. Transduction mechanisms involved in thrombin receptor-induced nerve growth factor secretion and cell division in primary cultures of astrocytes. *Journal of neurochemistry* **66**, 2320-2328 (1996).
45 Coughlin, S. R. Thrombin signalling and protease-activated receptors. *Nature* **407**, 258-264, doi:10.1038/35025229 (2000).
46 Wang, H. & Reiser, G. Thrombin signaling in the brain: the role of protease-activated receptors. *Biological chemistry* **384**, 193-202, doi:10.1515/bc.2003.021 (2003).
47 Yang, S. *et al.* Effects of thrombin on neurogenesis after intracerebral hemorrhage. *Stroke* **39**, 2079-2084, doi:10.1161/strokeaha.107.508911 (2008).
48 Xi, G., Reiser, G. & Keep, R. F. The role of thrombin and thrombin receptors in ischemic, hemorrhagic and traumatic brain injury: deleterious or protective? *Journal of neurochemistry* **84**, 3-9 (2003).
49 Abbott, N. J. Astrocyte-endothelial interactions and blood-brain barrier permeability. *Journal of anatomy* **200**, 629-638 (2002).
50 Keep, R. F. *et al.* Blood-brain barrier function in intracerebral hemorrhage. *Acta Neurochir Suppl* **105**, 73-77 (2008).
51 Babu, R., Bagley, J. H., Di, C., Friedman, A. H. & Adamson, C. Thrombin and hemin as central factors in the mechanisms of intracerebral hemorrhage-induced secondary brain injury and as potential targets for intervention. *Neurosurg Focus* **32**, E8, doi:10.3171/2012.1.focus11366 (2012).
52 Hanley, D. F. Intraventricular hemorrhage: severity factor and treatment target in spontaneous intracerebral hemorrhage. *Stroke* **40**, 1533-1538, doi:10.1161/STROKEAHA.108.535419 (2009).

53 Hallevi, H. *et al.* Inflammatory response to intraventricular hemorrhage: time course, magnitude and effect of t-PA. *J Neurol Sci* **315**, 93-95, doi:10.1016/j.jns.2011.11.019 (2012).
54 Wasserman, J. K., Zhu, X. & Schlichter, L. C. Evolution of the inflammatory response in the brain following intracerebral hemorrhage and effects of delayed minocycline treatment. *Brain Res* **1180**, 140-154, doi:10.1016/j.brainres.2007.08.058 (2007).
55 Fam, M. D. *et al.* CSF inflammatory response after intraventricular hemorrhage. *Neurology* **89**, 1553-1560, doi:10.1212/WNL.0000000000004493 (2017).
56 Hanley, D. F. *et al.* Thrombolytic removal of intraventricular haemorrhage in treatment of severe stroke: results of the randomised, multicentre, multiregion, placebo-controlled CLEAR III trial. *Lancet* **389**, 603-611, doi:10.1016/S0140-6736(16)32410-2 (2017).
57 Leao, A. A. Further observations on the spreading depression of activity in the cerebral cortex. *J Neurophysiol* **10**, 409-414, doi:10.1152/jn.1947.10.6.409 (1947).
58 Kraig, R. P. & Nicholson, C. Extracellular ionic variations during spreading depression. *Neuroscience* **3**, 1045-1059, doi:10.1016/0306-4522(78)90122-7 (1978).
59 Mutch, W. A. & Hansen, A. J. Extracellular pH changes during spreading depression and cerebral ischemia: mechanisms of brain pH regulation. *J Cereb Blood Flow Metab* **4**, 17-27, doi:10.1038/jcbfm.1984.3 (1984).
60 Fabricius, M., Jensen, L. H. & Lauritzen, M. Microdialysis of interstitial amino acids during spreading depression and anoxic depolarization in rat neocortex. *Brain Res* **612**, 61-69, doi:10.1016/0006-8993(93)91644-8 (1993).
61 Lauritzen, M. *et al.* Clinical relevance of cortical spreading depression in neurological disorders: migraine, malignant stroke, subarachnoid and intracranial hemorrhage, and traumatic brain injury. *J Cereb Blood Flow Metab* **31**, 17-35, doi:10.1038/jcbfm.2010.191 (2011).
62 Koide, M., Sukhotinsky, I., Ayata, C. & Wellman, G. C. Subarachnoid hemorrhage, spreading depolarizations and impaired neurovascular coupling. *Stroke Res Treat* **2013**, 819340, doi:10.1155/2013/819340 (2013).
63 Orakcioglu, B. *et al.* Evidence of spreading depolarizations in a porcine cortical intracerebral hemorrhage model. *Acta Neurochir Suppl* **114**, 369-372, doi:10.1007/978-3-7091-0956-4_71 (2012).
64 Shepro, D. & Morel, N. M. Pericyte physiology. *FASEB J* **7**, 1031-1038, doi:10.1096/fasebj.7.11.8370472 (1993).
65 Armulik, A. *et al.* Pericytes regulate the blood-brain barrier. *Nature* **468**, 557-561, doi:10.1038/nature09522 (2010).
66 Gautam, J. & Yao, Y. Roles of Pericytes in Stroke Pathogenesis. *Cell Transplant* **27**, 1798-1808, doi:10.1177/0963689718768455 (2018).
67 Hellstrom, M. *et al.* Lack of pericytes leads to endothelial hyperplasia and abnormal vascular morphogenesis. *J Cell Biol* **153**, 543-553, doi:10.1083/jcb.153.3.543 (2001).
68 Lindahl, P., Johansson, B. R., Leveen, P. & Betsholtz, C. Pericyte loss and microaneurysm formation in PDGF-B-deficient mice. *Science* **277**, 242-245, doi:10.1126/science.277.5323.242 (1997).
69 Ballabh, P. Pathogenesis and prevention of intraventricular hemorrhage. *Clin Perinatol* **41**, 47-67, doi:10.1016/j.clp.2013.09.007 (2014).

70 Chen, Y., Li, Q., Tang, J., Feng, H. & Zhang, J. H. The evolving roles of pericyte in early brain injury after subarachnoid hemorrhage. *Brain Res* **1623**, 110-122, doi:10.1016/j.brainres.2015.05.004 (2015).
71 Arnold, T. D. *et al.* Excessive vascular sprouting underlies cerebral hemorrhage in mice lacking alphaVbeta8-TGFbeta signaling in the brain. *Development* **141**, 4489-4499, doi:10.1242/dev.107193 (2014).
72 Li, Q., Liu, X., Ruan, H., Chen, Y. & Feng, H. Pericyte: Potential Target for Hemorrhagic Stroke Prevention and Treatment. *Curr Drug Deliv* **14**, 773-784, doi:10.2174/1567201813666160829103222 (2017).
73 Cheng, S. Y., Nagane, M., Huang, H. S. & Cavenee, W. K. Intracerebral tumor-associated hemorrhage caused by overexpression of the vascular endothelial growth factor isoforms VEGF121 and VEGF165 but not VEGF189. *Proc Natl Acad Sci U S A* **94**, 12081-12087, doi:10.1073/pnas.94.22.12081 (1997).
74 Greenberg, J. I. *et al.* A role for VEGF as a negative regulator of pericyte function and vessel maturation. *Nature* **456**, 809-813, doi:10.1038/nature07424 (2008).
75 Hall, C. N. *et al.* Capillary pericytes regulate cerebral blood flow in health and disease. *Nature* **508**, 55-60, doi:10.1038/nature13165 (2014).
76 Zurasky, J. A., Aiyagari, V., Zazulia, A. R., Shackelford, A. & Diringer, M. N. Early mortality following spontaneous intracerebral hemorrhage. *Neurology* **64**, 725-727, doi:10.1212/01.WNL.0000152045.56837.58 (2005).
77 Diringer, M. N. & Edwards, D. F. Admission to a neurologic/neurosurgical intensive care unit is associated with reduced mortality rate after intracerebral hemorrhage. *Crit Care Med* **29**, 635-640, doi:10.1097/00003246-200103000-00031 (2001).
78 Qureshi, A. I. *et al.* A prospective multicenter study to evaluate the feasibility and safety of aggressive antihypertensive treatment in patients with acute intracerebral hemorrhage. *J Intensive Care Med* **20**, 34-42, doi:10.1177/0885066604271619 (2005).
79 Anderson, C. S. *et al.* Intensive blood pressure reduction in acute cerebral haemorrhage trial (INTERACT): a randomised pilot trial. *Lancet Neurol* **7**, 391-399, doi:10.1016/S1474-4422(08)70069-3 (2008).
80 Qureshi, A. I. Antihypertensive Treatment of Acute Cerebral Hemorrhage (ATACH): rationale and design. *Neurocrit Care* **6**, 56-66, doi:10.1385/ncc:6:1:56 (2007).
81 Sjoblom, L. *et al.* Management and prognostic features of intracerebral hemorrhage during anticoagulant therapy: a Swedish multicenter study. *Stroke* **32**, 2567-2574, doi:10.1161/hs1101.098523 (2001).
82 Goldstein, J. N. *et al.* Timing of fresh frozen plasma administration and rapid correction of coagulopathy in warfarin-related intracerebral hemorrhage. *Stroke* **37**, 151-155, doi:10.1161/01.STR.0000195047.21562.23 (2006).
83 Roitberg, B., Emechebe-Kennedy, O., Amin-Hanjani, S., Mucksavage, J. & Tesoro, E. Human recombinant factor VII for emergency reversal of coagulopathy in neurosurgical patients: a retrospective comparative study. *Neurosurgery* **57**, 832-836; discussion 832-836, doi:10.1227/01.neu.0000180816.80626.c2 (2005).
84 Mayer, S. A. *et al.* Can a subset of intracerebral hemorrhage patients benefit from hemostatic therapy with recombinant activated factor VII? *Stroke* **40**, 833-840, doi:10.1161/STROKEAHA.108.524470 (2009).
85 Konkle, B. A. Monitoring target-specific oral anticoagulants. *Hematology Am Soc Hematol Educ Program* **2014**, 329-333, doi:10.1182/asheducation-2014.1.329 (2014).

86 Pollack, C. V., Jr. *et al.* Idarucizumab for Dabigatran Reversal - Full Cohort Analysis. *N Engl J Med* **377**, 431-441, doi:10.1056/NEJMoa1707278 (2017).
87 Siegal, D. M. *et al.* Andexanet Alfa for the Reversal of Factor Xa Inhibitor Activity. *N Engl J Med* **373**, 2413-2424, doi:10.1056/NEJMoa1510991 (2015).
88 Naidech, A. M. *et al.* Reduced platelet activity is associated with early clot growth and worse 3-month outcome after intracerebral hemorrhage. *Stroke* **40**, 2398-2401, doi:10.1161/STROKEAHA.109.550939 (2009).
89 Naidech, A. M. *et al.* Platelet activity and outcome after intracerebral hemorrhage. *Ann Neurol* **65**, 352-356, doi:10.1002/ana.21618 (2009).
90 Sansing, L. H. *et al.* Prior antiplatelet use does not affect hemorrhage growth or outcome after ICH. *Neurology* **72**, 1397-1402, doi:10.1212/01.wnl.0000342709.31341.88 (2009).
91 Steiner, T. *et al.* European Stroke Organisation (ESO) guidelines for the management of spontaneous intracerebral hemorrhage. *Int J Stroke* **9**, 840-855, doi:10.1111/ijs.12309 (2014).
92 Steiner, T., Al-Shahi Salman, R. & Ntaios, G. The European Stroke Organisation (ESO) guidelines. *Int J Stroke* **9**, 838-839, doi:10.1111/ijs.12369 (2014).
93 Wakai, A., McCabe, A., Roberts, I. & Schierhout, G. Mannitol for acute traumatic brain injury. *Cochrane Database Syst Rev*, CD001049, doi:10.1002/14651858.CD001049.pub5 (2013).
94 Stocchetti, N. *et al.* Refractory intracranial hypertension and "second-tier" therapies in traumatic brain injury. *Intensive Care Med* **34**, 461-467, doi:10.1007/s00134-007-0948-9 (2008).
95 Mendelow, A. D. *et al.* Early surgery versus initial conservative treatment in patients with spontaneous supratentorial intracerebral haematomas in the International Surgical Trial in Intracerebral Haemorrhage (STICH): a randomised trial. *Lancet* **365**, 387-397, doi:10.1016/S0140-6736(05)17826-X (2005).
96 Mendelow, A. D. *et al.* Early surgery versus initial conservative treatment in patients with spontaneous supratentorial lobar intracerebral haematomas (STICH II): a randomised trial. *Lancet* **382**, 397-408, doi:10.1016/S0140-6736(13)60986-1 (2013).
97 Wijdicks, E. F., St Louis, E. K., Atkinson, J. D. & Li, H. Clinician's biases toward surgery in cerebellar hematomas: an analysis of decision-making in 94 patients. *Cerebrovasc Dis* **10**, 93-96, doi:10.1159/000016036 (2000).
98 St Louis, E. K., Wijdicks, E. F. & Li, H. Predicting neurologic deterioration in patients with cerebellar hematomas. *Neurology* **51**, 1364-1369, doi:10.1212/wnl.51.5.1364 (1998).
99 Firsching, R., Huber, M. & Frowein, R. A. Cerebellar haemorrhage: management and prognosis. *Neurosurg Rev* **14**, 191-194, doi:10.1007/BF00310656 (1991).
100 Da Pian, R., Bazzan, A. & Pasqualin, A. Surgical versus medical treatment of spontaneous posterior fossa haematomas: a cooperative study on 205 cases. *Neurol Res* **6**, 145-151, doi:10.1080/01616412.1984.11739680 (1984).
101 Takeuchi, S., Wada, K., Nagatani, K., Otani, N. & Mori, K. Decompressive hemicraniectomy for spontaneous intracerebral hemorrhage. *Neurosurg Focus* **34**, E5, doi:10.3171/2013.2.FOCUS12424 (2013).
102 Fung, C. *et al.* Decompressive hemicraniectomy in patients with supratentorial intracerebral hemorrhage. *Stroke* **43**, 3207-3211, doi:10.1161/STROKEAHA.112.666537 (2012).
103 Hayes, S. B., Benveniste, R. J., Morcos, J. J., Aziz-Sultan, M. A. & Elhammady, M. S. Retrospective comparison of craniotomy and decompressive craniectomy for

surgical evacuation of nontraumatic, supratentorial intracerebral hemorrhage. *Neurosurg Focus* **34**, E3, doi:10.3171/2013.2.FOCUS12422 (2013).

104 Keric, N., Neulen, A., Kantelhardt, S. R. & Giese, A. Image-guided implantation of pre-calibrated catheters in the ICU: a feasibility study. *Acta Neurochir (Wien)* **155**, 1781-1786, doi:10.1007/s00701-013-1789-7 (2013).

105 Keric, N. *et al.* Optimization of Catheter Based rtPA Thrombolysis in a Novel In Vitro Clot Model for Intracerebral Hemorrhage. *Biomed Res Int* **2017**, 5472936, doi:10.1155/2017/5472936 (2017).

106 Masomi-Bornwassser, J. *et al.* Effect of irrigation on fibrinolytic rtPA therapy in a clot model of intracerebral haemorrhage: a systematic in vitro study. *Acta Neurochir (Wien)* **160**, 1159-1165, doi:10.1007/s00701-018-3517-9 (2018).

107 Masomi-Bornwasser, J. *et al.* Combination of ultrasound and rtPA enhances fibrinolysis in an In Vitro clot system. *PLoS One* **12**, e0188131, doi:10.1371/journal.pone.0188131 (2017).

108 Auer, L. M. *et al.* Endoscopic surgery versus medical treatment for spontaneous intracerebral hematoma: a randomized study. *J Neurosurg* **70**, 530-535, doi:10.3171/jns.1989.70.4.0530 (1989).

109 Schaller, C., Rohde, V., Meyer, B. & Hassler, W. Stereotactic puncture and lysis of spontaneous intracerebral hemorrhage using recombinant tissue-plasminogen activator. *Neurosurgery* **36**, 328-333; discussion 333-325, doi:10.1227/00006123-199502000-00012 (1995).

110 Mould, W. A. *et al.* Minimally invasive surgery plus recombinant tissue-type plasminogen activator for intracerebral hemorrhage evacuation decreases perihematomal edema. *Stroke* **44**, 627-634, doi:10.1161/STROKEAHA.111.000411 (2013).

111 Hanley, D. F. *et al.* Efficacy and safety of minimally invasive surgery with thrombolysis in intracerebral haemorrhage evacuation (MISTIE III): a randomised, controlled, open-label, blinded endpoint phase 3 trial. *Lancet* **393**, 1021-1032, doi:10.1016/S0140-6736(19)30195-3 (2019).

112 Keric, N. *et al.* Comparative analysis of fibrinolytic properties of Alteplase, Tenecteplase and Urokinase in an in vitro clot model of intracerebral haemorrhage. *J Stroke Cerebrovasc Dis* **29**, 105073, doi:10.1016/j.jstrokecerebrovasdis.2020.105073 (2020).

113 Kuramatsu, J. B. & Huttner, H. B. Management of oral anticoagulation after intracerebral hemorrhage. *Int J Stroke* **14**, 238-246, doi:10.1177/1747493019828555 (2019).

114 Ray, B. & Keyrouz, S. G. Management of anticoagulant-related intracranial hemorrhage: an evidence-based review. *Crit Care* **18**, 223, doi:10.1186/cc13889 (2014).

115 Mantia, C. *et al.* Predicting the higher rate of intracranial hemorrhage in glioma patients receiving therapeutic enoxaparin. *Blood* **129**, 3379-3385, doi:10.1182/blood-2017-02-767285 (2017).

116 Klionsky, D. J. *et al.* Guidelines for the use and interpretation of assays for monitoring autophagy (3rd edition). *Autophagy* **12**, 1-222, doi:10.1080/15548627.2015.1100356 (2016).

JOURNAL OF NEUROTRAUMA 37: 1481–1490 (June 15, 2020)

DOI: 10.1089/neu.2019.6582

The Cerebral Thrombin System Is Activated after Intracerebral Hemorrhage and Contributes to Secondary Lesion Growth and Poor Neurological Outcome in C57Bl/6 Mice

Harald Krenzlin,[1,2,*] Eva Gresser,[1,*] Daniel Jussen,[1,3] Nicole Riede,[1] Louise Taylor,[1] Christina Francisca Vogelaar,[4] Florian Ringel,[1,2] Oliver Kempski,[1] and Beat Alessandri[1]

Abstract

With increasing evidence for the existence of a cerebral thrombin system, coagulation factor IIa (thrombin) is suspected to influence the pathogenesis of secondary injury progression after intracerebral hemorrhage (ICH). We hypothesized that mechanisms associated with local volume expansion after ICH, rather than blood constituents, activate the cerebral thrombin system and are responsible for detrimental neurological outcome. To test this hypothesis, we examine the local thrombin expression after ICH in a C57BL/6N mouse model in the presence and absence of blood constituents. ICH was established using stereotaxic orthotopic injection of utologous blood ($n = 10$) or silicone oil as inert volume substance ($n = 10$) into the striatum. Intracranial pressure (ICP), cerebral blood flow (CBF), and mean arterial blood pressure (MAP) were monitored during and 30 min after the procedure. No significant differences between ICP, CBF, and MAP were found between both groups. Prothrombin messenger RNA expression was upregulated early after ICH. Immunohistochemistry showed an increase of perilesional thrombin in both groups (blood, 4.24-fold; silicone, 3.10-fold), whereas prothrombin fragment (F1.2) was elevated only in the absence of whole blood. Thrombin expression is colocalized with neuronal antigen expression. After 24 h, lesion size and neuronal loss were similar. Perihematomal thrombin correlated with increased neuronal loss and detrimental neurological outcome *in vivo*. In our study, we demonstrate, for the first time, that the local cerebral thrombin system is activated after ICH and that this activation is independent of the presence of whole-blood constituents. In our study, neuronal damage is driven by local thrombin expression and leads to an adverse clinical outcome.

Keywords: cerebral thrombin system; intracranial hemorrhage; secondary injury; thrombin

Introduction

Intracerebral hemorrhage (ICH) is a devastating form of stroke associated with considerable early mortality and long-term morbidity. ICH accounts for approximately 15% of all deaths from stroke.[1] Detailed knowledge about pathophysiology is still elusive, limiting therapy to mostly symptomatic treatments. An increasing number of studies indicate a key modulatory role of thrombin in traumatic brain injury (TBI) as well as ischemic and hemorrhagic stroke.[2]

The trypsin-like allosteric serine protease, thrombin, is one of the major actors within the coagulation cascade. It is derived from its inactive precursor, prothrombin, by proteolytic cleavage through the prothrombinase complex.[3] In the coagulation cascade, thrombin converts fibrinogen to fibrin, the main constituent of a blot clot. Further, thrombin acts as a polyfunctional signaling molecule binding to several substrates with a broad structural diversity.[4] Thus, generation of thrombin leads to receptor-mediated inflammatory responses, cell proliferation/modulation, cell protection, and apoptosis.[5,6] The majority of prothrombin is produced in the liver and in the bloodstream until it is converted into mature thrombin.[7] Because of its large, spherical shape, it is unable to pass the blood–brain barrier (BBB).[8] In cases of a BBB breakdown (e.g., during TBI, severe epilepsy, inflammation, and other pathological conditions), (pro-)thrombin enters the brain and reaches high concentrations.[8,9]

[1]Institute of Neurosurgical Pathophysiology, [2]Department of Neurosurgery, and [4]Department of Neurology, Johannes Gutenberg–University Mainz, Mainz, Germany.
[3]Department of Neurosurgery, HELIOS Dr. Horst-Schmidt-Kliniken, Wiesbaden, Germany.
*These authors contributed equally.

Yet, thrombin and thrombin associated factors, such as FX, protease nexin-1 (PN-1), AT III, and thrombin-activated receptors, have been demonstrated throughout the central nervous system (CNS) of rat and human specimens under various patho- and physiological conditions.[10] Local expression of prothrombin in neurons and glial cells might be the primary source of brain-derived thrombin and could, together with its activators and inhibitors, indicate an important role within the CNS.[10–13]

Lately, increasing evidence of protective and harmful thrombin effects in conditions such as stroke and hemorrhage became evident. When administered at pico- to nanomolar ranges (10 pM to 10 nM), thrombin was shown to be protective against a variety of cellular insults, such as glucose deprivation (oxygen-glucose deprivation), hypoglycemia, and reactive oxygen species.[14,15] Intracerebral thrombin administration (thrombin pre-conditioning) before the occurrence of intracerebral hemorrhage leads to edema reduction.[16] The instillation of thrombin in approximate 10-fold high concentrations (100 nM to 10 μM) increases neuronal death after ischemia and causes cellular damage *de novo* and tumor necrosis factor alpha (TNF-α) upregulation, with a consecutive increase of brain edema and neurological deficits in mice.[2,17] Release of proinflammatory factors (e.g., TNF-α and nitric oxide) contributes to neurodegeneration, neuroinflammation, and an increase of brain edema.[18,19]

These deleterious effects of thrombin are mediated by protease-activated receptor-1 (PAR-1) and matrix metalloproteinase-9 activation.[20] Activation of PAR-1 induces the mitogen-activated protein kinase pathway, thus leading to astrogliosis and glial scar formation impairing regeneration after ischemia and ICH.[21–24]

We hypothesized that effects associated with local volume expansion after ICH, not blood constituents, activate the cerebral thrombin system. We speculated that local thrombin expression, rather than influx of systemic thombin, is responsible for secondary injury and detrimental neurological outcome. To test this hypothesis, we examined local thrombin expression after ICH in a C57BL/6N mouse model in the presence and absence of blood-derived thrombin. In this study, silicone oil was used as inert volume substance to replace whole blood and thus circumvent thrombin influx and altercation by blood constituents. We generated a stereotaxic ICH mouse model and inoculated either autologous blood or silicone oil. Sham-operated animals were used as a control. Intracranial pressure (ICP), cerebral blood flow (CBF), and mean arterial blood pressure (MAP) were monitored continually during some operations. Lesion size and localization were examined using hematoxylin/eosin staining in frozen sections. We performed immunohistochemistry (IHC) to analyze prothrombin and thrombin expression. Neuronal damage, astrocyte, and microglia attraction were measured in both lesion groups and compared to sham-operated animals.

Methods

Experimental design

To investigate the occurrence and influence of ICH on the local cerebral thrombin system, either 30 μL of autologous blood or silicone oil was injected into the striatum of 20 C57Bl/6N mice (Charles River, Sulzfeld, Germany). Silicone oil is a man-made synthetic substance composed of repeating units of siloxane. Silicone oil has long been used in experimental settings and as a tamponade in vitreoretinal surgery given that it is supposed to be chemically inert.[25] It was assumed that silicone oil acts as a chemically inert substance, thus mimicking the properties of whole blood and avoiding the bias of blood constituents.[25] In the sham group, 7 mice received needle insertion only. Monitoring of physiological parameters, intracranial pressure (ICP), and CBF was performed on additional mice (5 blood, 5 silicone oil, and 2 sham), starting with the application of blood or silicone oil respectively and continued for 30 min. All animals were then returned into their housing for 24 h. Ultimately, all animals were euthanized and the lesion size histologically analyzed. For quantitative reverse-transcriptase polymerase chain reaction (qRT-PCR) analysis, 6 mice were injected with either blood or silicone oil and euthanized 4 h after injection.

Animal care and anesthesia

All experimental animal procedures were planned and performed according to the German guidelines for animal use and care and approved by the local ethics committee. A total of 45 male wild-type C57BL/6N mice (Charles River), weighing 25–28 g, were used in this study. All animals were housed at room temperature of 22 ± 2°C and humidity >50%. Mice were anesthetized with medetomidine (0.5 mg/kg), tramadol (350 mg/kg), and midazolam (5 mg/kg) by intraperitoneal injection in a body-weight–adapted dosage. Body temperature was closely kept at 37.5°C throughout the operation using a heating pad (Homeothermic Blanket Unit, Harvard, UK).

Intracranial hemorrhage

All procedures were performed using sterile techniques. Animals were fixed in a stereotaxic frame (David Kopf Instruments, Tujunga, CA). Blood pressure measurement was established using a CODA Monitor (Kent Scientific Corporation, Torrington, CT). The tail vein was cannulated for withdrawal of blood in animals subjected to autologous blood injection. The skull was exposed through a midline incision. A 1-mm burr-hole craniotomy for striatal blood injection was performed using a high-speed drill (Aesculap/B. Braun, Melsungen, Germany) on the left frontal bone (1 mm anterior to bregma and 2 mm lateral to sagittal suture). For ICP monitoring, a minicraniotomy of 1 × 1 mm was made on the right parietal bone and a pressure probe (Raumedic, Helmbrechts, Germany) was placed epidurally. CBF measurement was performed using a laser Doppler probe placed on the ipsilateral hemisphere posterior to the burr hole (Laserflo BPM2; Vasamedics, St. Paul, MN).

Briefly, intracranial hemorrhage was established using a two-step model. A blunt 26G cannula (Becton, Dickinson and Company, Franklin Lakes, NJ) was inserted to a depth of 3 mm from dural level. In a first step, 5 μL of autologous blood or silicone oil was injected using a syringe pump (KD Scientific Inc., Holliston, MA) at 10 μL/min. The needle was then advanced to 4-mm depth and a further 25 μL was injected. To allow for proper clotting, the needle was left in place for either 10 min or for the time of monitoring. After injection, the needle was removed, the burr hole sealed using tissue glue (Histoacryl; B. Braun), and the scalp was sutured. All animals were left to recover and then returned to regular housing for 24 h under continued analgesia. Sham-operated animals were handled identically, but received no intracerebral infusion.

Primary neuronal cultures

Dissociated cortical neurons were prepared as previously described.[26] Briefly, the cerebral cortex of E17 C57Bl6 embryos was digested with trypsin/ethylenediaminetetraacetic acid solution (Gibco, Grand Island, NY), containing 1% DNase (Roche, Basel, Switzerland), for 30 min at 37°C. After trituration, 106 cells were plated in poly-D-lysine–coated (0.5 mg/m; Sigma-Aldrich, St.

Louis, MO) six-well plates or 24-well plates with glass cover-slips. Cells were cultivated for 7 days in neurobasal medium (Gibco).

Quantitative reverse-transcriptase polymerase chain reaction

Total RNA was extracted using TRIzol and treated with RNase-free DNase (QIAGEN, Hilden, Germany). Messenger RNA (mRNA) expression analysis was carried out using Power SYBR Green (Applied Biosystems, Foster City, CA). RNA concentration was quantified using a Nanodrop RNA 6000 (Thermo Fisher Scientific, Waltham, MA) and analyzed using the Applied Biosystems StepOnePlus PCR machine (Thermo Fisher Scientific). Primer sequences were as follows: 18s-forward %'- GTAACCCGTT GAACCCCATT-3', 18s-reverse 5'- CCATCCAATCGGTAGTA GCG-3'; Prothrombin-forward 5'-CTGGGAGTTCTGGGCAAC TA-3', Prothrombin-reverse 5'- ACCTAAGCAGGCCATTAA CCC-3'.

Histological evaluation

Mice were kept under deep anesthesia and euthanized using atlantooccipital dislocation. Brains were removed and snap frozen using methyl butane (isopentane) cooled to −72°C. Coronal sections (6 μm) were cut throughout the visible lesion and stained with hematoxylin and eosin (H&E) to visualize lesion localization and composure. Staining for prothrombin (anti-prothrombin fragment 1+2, PAA710Ra01, dilution 1:500; Cloud-Clone Corp, Houston, TX), thrombin (anti-thrombin, cat. no. sc-23335, dilution 1:500; Santa Cruz Biotechnology, Santa Cruz, CA), protease-activated receptor-1 (PAR-1; anti-PAR-1, cat. no. 251324, dilution 1:500; Abbiotec LLC, San Diego, CA), neuronal nuclear antigen (anti-NeuN [neuronal nuclei], cat. no. 702022, dilution 1:500; Thermo Fisher Scientific), glial fibrillary acidic protein (GFAP; marker of astrocytes; anti-GFAP, cat. no. 556330, dilution 1:500; BD Biosciences), and ionized calcium-binding adapter molecule 1 (Iba-1; marker of microglia/macrophages; anti-Iba-1, cat. no. 019-19741, dilution 1:500; Wako Chemicals USA, Inc., Richmond, VA) were visualized using avidin-biotin-peroxidase complex (Vector VIP peroxidase substrate kit, cat. no. SK-4600; Vector Laboratories, Burlingame, CA) or matching secondary immunofluorescence antibodies.

Tissue injury was analyzed by staining and counting NeuN-positive neurons and expressed as a percent of the contralateral (uninjected) side. The average of three to four comparable regions of interest (ROIs; each 0.11×0.22 mm) on three adjacent slides in an increasing distance from the site of injury was calculated. ROI 1 was placed directly adjacent to the blot or silicone oil clot. Staining within each ROI was quantified using Optimas analyzing software (Optimas 6.51; VSG; Fig. 1).

Neurological examination

Deficits caused by ICH result from disruption of complex motor pathways and sensorimotor integration and thus can be assessed using sensorimotor function tests such as the Rotarod, grip strength, beam walk, and beam balance tests. Sensory and motor integrity were tested using a neuroscore by evaluating motor activity, orientation, and reaction to tactile, visual, and auditory stimuli. Neurological and behavioral testing was performed in a quiet room in dim light starting 24 h before and repeated daily until 5 days after ICH.

Statistical analysis

Data are expressed as mean ± standard error of the mean. Comparison of different groups was performed using the one-way analysis oif variance or the Kruskal-Wallis one-way variance on ranks with an $\alpha = 0.05$ (Sigma-Plot 11.0; Systat Software, Inc., San Jose, CA). Subgroup analysis with autologous blood and silicone oil injection was performed using the post-hoc Mann–Whitney U test. Differences were considered statistically significant at $p < 0.05$.

Results

Neuromonitoring in the acute phase during and after intracerebral hemorrhage

To characterize our model of ICH in mice, 12 C57BL/6J mice (blood, $n = 5$, silicone oil, $n = 5$; sham operation, $n = 2$) were subjected to multi-modal monitoring during and after the procedure. ICP, CBF, and MAP were chosen as standard monitoring parameters. ICP increased during ICH induction with peak values of 54.0 ± 10 mm Hg in the blood and 40.8 ± 9 mm Hg in the silicone group at the end of the injection ($p = 0.34$). In both groups, ICP normalized within 30 min. Inversely, CBF dropped to 32.0% ± 8.1% of baseline in blood and 37.6% ± 10.3% of baseline in silicone-oil–injected animals. CBF partially recovered after the end of the injection, but remained low throughout the monitoring period (no statistical significance between blood and silicone oil). MAP increased reflexively during the injection period (Cushing reflex; data not shown). No statistically significant disparities were detected between ICP, MAP, and CBF measurements of blood and silicone oil groups (Fig. 2).

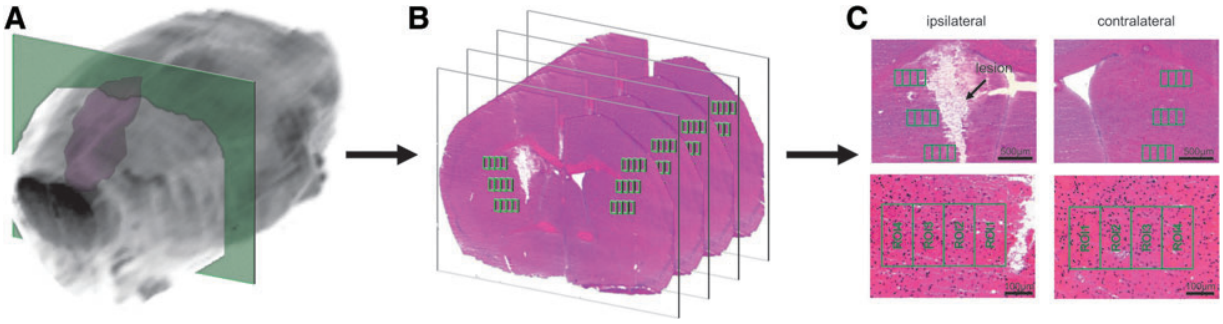

FIG. 1. (**A**) 3D-volume rendering of a mouse brain after intracranial hemorrhage induction (hematoma depicted in red). (**B** and **C**) Tissue injury was analyzed by calculating the average of three comparable ROIs with a similar distance from the site of injury (ROI, 0.11×0.22 mm) on three adjacent slides. Multiple sites with increasing distance from the lesion were compared. Staining within each ROI was quantified using Optimas analyzing software (Optimas 6.51; VSG, Northampton, UK). 3D, three-dimensional; ROI, region of interest. Color image is available online.

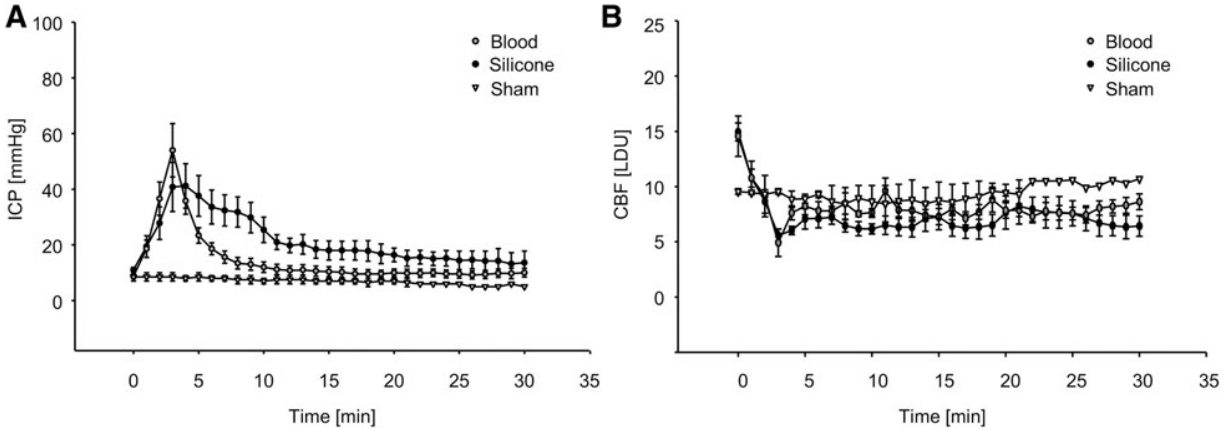

FIG. 2. Measurement of ICP and CBF during ICH induction. ICP and CBF were recorded from the beginning of the intracerebral injection of 30 μL of autologous blood or the same amount of silicon oil and continued for 30 min ($n = 12$/group). (**A**) ICP showed no differences in peak values between both groups ($p = 0.34$), but recovered slower in those animals injected with silicon oil. (**B**) CBF dropped to 32.0% ± 8.1% of baseline in blood and 37.6% ± 10.3% of baseline in silicon-oil–injected animals. No statistically significant difference was detected in both groups. ICP and CBF returned to baseline within 30 min. CBF, cerebral blood flow; ICH, intracerebral hemmorhage; ICP, intracranial pressure; LDU, laser Doppler units.

Lesion characteristics and neuronal loss after intracerebral hemorrhage

To investigate the effects of intracerebral injection of autologous blood and silicone oil on lesion size, brains were frozen, sectioned, and H&E stained. Reproducible lesions were found within the ipsilateral striatum 24 h after ICH induction (Fig. 2). No significant differences were found between the maximum lesion extension in both groups (cranial-caudal, 2.0 ± 0.4 mm [blood] and 2.3 ± 0.7 mm [silicone]; medial-lateral, 0.7 ± 0.1 mm [blood] and 1.0 ± 0.2m [silicone]; anterior-posterior, 0.7 ± 0.2m [blood] and 0.9 ± 0.4m [silicone]). Neuronal loss was analyzed using NeuN IHC staining as a marker of mature neurons. Adjacent to the lesion, the number of neurons was decreased to 53.96 ± 4.40% ($p = < 0.05$) in blood-injected animals and 61.82 ± 7.39% ($p = 0.02$) in silicone-oil–injected animals. Neuronal loss decreased with growing distance from the injection and normalized in both groups within a radius of 440 μm. Analysis revealed no statistically significant disparities between blood and silicone lesions, whereas both were significantly lower compared to sham-operated animals (blood vs. sham, $p < 0.001$; silicone oil vs. sham, $p = 0.001$; Fig. 3).

Neuronal prothrombin expression in vitro *and* in vivo

To verify whether silicone oil affects neuronal thrombin expression directly or indirectly by the mass effect, we resorted to qPCR analysis of prothrombione mRNA expression. *In vivo*, prothrombin mRNA expression was upregulated 4 h after blood or silicone oil injection in the ipsilateral side compared to contralateral. After 24 h, prothrombin expression was no longer upregulated (Supplementary Fig. S1A). *In vitro*, treatment of murine primary neuronal cells with silicone oil emulsified in neuronal media did not lead to upregulation of prothrombin mRNA at 10 or 30 min after addition of the treatment (Supplementary Fig. S1B).

Perilesional thrombin accumulation after intracerebral hemorrhage

Twenty-four hours after ICH, a significant perilesional increase in thrombin was detected. Animals receiving blood injections

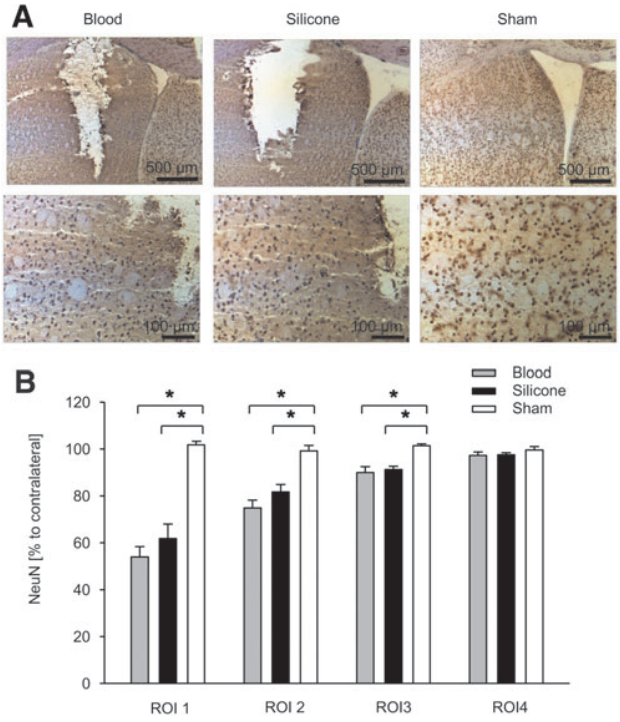

FIG. 3. (**A**) Neuronal loss was analyzed using NeuN IHC staining as marker of mature neurons. (**B**) NeuN-positive cells of three individual ROIs on three consecutive brain sections compared to contralateral. Adjacent to the lesion, the number of neurons was decreased to 53.96 ± 4.40% ($p = < 0.05$) in blood-injected animals and 61.82 ± 7.39 ($p = 0.02$) in silicon-oil–injected animals. Analysis revealed no statistically significant disparities between blood and silicon lesions, whereas both were significantly lower compared to sham-operated animals (blood vs. sham, $p < 0.001$; silicon oil vs. sham, $p = 0.001$). IHC, immunohistochemistry; NeuN, neuronal nuclei; ROI, region of interest. Color image is available online.

showed a 4.24 ± 0.50-fold ($p < 0.05$) increase in perilesional thrombin compared to contralateral and in those receiving silicone oil a 3.10 ± 0.54-fold ($p < 0.05$) increase, respectively. Thrombin decreased in both groups with growing distance from the site of damage toward the periphery and normalized within a distance of 220 μm to levels equal to sham animals. No statistically significant differences were found in subgroup analysis comparing blood to silicone oil ($p = 0.16$; Fig. 4).

Perilesional expression levels of the thrombin ligand receptor (PAR-1) was measured as mean immunoreactivity of three ROIs

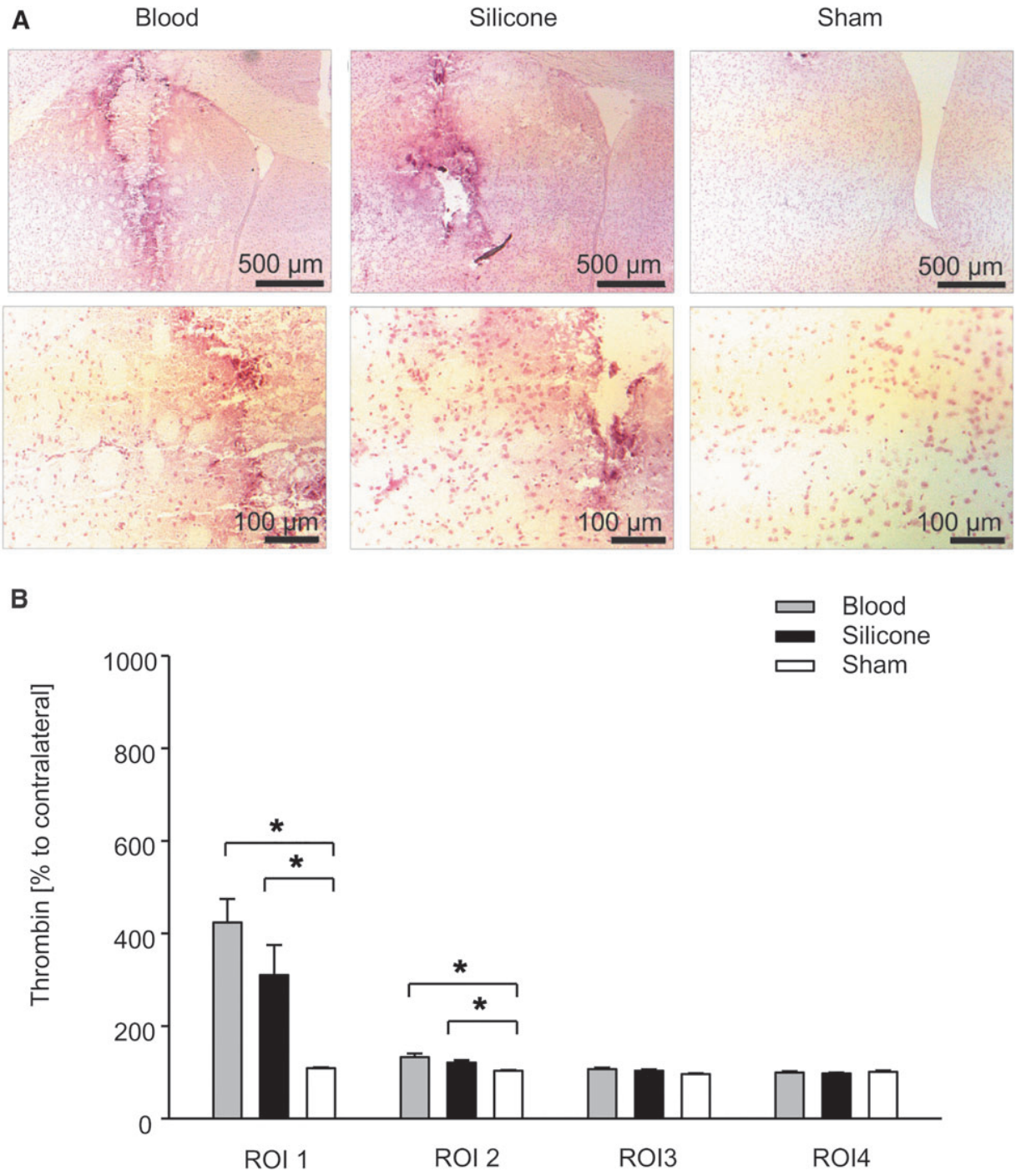

FIG. 4. (**A**) Perilesional thrombin was measured as mean immunoreactivity of three individual ROIs compared to contralateral. (**B**) Twenty-four hours after ICH, animals receiving blood injections showed a 4.24 ± 0.50-fold increase in thrombin (compared to contralateral, $p < 0.05$), whereas those receiving silicon oil showed 3.10 ± 0.54 (compared to contralateral, $p < 0.05$). No statistically significant differences were found in subgroup analysis comparing blood versus silicon oil. ICH, intracerebral hemmorhage; ROI, region of interest. Color image is available online.

compared to contralateral. Twenty-four hours after ICH, no changes in PAR-1 expression levels were observed (Fig. 5).

Perilesional expression of thrombin (ROIs 1 and 2) in both groups positively correlated with a neuronal loss (spearman coefficient, $\rho = -0.679$; $p < 0.001$; Fig. 7).

Perilesional prothrombin expression after intracerebral hemorrhage

Prothrombin was increased 2.07 ± 0.39-fold ($p = 0.02$) in silicone-oil– and 1.37 ± 0.2-fold in blood-injected animals without

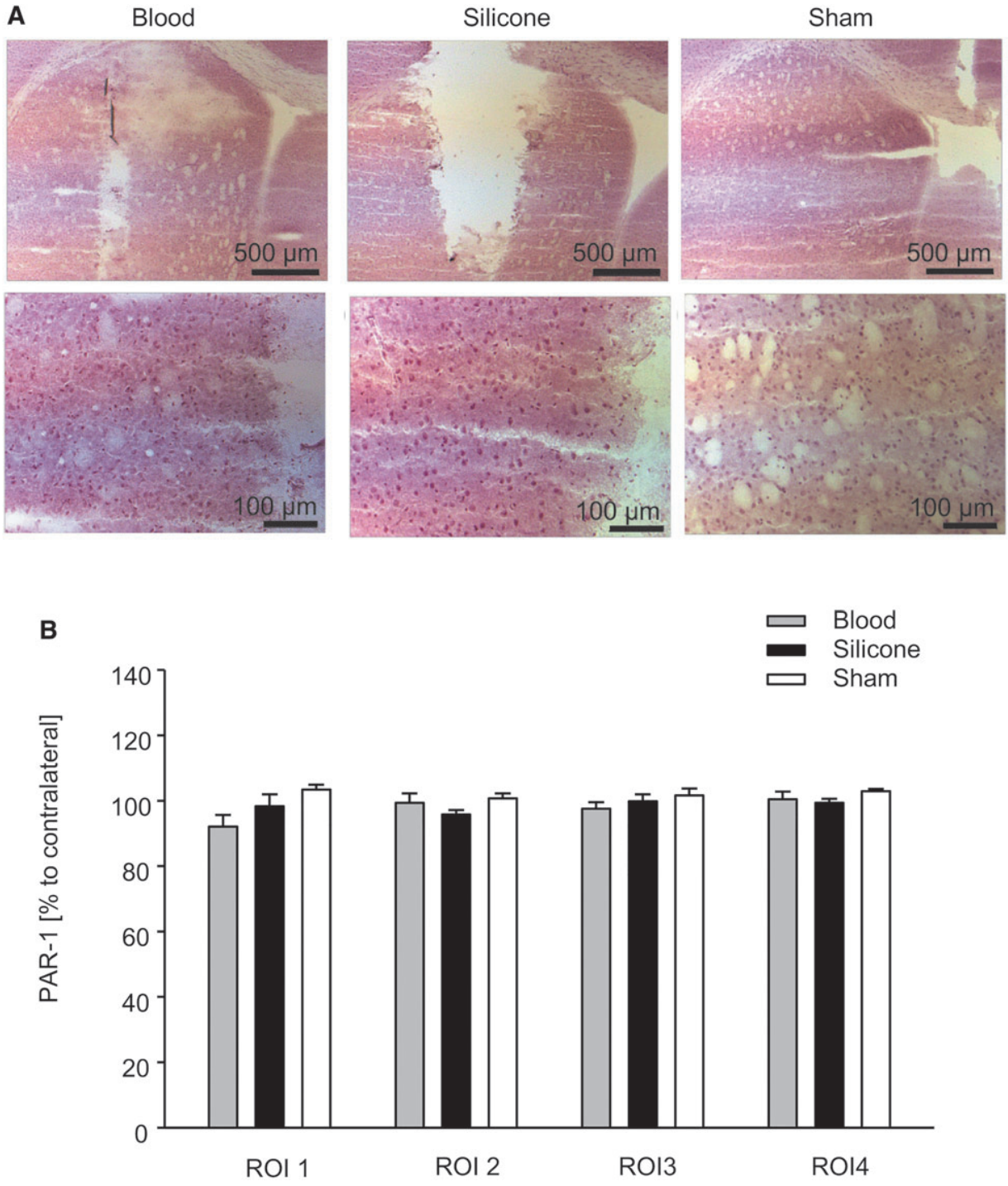

FIG. 5. (**A**) Perilesional expression levels of the thrombin ligand receptor, PAR-1, was measured as mean immunoreactivity of three ROIs compared to contralateral. (**B**) Twenty-four hours after ICH, no changes in PAR-1 expression levels were observed. ICH, intracerebral hemmorhage; PAR-1, protease-activated receptor-1; ROI, region of interest. Color image is available online.

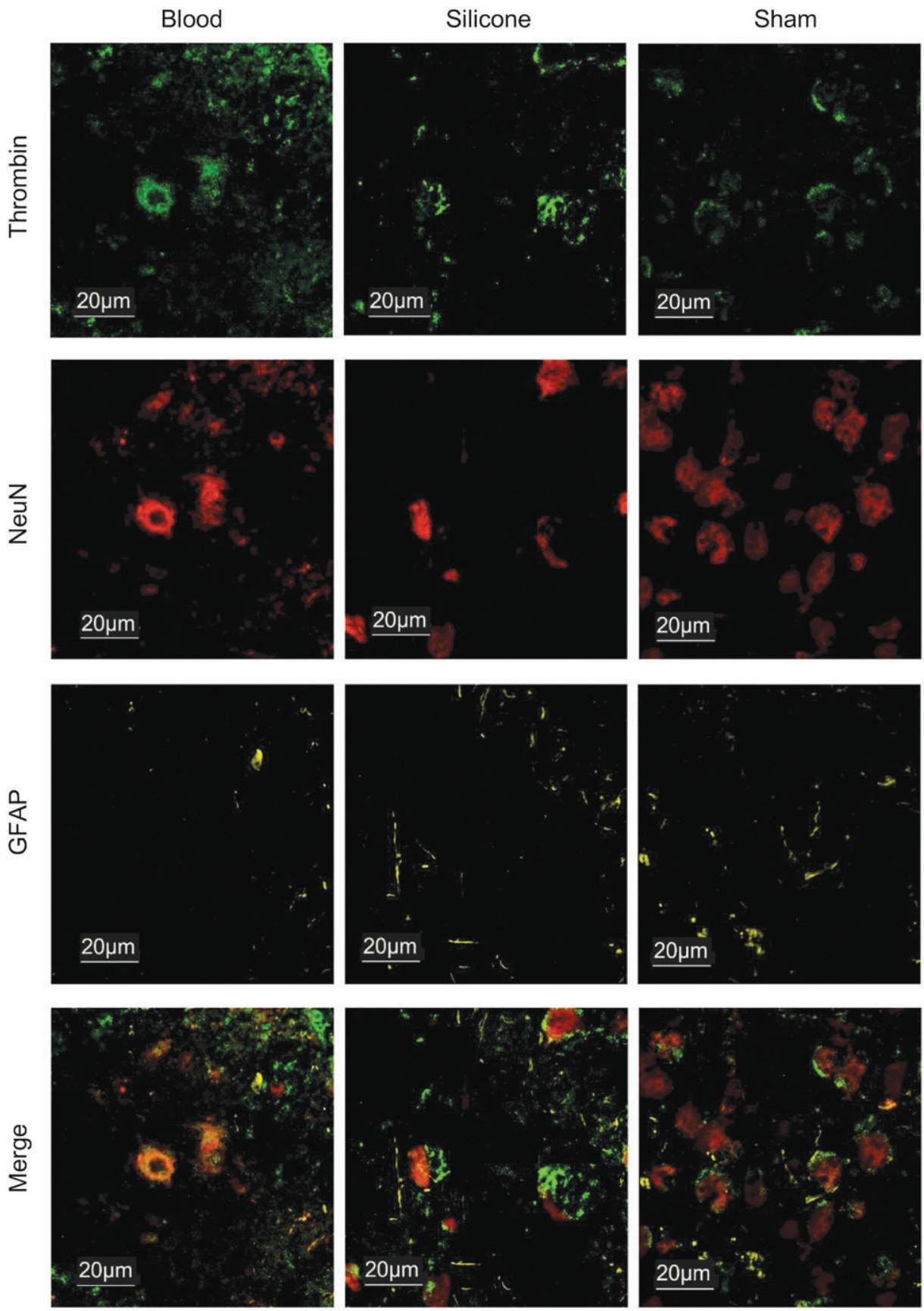

FIG. 6. Immunofluorescence staining of thrombin (anti-thrombin; Alexa Fluor 488), neuronal nuclear antigen (anti-NeuN; Alexa Fluor 594), and GFAP (Alexa Fluor 647; anti-GFAP, dilution 1:500; BD Biosciences, Santa Jose CA). *Thrombin expression colocalizes with NeuN in the vicinity of intracerebral hemorrhage. GFAP, glial fibrillary acidic protein; NeuN, neuronal nuclei. Color image is available online.

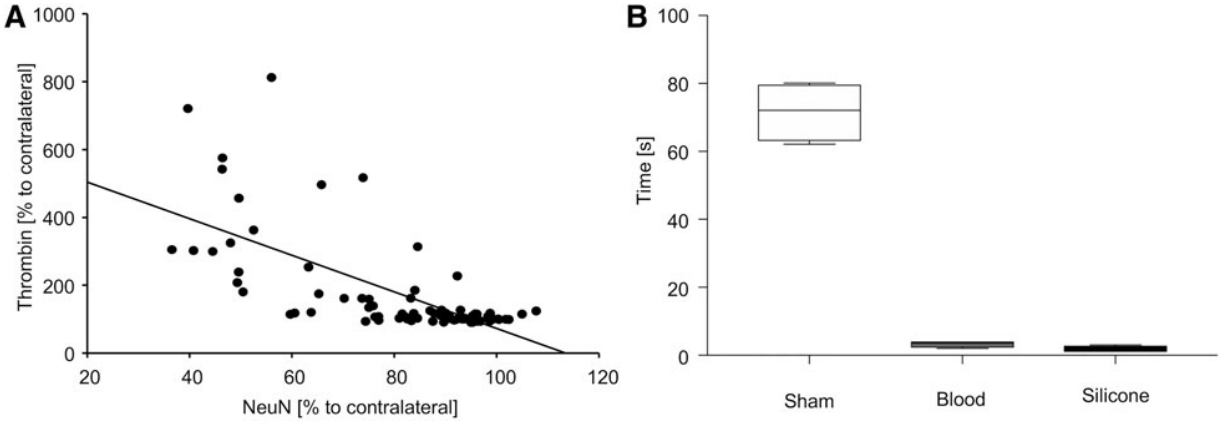

FIG. 7. (**A**) Perilesional expression of thrombin positively correlates with neuronal loss ($r^2 = 0.23$; spearman coefficient, $\rho = -0.679$; $p < 0.001$) and (**B**) diminished rotarod performance ($p < 0.001$). NeuN, neuronal nuclei.

reaching significance in the latter group. Prothrombin levels in both groups were within a 660-μm perimeter around the lesion. In subgroup analysis, no statistically significant differences were found.

Cellular localization of thrombin expression after intracerebral hemorrhage

To differentiate more precisely between local thrombin expression and circulatory influx, immunofluorescence costaining of thrombin and NeuN were performed. A strong colocalization of thrombin and NeuN after blood as well as after silicone oil was observed. Thrombin was predominantly detected in mature neurons and the extracellular matrix, but not in glial cells. No differences were found between blood versus silicone oil.

Inflammatory response 24 h after intracerebral hemorrhage

IHC staining for GFAP and IBA-1 showed no differences between blood or silicone lesions compared to sham lesions. No different regulation in proximity of the lesion was detected in any group (data not shown).

Inter-relation of perilesional thrombin and neurological outcome

Assessment of balance, grip strength, and motor coordination were done using the Rotarod® performance test. The test was performed 24 h after ICH to match histological sections. The biggest differences between all groups were detected 3 days after ICH. Mice receiving blood injection remained for 3.25 ± 0.90 sec, those receiving silicone oil for 1.75 ± 0.90 sec, and sham-operated animals 71.5 ± 8.8 sec. No statistically significant difference was found between blood and silicone animals, whereas both differed from sham controls ($p < 0.0001$; Fig. 7).

Discussion

ICH accounts for 10–15% of all strokes and has a dismal prognosis. Brain damage occurs through primary tissue disruption and secondary detrimental effects of ischemia and accumulation of neurotoxic substances. Despite extensive research efforts, treatment is restricted to symptomatic therapy. Recent studies turned the focus on thrombin acting as modulator in ischemia, TBI, and ICH. Despite the mainly hepatic genesis of prothrombin, smaller amounts are produced within the CNS by neurons and astrocytes.[8] It is hypothesized that thrombin regulates brain maturation, neuron and astrocyte modification, induces glial cell proliferation, and exerts, in low concentrations, a neuroprotective influence in cases of ischemia.[27]

We previously showed that subdural infusion with an inert volume substance (e.g., paraffin oil) resulted in similar alterations of ICP, CBF, and MAP, compared to autologous blood infusion in a subdural hematoma model in rats.[28] Thus, we inferred that similar characteristics apply in our stereotaxic ICH mouse model. In this study, we show that the injection of silicone oil, an inert substance with blood-like fluid characteristics, leads to similar changes in ICP, CBF, and MAP compared to autologous blood.[29] We further investigated the varying effects of an intracranial mass lesion on activation of the cerebral thrombin system in the presence and absence of whole-blood constituents. We provide evidence that local thrombin production is initiated after primary brain damage independently from the influx of whole-blood constituents. Further, neuronal loss was found to be dependent on the amount of thrombin expression.

In our study, thrombin production was initiated by ICH, but did not lead to consecutive increase of astrocytes or microglia. These findings differ from the current literature, where thrombin-induced astrogliosis was mediated by PAR-1 activation.[30] We were able to colocalize cerebral thrombin expression to mature neurons around the initial ICH lesion, whereas systemic thrombin influx accounted for the lesser part of the perilesional thrombin concentration.

The results of the presented study fall in line with previously published data demonstrating the comparability of blood and paraffin oil subdural hematomas in terms of neuromonitoring parameters.[31] Our PubMed research delivered no other study addressing silicone oil as an inert volume substance to mimic ICH. So far, there are only limited data addressing the local cerebral thrombin system. It is still controversially debated whether thrombin is washed in as a result of blood extravasation and BBB breakdown or produced locally.

Whelihan and colleagues demonstrated that red blood cells (RBCs) and platelets both contribute to prothrombin to thrombin conversion.[32] In the absence of whole-blood constituents, prothrombin to thrombin conversion might be delayed, leading to increased thrombin synthesis attributable to a putative activation of the local cerebral thrombin system. Further, prothrombin to thrombin conversion is increased by RBCs and platelets, thus

contributing to prothrombin depletion. It is discussed that continued deterioration of patients suffering from ICH days after the initial insult might be attributed to cytotoxic, excitotoxic, oxidative, and inflammatory effects of intraparenchymal blood.[33]

In our study, we observed similar parenchymal damage 24 h after ICH independent from the presence of blood. Thus, it is speculated that activation of the cerebral thrombin system might be an important contributor for secondary brain damage and should therefore be in the focus of future therapeutic efforts. This hypothesis is further strengthened by variable reports stressing the inter-relation of focal thrombin accumulation and neuronal damage.[34] We found that thrombin was increased 24 h after ICH. Although not statistically significant, those animals with blood lesions seem to have had higher concentrations than those with silicone lesions. These findings did not translate into more elevated neuronal damage by whole blood in our study. Similar results were reported by Gong and colleagues, reporting increased thrombin activity 24 h after ICH in mice. Here, the average amount accumulated to 3.3 U/g, an amount exceeding the assumed neuroprotective levels of 1 U/g and capable of inflicting substantial neuronal damage.[35]

Activation of microglia seems to impose detrimental effects after ischemic stroke and ICH.[36] Microglia/macrophage activation is described upon stereotaxic injection of thrombin (1 U/4 μL 0.9% NaCl) into the striatum of mice.[37] Microglia and astrocyte activation is observed already 4 h after ICH and peaks at day 3. It then wears off until day 7 after autologous blood as well as collagenase injection in murine ICH models.[38] Activation could be ameliorated using anti-inflammatory or -thrombin agents. Mice receiving thrombin injections without therapy showed no motor, but spatial memory impairments 5 days after operation. These deficits were partly reversed under anti-inflammatory or -thrombin therapy.[37] Microglia or astrocyte activation is not essential for thrombin-induced neuronal damage.[34] Besides activation of microglia and macrophages, no influx of these cells in response to thrombin or ICH has been reported so far. Microglia migration and proliferation were reported in response to cerebral microbleeds and began 40 h after occurrence of these bleedings.[39] This falls in line with our observation, given that we observed no increase in GFAP- or IBA-1-positive cells 24 h after ICH.

In summary, intrastriatal injection of either whole blood or silicone oil produced similar neurophysiological alterations detected by neuromonitoring. We showed that silicone oil injection is a suitable replacement in ICH mouse models to analyze ICH pathophysiology in the absence of whole-blood constituents. We demonstrated that the local thrombin system is upregulated after ICH in a blood-independent manner. Neuronal damage in the early stages after ICH correlates with thrombin occurrence and does not coincide with an inflammatory response. In our model, neurological deficits after ICH do not depend on the presence of extravasated blood, but correlate with activation of the cerebral thrombin system. Thus, our findings further substantiate the existence of a cerebral thrombin system and highlight its importance as a future target of targeted ICH treatment efforts.

Acknowledgment

We thank A. Ehlert, F. Kafai, L. Kopacz, and M. Malzahn for their technical and secretarial support during the experiments.

Funding Information

No funding was received for this study.

Author Disclosure Statement

No financial conflicts exist.

References

1. Qureshi, A.I., Mendelow, A.D., and Hanley, D.F. (2009). Intracerebral haemorrhage. Lancet 373, 1632–1644.
2. Xi, G., Reiser, G., and Keep, R.F. (2003). The role of thrombin and thrombin receptors in ischemic, hemorrhagic and traumatic brain injury: deleterious or protective? J. Neurochem. 84, 3–9.
3. Grand, R.J., Turnell, A.S., and Grabham, P.W. (1996). Cellular consequences of thrombin-receptor activation. Biochem. J. 313, Pt. 2, 353–368.
4. Yamada, T., and Nagai, Y. (1996). Immunohistochemical studies of human tissues with antibody to factor Xa. Histochem. J. 28, 73–77.
5. Ossovskaya, V.S., and Bunnett, N.W. (2004). Protease-activated receptors: contribution to physiology and disease. Physiol. Rev. 84, 579–621.
6. Steinhoff, M., Buddenkotte, J., Shpacovitch, V., Rattenholl, A., Moormann, C., Vergnolle, N., Luger, T.A., and Hollenberg, M.D. (2005). Proteinase-activated receptors: transducers of proteinase-mediated signaling in inflammation and immune response. Endocr. Rev. 26, 1–43.
7. Shikamoto, Y., and Morita, T. (1999). Expression of factor X in both the rat brain and cells of the central nervous system. FEBS Lett. 463, 387–389.
8. Dihanich, M., Kaser, M., Reinhard, E., Cunningham, D., and Monard, D. (1991). Prothrombin mRNA is expressed by cells of the nervous system. Neuron 6, 575–581.
9. Sokolova, E., and Reiser, G. (2008). Prothrombin/thrombin and the thrombin receptors PAR-1 and PAR-4 in the brain: localization, expression and participation in neurodegenerative diseases. Thromb. Haemost. 100, 576–581.
10. Deschepper, C.F., Bigornia, V., Berens, M.E., and Lapointe, M.C. (1991). Production of thrombin and antithrombin III by brain and astroglial cell cultures. Brain research. Mol. Brain Res. 11, 355–358.
11. Mansuy, I.M., van der Putten, H., Schmid, P., Meins, M., Botteri, F.M., and Monard, D. (1993). Variable and multiple expression of Protease Nexin-1 during mouse organogenesis and nervous system development. Development 119, 1119–1134.
12. Arai, T., Miklossy, J., Klegeris, A., Guo, J.P., and McGeer, P.L. (2006). Thrombin and prothrombin are expressed by neurons and glial cells and accumulate in neurofibrillary tangles in Alzheimer disease brain. J. Neuropathol. Exp. Neurol. 65, 19–25.
13. Niclou, S.P., Suidan, H.S., Pavlik, A., Vejsada, R., and Monard, D. (1998). Changes in the expression of protease-activated receptor 1 and protease nexin-1 mRNA during rat nervous system development and after nerve lesion. Eur. J. Neurosci. 10, 1590–1607.
14. Striggow, F., Riek, M., Breder, J., Henrich-Noack, P., Reymann, K.G., and Reiser, G. (2000). The protease thrombin is an endogenous mediator of hippocampal neuroprotection against ischemia at low concentrations but causes degeneration at high concentrations. Proc. Natl. Acad. Sci. U. S. A. 97, 2264–2269.
15. Vaughan, P.J., Pike, C.J., Cotman, C.W., and Cunningham, D.D. (1995). Thrombin receptor activation protects neurons and astrocytes from cell death produced by environmental insults. J. Neurosci. 15, 5389–5401.
16. Xi, G., Keep, R.F., Hua, Y., Xiang, J., and Hoff, J.T. (1999). Attenuation of thrombin-induced brain edema by cerebral thrombin preconditioning. Stroke 30, 1247–1255.
17. Wu, X., Zhang, W., Li, J.Y., Chai, B.X., Peng, J., Wang, H., and Mulholland, M.W. (2011). Induction of apoptosis by thrombin in the cultured neurons of dorsal motor nucleus of the vagus. Neurogastroenterol. Motil. 23, 279–285, e123–e274.
18. Coughlin, S.R. and Camerer, E. (2003). PARticipation in inflammation. J. Clin. Invest. 111, 25–27.
19. Hua, Y., Wu, J., Keep, R.F., Nakamura, T., Hoff, J.T., and Xi, G. (2006). Tumor necrosis factor-alpha increases in the brain after intracerebral hemorrhage and thrombin stimulation. Neurosurgery 58, 542–550; discussion, 542–550.
20. Svedin, P., Hagberg, H., Savman, K., Zhu, C., and Mallard, C. (2007). Matrix metalloproteinase-9 gene knock-out protects the immature brain after cerebral hypoxia-ischemia. J. Neurosci. 27, 1511–1518.
21. Wang, H., Ubl, J.J., Stricker, R., and Reiser, G. (2002). Thrombin (PAR-1)-induced proliferation in astrocytes via MAPK involves multiple signaling pathways. Am. J. Physiol. Cell Physiol. 283, C1351–C1364.

22. Wang, Y., Luo, W., and Reiser, G. (2007). Activation of protease-activated receptors in astrocytes evokes a novel neuroprotective pathway through release of chemokines of the growth-regulated oncogene/cytokine-induced neutrophil chemoattractant family. Eur. J. Neurosci. 26, 3159–3168.
23. Nicole, O., Goldshmidt, A., Hamill, C.E., Sorensen, S.D., Sastre, A., Lyuboslavsky, P., Hepler, J.R., McKeon, R.J., and Traynelis, S.F. (2005). Activation of protease-activated receptor-1 triggers astrogliosis after brain injury. J. Neurosci. 25, 4319–4329.
24. Ohnishi, M., Katsuki, H., Fujimoto, S., Takagi, M., Kume, T., and Akaike, A. (2007). Involvement of thrombin and mitogen-activated protein kinase pathways in hemorrhagic brain injury. Exp. Neurol. 206, 43–52.
25. Stappler, T., Morphis, G., Irigoyen, C., and Heimann, H. (2011). Is there a role for long-term silicone oil tamponade for more than twelve months in vitreoretinal surgery? Ophthalmologica 226, Suppl. 1, 36–41.
26. Vogelaar, C.F., Mandal, S., Lerch, S., Birkner, K., Birkenstock, J., Buhler, U., Schnatz, A., Raine, C.S., Bittner, S., Vogt, J., Kipnis, J., Nitsch, R., and Zipp, F. (2018). Fast direct neuronal signaling via the IL-4 receptor as therapeutic target in neuroinflammation. Sci. Transl. Med. 10, eaao2304.
27. Wang, H., and Reiser, G. (2003). Thrombin signaling in the brain: the role of protease-activated receptors. Biol. Chem. 384, 193–202.
28. Jussen, D., Krenzlin, H., Papaioannou, C., Ens, S., Kempski, O., and Alessandri, B. (2017). Blood aggravates histological and functional damage after acute subdural hematoma in rats. J. Neurotrauma 34, 906–913.
29. Jenkins, A., Mendelow, A.D., Graham, D.I., Nath, F.P., and Teasdale, G.M. (1990). Experimental intracerebral haematoma: the role of blood constituents in early ischaemia. Br. J. Neurosurg. 4, 45–51.
30. Radulovic, M., Yoon, H., Wu, J., Mustafa, K., and Scarisbrick, I.A. (2016). Targeting the thrombin receptor modulates inflammation and astrogliosis to improve recovery after spinal cord injury. Neurobiol. Dis. 93, 226–242.
31. Jussen, D., Krenzlin, H., Papaioannou, C., Ens, S., Kempski, O., and Alessandri, B. (2017). Blood aggravates histological and functional damage after acute subdural hematoma in rats. J. Neurotrauma 34, 906–913.
32. Whelihan, M.F., Zachary, V., Orfeo, T., and Mann, K.G. (2012). Prothrombin activation in blood coagulation: the erythrocyte contribution to thrombin generation. Blood 120, 3837–3845.
33. Babu, R., Bagley, J.H., Di, C., Friedman, A.H., and Adamson, C. (2012). Thrombin and hemin as central factors in the mechanisms of intracerebral hemorrhage-induced secondary brain injury and as potential targets for intervention. Neurosurg. Focus 32, E8.
34. Chen, B., Friedman, B., Whitney, M.A., Winkle, J.A., Lei, I.F., Olson, E.S., Cheng, Q., Pereira, B., Zhao, L., Tsien, R.Y., and Lyden, P.D. (2012). Thrombin activity associated with neuronal damage during acute focal ischemia. J. Neurosci. 32, 7622–7631.
35. Gong, Y., Xi, G., Hu, H., Gu, Y., Huang, F., Keep, R.F., and Hua, Y. (2008). Increase in brain thrombin activity after experimental intracerebral hemorrhage. Acta Neurochir. Suppl. 105, 47–50.
36. Taylor, R.A., and Sansing, L.H. (2013). Microglial responses after ischemic stroke and intracerebral hemorrhage. Clin. Dev. Immunol. 2013, 746068.
37. Yang, Y., Zhang, M., Kang, X., Jiang, C., Zhang, H., Wang, P., and Li, J. (2015). Thrombin-induced microglial activation impairs hippocampal neurogenesis and spatial memory ability in mice. Behav. Brain Funct. 11, 30.
38. Barratt, H.E., Lanman, T.A., and Carmichael, S.T. (2014). Mouse intracerebral hemorrhage models produce different degrees of initial and delayed damage, axonal sprouting, and recovery. J. Cerebr. Blood Flow Metab. 34, 1463–1471.
39. Ahn, S.J., Anrather, J., Nishimura, N., and Schaffer, C.B. (2018). Diverse inflammatory response after cerebral microbleeds includes coordinated microglial migration and proliferation. Stroke 49, 1719–1726.

Address correspondonce to:
Harald Krenzlin, MD
Department of Neurosurgery
University Medicine of the Johannes
Gutenberg–University Mainz
Langenbeckstraße 1
55131 Mainz
Germany

E-mail: harald.krenzlin@unimedizin-mainz.de

PLOS ONE

RESEARCH ARTICLE

High CSF thrombin concentration and activity is associated with an unfavorable outcome in patients with intracerebral hemorrhage

Harald Krenzlin[1]*, Christina Frenz[1], Jan Schmitt[1], Julia Masomi-Bornwasser[1], Dominik Wesp[1], Darius Kalasauskas[1], Thomas Kerz[1], Johannes Lotz[2], Beat Alessandri[1], Florian Ringel[1], Naureen Keric[1]

1 Department of Neurosurgery, University Medical Center Mainz, Mainz, Germany, **2** Institute of Clinical Chemistry and Laboratory Medicine, University Medical Center Mainz, Mainz, Germany

* harald.krenzlin@unimedizin-mainz.de

Citation: Krenzlin H, Frenz C, Schmitt J, Masomi-Bornwasser J, Wesp D, Kalasauskas D, et al. (2020) High CSF thrombin concentration and activity is associated with an unfavorable outcome in patients with intracerebral hemorrhage. PLoS ONE 15(11): e0241565. https://doi.org/10.1371/journal.pone.0241565

Editor: Tamil Selvan Anthonymuthu, University of Pittsburgh, UNITED STATES

Received: July 15, 2020

Accepted: October 18, 2020

Published: November 11, 2020

Peer Review History: PLOS recognizes the benefits of transparency in the peer review process; therefore, we enable the publication of all of the content of peer review and author responses alongside final, published articles. The editorial history of this article is available here: https://doi.org/10.1371/journal.pone.0241565

Data Availability Statement: All relevant data are within the paper and its Supporting Information files.

Abstract

Background

The cerebral thrombin system is activated in the early stage after intracerebral hemorrhage (ICH). Expression of thrombin leads to concentration dependent secondary neuronal damage and detrimental neurological outcome. In this study we aimed to investigate the impact of thrombin concentration and activity in the cerebrospinal fluid (CSF) of patients with ICH on clinical outcome.

Methods

Patients presenting with space-occupying lobar supratentorial hemorrhage requiring extraventricular drainage (EVD) were included in our study. The CSF levels of thrombin, its precursor prothrombin and the Thrombin-Antithrombin complex (TAT) were measured using enzyme linked immune sorbent assays (ELISA). The oxidative stress marker Superoxide dismutase (SOD) was assessed in CSF. Initial clot size and intraventricular hemorrhage (IVH) volume was calculated based on by computerized tomography (CT) upon admission to our hospital. Demographic data, clinical status at admission and neurological outcome were assessed using the modified Rankin Scale (mRS) at 6-weeks and 6-month after ICH.

Results

Twenty-two consecutive patients (9 females, 11 males) with supratentorial hemorrhage were included in this study. CSF concentrations of prothrombin ($p < 0.005$), thrombin ($p = 0.005$) and TAT ($p = 0.046$) were statistical significantly different in patients with ICH compared to non-hemorrhagic CSF samples. CSF concentrations of thrombin 24h after ICH correlated with the mRS index after 6 weeks ($r^2 = 0.73$; < 0.005) and 6 months ($r^2 = 0.63$; < 0.005) after discharge from hospital. Thrombin activity, measured via TAT as surrogate parameter of coagulation, likewise correlated with the mRS at 6 weeks ($r^2 = 0.54$; < 0.01) and 6 months ($r^2 = 0.66$; < 0.04). High thrombin concentrations coincide with higher SOD levels 24h after ICH ($p = 0.01$).

Funding: The funders had no role in study design, data collection and analysis, decision to publish, or preparation of the manuscript. The authors received no specific funding for this work.

Competing interests: The authors have declared that no competing interests exist.

Conclusion

In this study we found that initial thrombin concentration and activity in CSF of ICH patients did not correlate with ICH and IVH volume but are associated with a poorer functional neurological outcome. These findings support mounting evidence of the role of thrombin as a contributor to secondary injury formation after ICH.

Background

Intracerebral hemorrhage (ICH) accounts for 10–15% of all strokes worldwide [1]. With an annual incidence of 10–30 per 100,000 population, it represents a major public health burden [1]. It is associated with considerable mortality and long-term morbidity [2]. Neuronal damage after ICH is caused by primary tissue disruption and secondary progression due to detrimental processes in the perihematomal zone. Despite ongoing clinical and preclinical research efforts, the underlying pathophysiological mechanisms of secondary deterioration are poorly understood. So far, good prognostic factors and specific treatment targets are missing.

Recently, the importance of the blood coagulation factor IIa (thrombin, FIIa) as key effector after traumatic brain injury and hemorrhagic stroke has become evident [3–5]. Thrombin signaling is mostly mediated through the family of protease-activated receptors (PARs) causing inflammatory responses, cell proliferation/modulation, cell protection and apoptosis [6, 7]. The majority of prothrombin is produced in the liver and, due to its large, spherical shape, it is unable to pass the blood-brain barrier (BBB) [8]. Nevertheless, thrombin and associated factors such as Anti-thrombin III (AT III) have also been detected throughout the central nervous system under physiological conditions [9]. Within the central nervous system (CNS) thrombin exerts both protective and detrimental effects. In pico- to nanomolar ranges (10pM– 10nM), thrombin is protective against a variety of cellular insults, such as glucose deprivation, reactive oxygen species (ROS) or edema formation after ICH [10, 11]. In high concentrations (100 nM–10 μM) thrombin increases edema by TNF-α up-regulation, neuronal damage and death after ischemia in mice [12–14]. These processes lead to extended neuronal injury predominantly mediated via protease-activated receptor-1 signaling [15]. Interestingly, the majority of perihematomal thrombin accumulation has been linked to neuronal expression, rather than systemic influx [16]. The CNS is the only known site of extra-hepatic thrombin production [17]. Neuronal cell loss within the tissue at risk and neurological deficits are associated with higher concentrations of thrombin in mice [16]. This supports the potential role of thrombin as a target of novel therapeutic regimens in the treatment of intracerebral hemorrhage. As human perihematomal tissue samples are not readily available, other specimens need to be analyzed to gain insight into the role of thrombin after ICH. It has previously been shown that thrombin and its inactive precursor prothrombin are detectable in human CSF [5]. However, no published data are available addressing thrombin within CSF after ICH.

We hypothesized that thrombin accumulation occurs in all compartments including the cerebrospinal fluid (CSF) after ICH and, in higher concentrations, might contribute to detrimental neurological outcome. In this study, prothrombin, thrombin and TAT were analyzed in the CSF of ICH patients and correlated with their functional neurological outcome.

Methods

Patient population

From February 2017 to February 2019, 20 consecutive patients (9 female and 11 male) that required extra-ventricular drainage due to space-occupying supratentorial ICH with

ventricular hemorrhage were included in our study. Age ranged from 40 to 80 years (66±12 years). All patients had one or more underlying conditions. Arterial hypertension was most common and present in 75% of all patients, chronic heart disease (35%) and malignancies (30%) ranked 2nd and 3rd (S1 Table). All patients received standard intensive care medical treatment according to current clinical guidelines. EVD was established on admission on our neurosurgical intensive care unit. Patients were followed up until six months after discharge or until death occurred. CSF and clinical data were collected and analyzed prospectively. All patients received a thorough clinical examination on admission and before discharge from our hospital. CT was used to analyze hematoma volume and localization as described before [18]. The clinical data and baseline characteristics are summarized in Table 1. Each patient's clinical status was graded according to the modified Rankin scale (mRS) and Glasgow coma scale (GCS) prior to admission. The neurological outcome was measured using the mRS and Glasgow outcome scale extended (GOSE) at 6 weeks and 6 months after ICH occurrence. CSF from patients with normal pressure hydrocephalus was collected and served as controls.

Sampling procedure

CSF was obtained through extra-ventricular drainage at day 1 and 3 after ICH onset. Concordant blood samples were obtained via an arterial canula. CSF of controls were obtained from either lumbar drainages placed for normal pressure hydrocephalus evaluation or from intraoperative opening of CSF spaces in meningioma and schwannoma patients. Samples were collected in a sterile plastic tube. The tube was centrifuged at 1500 G at 4˚C for 5 min. The supernatant was frozen, and aliquots were stored at -80˚C until analysis.

Measurement of analytes in CSF and blood samples

The prothrombin (NBP2-60624, Novus Biologicals, Abingdon, UK), thrombin (NBP2-60590, Novus Biologicals, Abingdon, UK) and TAT (NBP2-60605, Novus Biologicals, Abingdon, UK)

Table 1. Baseline demographics and patients characteristics.

	ICH patients	Control subject
No of subjects	22	4
Mean age (SD)	65.6 (12.3)	67.0 (5.7)
Sex		
Female	8	2
Male	14	2
ICH score	3 (1)	
Hematoma localization		
frontal	12	n.a.
parietal	8	n.a.
occipital	0	n.a.
Basal ganglia	2	n.a.
Clot volume (cm^3) (SD)	26.61 (29.93)	n.a.
Intraventricular clot (cm^3) (SD)	76.96 (94.88)	n.a.
Perihematomal zone (cm3) (SD)	90.54 (44.27)	n.a.
CSF concentration (ng/ml)		
Prothrombin	20.18 (1.4)	16.68 (1.17)
Thrombin	4.12 (1.3)	0.86 (0.36)
TAT	1.95 (1.7)	0.57 (0.11)
SOD	2.05 (0.95)	1.21 (0.05)

https://doi.org/10.1371/journal.pone.0241565.t001

concentration of each sample was measured with an enzyme-linked immunosorbent assay. SOD and fibrinogen were measured via photometry.

Measurement of hematoma volume

ICH and IVH volumes were calculated by CT, with a slice thickness of 1 mm. On serial slices in one direction, the intraventricular and intracerebral hematomas were segmented separately, while the volume were calculated using the Brainlab software (Brainlab, Munich, Germany) (Tables 1 and 2).

Statistical analysis

Findings were reported as mean or median ± SD. For statistical analysis, we used the non-parametric Mann-Whitney U-test. Relations among FII, FIIa, TAT, SOD and clinical outcome parameters two-way analysis of variance (ANOVA) with Tukey's multiple comparison post hoc test were performed using GraphPad Prism version 8.4.2 for macOS, GraphPad Software, La Jolla California USA, www.graphpad.com. A value of $P < 0.05$ was accepted as statistically significant.

Ethical approval

Data acquisition and analysis was performed in an anonymous fashion and was approved by the Ethics Committees of the medical association of Rhineland Palatinate and Lower Saxony, Germany (837.374.16). According to the local laws, no informed consent is necessary for such kind of analysis.

Results

Patient outcome and follow-up

Median GCS on admission was 10 ± 5. The mean ICH score on admission was 3 ± 1. Median historical mRS was 1 ± 1. The mRS deteriorated after ICH to 5 ± 1 at week 6 after ICH. The median mRS remained at 5 ± 2 at 6 months after ICH. (Table 2)

CSF FII, FIIa and TAT of controls and ICH patients

24h after ICH mean CSF levels of thrombin were 4.12±1.3 ng/ml compared to 0.86±0.36 ng/ml in healthy controls. Likewise, mean levels of prothrombin within the CSF was 20.18±1.4 ng/ml in patients with ICH and 16.68±1.17 ng/ml in controls. Mean TAT levels were 1.95±1.7 ng/ml or 0.57±0.11 ng/ml respectively. A statistically significant difference was evident between CSF concentrations of prothrombin ($p = 0.001$), thrombin ($p = 0.005$) and TAT ($p = 0.046$) in patients with ICH compared to healthy controls. (Table 1) Plasma levels of FII and FIIa did not correlate with their corresponding CSF levels. (Table 3)

Table 2. Disability and dependence over time (median; IQR).

	Admission / prior to ICH	6 weeks	6 month
GCS	10 (3, 14)	n.a.	n.a.
mRS	1 (0, 1)	5 (3, 5)	5 (3, 6)
GOSE	n.a.	3 (2, 3)	1 (1, 3)

https://doi.org/10.1371/journal.pone.0241565.t002

Table 3. CSF prothrombin, thrombin and TAT of patients with ICH and controls.

	Prothrombin (FII)		Thrombin (FIIa)		TAT	
	Spearman's ρ	p	Spearman's ρ	p	Spearman's ρ	p
ICH score	0.69	0.005	0.68	0.004	0.04	0.45
mRS 6 weeks	0.3	0.28	0.61	0.004	0.65	0.013
mRS 6 month	0.33	0.22	0.57	0.009	0.65	0.015
Clot size	0.47	0.07	0.23	.35	0.01	0.53
Plasma / CSF	0.007	0.77	0.08	0.3	-	-

https://doi.org/10.1371/journal.pone.0241565.t003

CSF fibrinogen and SOD after ICH

CSF levels of fibrinogen were 1.57±0.74 ng/ml 24h- and 1.5±0.89 ng/ml 72h after ICH. SOD levels within the CSF were 2.05±0.9 U/l 24h after ICH and 1.21±0.05 U/l in controls.

While initial levels of CSF fibrinogen and thrombin showed no correlation, both were inversely correlated 72h after onset of ICH (r = -0.68; p = 0.01). Higher levels of CSF thrombin correlate with higher levels of SOD 24h after ICH occurrence (r = 0.64; p = 0.095). (Fig 1)

Correlation of CSF FII, FIIa and TAT with clinical outcome

CSF concentrations of FIIa 24h after ICH correlated with the initial ICH score (r = 0.68; p = 0.004), as well as the mRS disability index 6 weeks (r = 0.61; p = 0.004) and 6 months (r = 0.57; p = 0.009) after discharge from hospital. Further, the TAT-complex as surrogate parameter of coagulation correlated with the mRS disability index at 6 weeks (r = 0.65; p = 0.013) and 6 months (r = 0.65; p = 0.015). (Table 3, Figs 1 and 2) In contrast, Prothrombin, Thrombin and TAT had no statistically significant correlation neither to the initial ICH volume nor to the IVH volume. Likewise, plasma levels of FII, FIIa and TAT did not correlate with the clinical outcome. (Table 3)

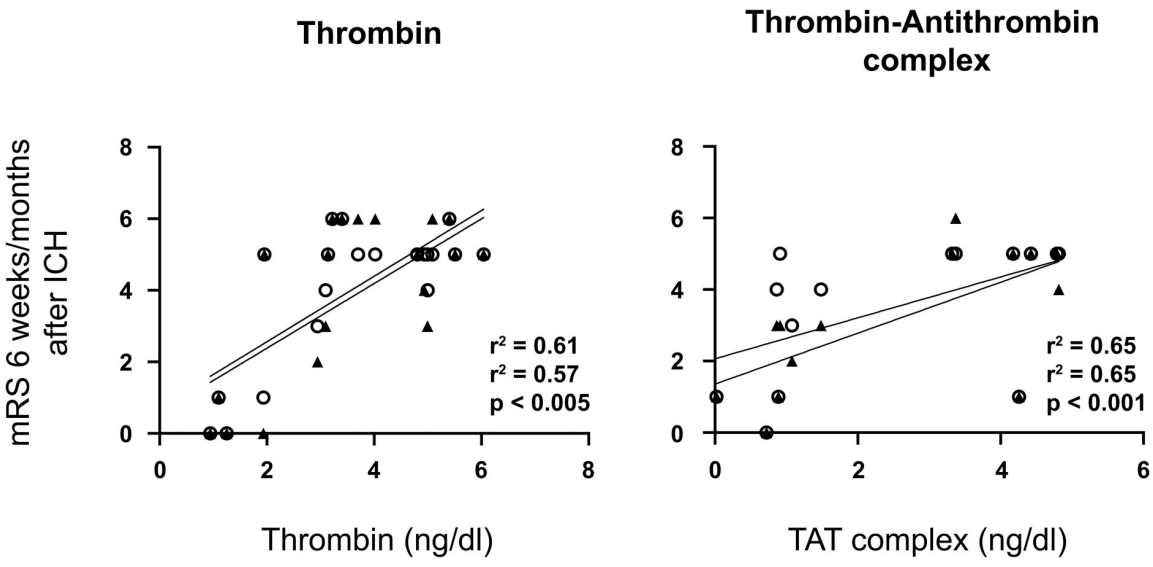

Fig 1. mRS after ICH is dependent on CSF FIIa and TAT concentrations. CSF concentrations of FIIa 24h after ICH correlated with the mRS disability index 6 weeks (r = 0.61; p = 0.004) and 6 months (r = 0.57; p = 0.009) after discharge from hospital. Further, the TAT-complex as surrogate parameter of coagulation correlated with the mRS disability index at 6 weeks (r = 0.65; p = 0.013) and 6 months (r = 0.65; p = 0.015).

https://doi.org/10.1371/journal.pone.0241565.g001

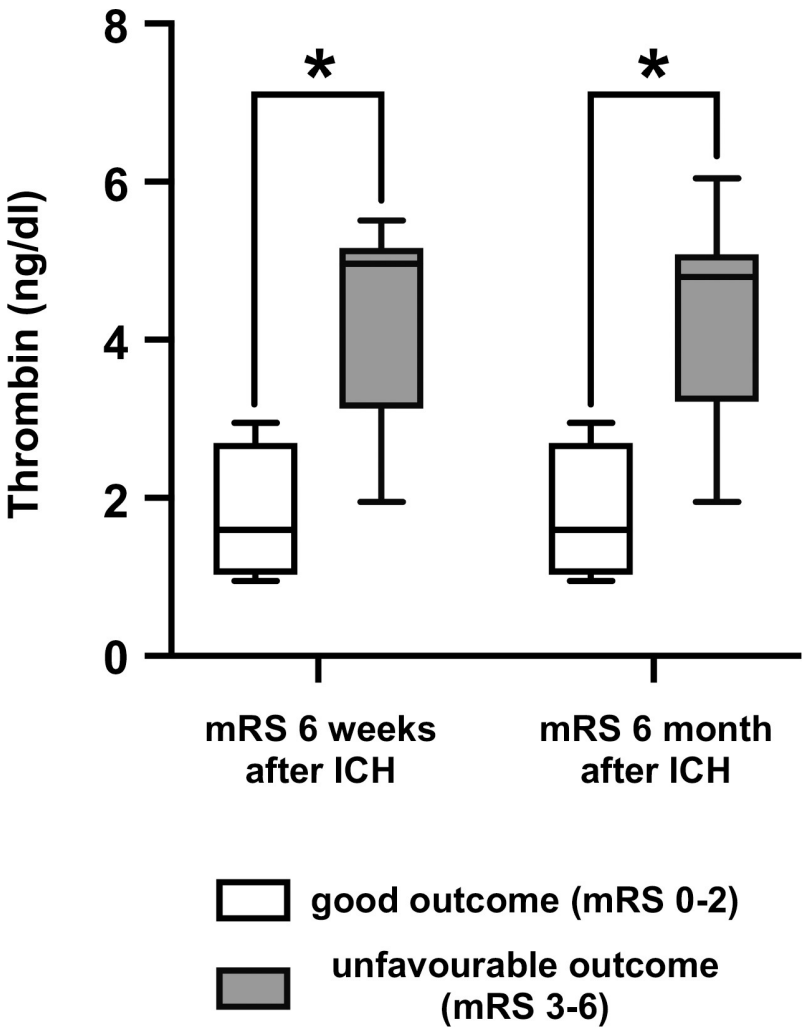

Fig 2. Higher CSF concentrations of thrombin are associated with an unfavourble outcome. Higher FIIa CSF concentrations 24h after ICH correlated with an unfavorable outcome after 6 weeks and 6 months.

https://doi.org/10.1371/journal.pone.0241565.g002

Correlation of CSF FII, FIIa and TAT with clinical outcome was independent from the type of surgical intervention. In our data, clot evacuation or lysis did not lead to better neurological outcome after 6 weeks or 6 months compared to conservative medical treatment ($p = 0.71$). High concentrations of FII, FIIa or TAT in CSF did not increase the likelihood of necessary surgical interventions during the acute phase of hospital care.

Discussion

In our study, higher concentrations of thrombin in the CSF of patients suffering from ICH correlated with an unfavorable outcome at 6 weeks and 6 months after discharge from hospital. We further show that prothrombin and thrombin within the CSF does correlate with the ICH score at the time of admission. This is plausible as thrombin has been shown to be neurotoxic both *in vitro* and *in vivo* if exceeding a threshold of 100nM [19]. Thrombin is inhibited by antithrombin III, resulting in an inactive proteinase/inhibitor complex (TAT). Interestingly, exceeding concentrations of antithrombin III are also detrimental to neuronal health

and might add to adverse thrombin effects [19]. In contrast to thrombin, ATIII mRNA expression has not been detected within normal CNS tissue and is supposed to be largely derived from passage across the blood-brain barrier [20]. It is about 100x higher in plasma, than it is in CSF. In times of BBB disruption, ATIII might enter then CNS and contribute to neuronal damage in the wake of ICH [20]. In our cohort, higher concentrations of thrombin and TAT complex within CSF correlated with a higher mRS at 6 weeks and 6 months after ICH, similar to those of unbound thrombin. These results fall in line with data published from patients with SAH where thrombin activity correlated with the degree of SAH (according to Fisher's CT classification), the persistence of a subarachnoid clot and the development of vasospasm [14]. In SAH, the Thrombin-Anti-Thrombin complex as surrogate of thrombin activity was found to correlate with the Hunt and Hess grading on admission. Although not statistically significant, larger amounts of TAT persisting over a longer period of time were found to be present in patients with worse neurological outcome [15]. In a preclinical study, nude mice developed hydrocephalus after injection of human hemorrhagic CSF [21]. The authors suggest that various acellular components of CSF inducing secondary brain injury and post-hemorrhagic hydrocephalus. However, in our small patient cohort, the severity and volume of ICH and IVH did not correlate neither with thrombin nor with the occurrence of a post-hemorrhagic hydrocephalus proving the complexity of the underlying pathophysiology.

It is speculated that thrombin induced neurotoxicity is mediated via Par-1, one of 4 members of the protease activated receptors family as activation of Par-1 per se has been linked to neuronal cell death [22]. The increases of oxidative stress and reduction of mitochondrial membrane potential might serve as possible explanation how Par-1 activation subsequently leads to cellular toxicity [23]. Another pathway leading to reactive oxygen species involves activation of microglial NADPH oxidase by thrombin induced upregulation of NADPH oxidation proteins gp91, p47-phox and p67-phox [22]. In our study SOD, higher concentration of thrombin coincided with higher concentrations of SOD at day 1, indirectly indicating the increased occurrence of ROS. Further, higher concentrations of CSF thrombin lead to decreased amounts of fibrinogen 3 days after ICH. As Inhibition of fibrin formation reduces neuroinflammation and improves long-term outcome after intracerebral hemorrhage, this might hint at another mechanism leading to secondary damage induction mediated by thrombin [24].

In contrast to our expectations, thrombin did not correlate with ICH or the IVH volume in our study. It remains a matter of debate, whether thrombin is washed in as a result of blood extravasation and BBB breakdown or mainly produced within the CNS as response to various stressors. Local thrombin expression in the perihematomal zone after ICH might contribute to thrombin levels in CSF [16]. As numerous MRI studies suggests the existence of a perihematomal penumbra with functionally impaired, but potentially reversible neuronal injury, this thin rim of 2 mm to a maximum width of 1 cm surrounding the site of injury, might as well be the area most devastatingly influenced by thrombin [16, 25].

Limitations of the study are due to a rather small and heterogeneous group of patients suffering from severe intracerebral hemorrhage. Limited knowledge of events prior to hospital admission and the number of concomitant illnesses might constitute an additional limitation of our study. Further research combining larger patient cohorts and multivariate analysis could lead to more definitive conclusions on the role of the cerebral thrombin system in the development of secondary brain injury after ICH.

Conclusion

In summary, in the presented data thrombin concentration and activity correlate with the neurological outcome after ICH. Further, generation of ROS seems to be involved in these

processes. Our data adds to a mounting body of evidence hinting at the importance of thrombin as a contributor to secondary injury formation after ICH.

Supporting information

S1 Fig. Clot volume is independent from CSF FIIa and TAT concentrations. CSF concentrations of FIIa (r = 0.13; p = 0.68) and TAT (r = -0.18; p = 0.51) show no correlation with clot volume 24h after ICH. Likewise, no correlation between FIIa (r = 0.36; p = 0.137) and TAT (r = 0.23; p = 0.422) with intraventricular clot volume were found 24h after ICH.
(TIF)

S1 Table. Underlying conditions.
(DOCX)

Author Contributions

Conceptualization: Harald Krenzlin, Julia Masomi-Bornwasser, Dominik Wesp, Thomas Kerz, Beat Alessandri, Florian Ringel, Naureen Keric.

Data curation: Harald Krenzlin, Christina Frenz, Jan Schmitt, Julia Masomi-Bornwasser, Dominik Wesp, Thomas Kerz, Johannes Lotz.

Formal analysis: Harald Krenzlin, Christina Frenz, Darius Kalasauskas, Beat Alessandri, Naureen Keric.

Project administration: Harald Krenzlin, Florian Ringel.

Resources: Florian Ringel.

Supervision: Harald Krenzlin, Dominik Wesp, Thomas Kerz, Beat Alessandri, Florian Ringel, Naureen Keric.

Validation: Naureen Keric.

Visualization: Harald Krenzlin.

Writing – original draft: Harald Krenzlin.

Writing – review & editing: Julia Masomi-Bornwasser, Darius Kalasauskas, Johannes Lotz, Beat Alessandri, Florian Ringel, Naureen Keric.

References

1. Qureshi AI, Tuhrim S, Broderick JP, Batjer HH, Hondo H, Hanley DF. Spontaneous intracerebral hemorrhage. N Engl J Med. 2001; 344(19):1450–60. Epub 2001/05/11. https://doi.org/10.1056/NEJM200105103441907 PMID: 11346811.
2. Qureshi AI, Mendelow AD, Hanley DF. Intracerebral haemorrhage. Lancet. 2009; 373(9675):1632–44. Epub 2009/05/12. https://doi.org/10.1016/S0140-6736(09)60371-8 PMID: 19427958; PubMed Central PMCID: PMC3138486.
3. Xi G, Reiser G, Keep RF. The role of thrombin and thrombin receptors in ischemic, hemorrhagic and traumatic brain injury: deleterious or protective? J Neurochem. 2003; 84(1):3–9. Epub 2002/12/18. https://doi.org/10.1046/j.1471-4159.2003.01268.x PMID: 12485396.
4. Gong Y, Xi G, Hu H, Gu Y, Huang F, Keep RF, et al. Increase in brain thrombin activity after experimental intracerebral hemorrhage. Acta Neurochir Suppl. 2008; 105:47–50. Epub 2008/12/11. https://doi.org/10.1007/978-3-211-09469-3_10 PMID: 19066081.
5. Smirnova IV, Salazar A, Arnold PM, Glatt S, Handler M, Festoff BW. Thrombin and its precursor in human cerebrospinal fluid. Thromb Haemost. 1997; 78(6):1473–9. Epub 1998/01/10. PMID: 9423797.

6. Ossovskaya VS, Bunnett NW. Protease-activated receptors: contribution to physiology and disease. Physiological reviews. 2004; 84(2):579–621. Epub 2004/03/27. https://doi.org/10.1152/physrev.00028.2003 PMID: 15044683.

7. Steinhoff M, Buddenkotte J, Shpacovitch V, Rattenholl A, Moormann C, Vergnolle N, et al. Proteinase-activated receptors: transducers of proteinase-mediated signaling in inflammation and immune response. Endocrine reviews. 2005; 26(1):1–43. Epub 2005/02/04. https://doi.org/10.1210/er.2003-0025 PMID: 15689571.

8. Shikamoto Y, Morita T. Expression of factor X in both the rat brain and cells of the central nervous system. FEBS letters. 1999; 463(3):387–9. Epub 1999/12/22. https://doi.org/10.1016/s0014-5793(99)01657-9 PMID: 10606759.

9. Deschepper CF, Bigornia V, Berens ME, Lapointe MC. Production of thrombin and antithrombin III by brain and astroglial cell cultures. Brain Res Mol Brain Res. 1991; 11(3–4):355–8. Epub 1991/10/01. https://doi.org/10.1016/0169-328x(91)90045-y PMID: 1661827.

10. Striggow F, Riek M, Breder J, Henrich-Noack P, Reymann KG, Reiser G. The protease thrombin is an endogenous mediator of hippocampal neuroprotection against ischemia at low concentrations but causes degeneration at high concentrations. Proceedings of the National Academy of Sciences of the United States of America. 2000; 97(5):2264–9. Epub 2000/02/19. https://doi.org/10.1073/pnas.040552897 PMID: 10681455; PubMed Central PMCID: PMC15789.

11. Vaughan PJ, Pike CJ, Cotman CW, Cunningham DD. Thrombin receptor activation protects neurons and astrocytes from cell death produced by environmental insults. The Journal of neuroscience: the official journal of the Society for Neuroscience. 1995; 15(7 Pt 2):5389–401. Epub 1995/07/01. https://doi.org/10.1523/JNEUROSCI.15-07-05389.1995 PMID: 7623161.

12. Coughlin SR, Camerer E. PARticipation in inflammation. The Journal of clinical investigation. 2003; 111(1):25–7. Epub 2003/01/04. https://doi.org/10.1172/JCI17564 PMID: 12511583; PubMed Central PMCID: PMC151847.

13. Hua Y, Wu J, Keep RF, Nakamura T, Hoff JT, Xi G. Tumor necrosis factor-alpha increases in the brain after intracerebral hemorrhage and thrombin stimulation. Neurosurgery. 2006; 58(3):542–50; discussion -50. Epub 2006/03/11. https://doi.org/10.1227/01.NEU.0000197333.55473.AD PMID: 16528196.

14. Kasuya H, Shimizu T, Takakura K. Thrombin activity in CSF after SAH is correlated with the degree of SAH the persistence of subarachnoid clot and the development of vasospasm. Acta Neurochir (Wien). 1998; 140(6):579–84. Epub 1998/10/02. https://doi.org/10.1007/s007010050143 PMID: 9755325.

15. Hirashima Y, Nakamura S, Suzuki M, Kurimoto M, Endo S, Ogawa A, et al. Cerebrospinal fluid tissue factor and thrombin-antithrombin III complex as indicators of tissue injury after subarachnoid hemorrhage. Stroke. 1997; 28(9):1666–70. Epub 1997/09/26. https://doi.org/10.1161/01.str.28.9.1666 PMID: 9303007.

16. Krenzlin H, Gresser E, Jussen D, Riede N, Taylor LE, Vogelaar CF, et al. The cerebral thrombin system is activated after intracerebral hemorrhage and contributes to secondary lesion growth and poor neurological outcome in C57Bl/6 mice. J Neurotrauma. 2019. Epub 2019/12/14. https://doi.org/10.1089/neu.2019.6582 PMID: 31830857.

17. Wang H, Reiser G. Thrombin signaling in the brain: the role of protease-activated receptors. Biol Chem. 2003; 384(2):193–202. Epub 2003/04/05. https://doi.org/10.1515/BC.2003.021 PMID: 12675511.

18. Bhattathiri PS, Gregson B, Prasad KS, Mitchell P, Soh C, Mitra D, et al. Reliability assessment of computerized tomography scanning measurements in intracerebral hematoma. Neurosurg Focus. 2003; 15(4):E6. Epub 2004/09/04. https://doi.org/10.3171/foc.2003.15.4.6 PMID: 15344899.

19. Garcia PS, Ciavatta VT, Fidler JA, Woodbury A, Levy JH, Tyor WR. Concentration-Dependent Dual Role of Thrombin in Protection of Cultured Rat Cortical Neurons. Neurochem Res. 2015; 40(11):2220–9. Epub 2015/09/08. https://doi.org/10.1007/s11064-015-1711-1 PMID: 26342829; PubMed Central PMCID: PMC4644093.

20. Zetterberg H, Andreasson U, Blennow K. CSF antithrombin III and disruption of the blood-brain barrier. J Clin Oncol. 2009; 27(13):2302–3; author reply 3–4. Epub 2009/04/01. https://doi.org/10.1200/JCO.2008.19.8598 PMID: 19332721.

21. Wan S, Wei J, Hua Y, Koduri S, Keep RF, Xi G, et al. Cerebrospinal Fluid from Aneurysmal Subarachnoid Hemorrhage Patients Leads to Hydrocephalus in Nude Mice. Neurocrit Care. 2020. Epub 2020/07/03. https://doi.org/10.1007/s12028-020-01031-0 PMID: 32613425.

22. Choi SH, Lee DY, Kim SU, Jin BK. Thrombin-induced oxidative stress contributes to the death of hippocampal neurons in vivo: role of microglial NADPH oxidase. J Neurosci. 2005; 25(16):4082–90. Epub 2005/04/22. https://doi.org/10.1523/JNEUROSCI.4306-04.2005 PMID: 15843610; PubMed Central PMCID: PMC6724962.

23. Antoniak S, Tatsumi K, Schmedes CM, Grover SP, Pawlinski R, Mackman N. Protease-activated receptor 1 activation enhances doxorubicin-induced cardiotoxicity. J Mol Cell Cardiol. 2018; 122:80–7.

Epub 2018/08/14. https://doi.org/10.1016/j.yjmcc.2018.08.008 PMID: 30098988; PubMed Central PMCID: PMC6173317.

24. Li X, Zhu Z, Gao S, Zhang L, Cheng X, Li S, et al. Inhibition of fibrin formation reduces neuroinflammation and improves long-term outcome after intracerebral hemorrhage. Int Immunopharmacol. 2019; 72:473–8. Epub 2019/05/01. https://doi.org/10.1016/j.intimp.2019.04.029 PMID: 31039464.

25. Siddique MS, Mendelow AD. Surgical treatment of intracerebral haemorrhage. Br Med Bull. 2000; 56 (2):444–56. Epub 2000/11/25. https://doi.org/10.1258/0007142001903085 PMID: 11092093.

Acta Neurochir (2014) 156:1729–1734
DOI 10.1007/s00701-014-2141-6

CLINICAL ARTICLE - VASCULAR

Surgical treatment of intraparenchymal hemorrhage during mechanical circulatory support for heart-failure – a single-centre experience

Harald Krenzlin · Christoph Rosenthal · Stefan Wolf · Juliane Vierecke · Alexander Kowski · Roland Hetzer · Peter Vajkoczy · Marcus Czabanka

Received: 2 April 2014 / Accepted: 21 May 2014 / Published online: 13 June 2014

Abstract
Background Cranial intraparenchymal hemorrhage represents a critical complication of mechanical circulatory support requiring constant antithrombotic treatment. Surgery of intraparenchymal hemorrhage under anticoagulation represents a challenge and imposes significant risks for patients. It was the aim to analyse surgical and clinical outcome of patients requiring surgical treatment due to intraparenchymal hemorrhage.
Methods Patients with mechanical circulatory support requiring surgical therapy due to space-occupying lobar supratentorial or infratentorial hemorrhage from January 1, 2009 to January 1, 2014 were included in our study. Baseline parameters are preoperative International Normalized Ratio (INR) values, postoperative anticoagulation regiment, bleeding size and localization. Co-primary outcome parameters were the extent of hematoma evacuation and the Modified Rankin Scale at discharge from hospital. Secondary outcome parameters included rate of recurrent hemorrhage, rate of revision surgery and in-hospital mortality.
Results Twelve patients (mean age 44±18 years, nine supratentorial-/three infratentorial hemorrhages, 11 left ventricular assist devices, and one extracorporeal membrane oxygenation) were included. Surgical hematoma evacuation was performed in 11 patients, one patient received decompressive hemicraniectomy. Hematoma evacuation was complete in no patients, and partial in 11 patients. Initial INR was 2,7±1,6. Rate of recurrent hemorrhage was 75 %. Revision surgery was performed in three patients achieving partial hematoma evacuation in two patients and complete evacuation in one patient. Modified Rankin Scale at discharge from hospital was six in nine patients (in-hospital mortality of 75 %), five in two patients and four in one patient.
Conclusions Surgical treatment of life threatening, space-occupying intraparenchymal hemorrhage under mechanical circulation support is of limited efficacy with high rates of recurrent hemorrhage and in-hospital mortality. We provide additional data that postponing anticoagulation is feasible and may lead to improved clinical outcome and survival.

Keywords Intracerebral hemorrhage · Left ventricular assist device · Surgical hematoma evacuation · Anticoagulation · Heart failure · Complication of left ventricular assist device · Extracorporeal membrane oxygenation

The results of this study were presented at the Annual Meeting of the German Neurosurgical Society (DGNC) 2014.

H. Krenzlin · S. Wolf · P. Vajkoczy · M. Czabanka (✉)
Department of Neurosurgery, Campus Virchow Klinikum, Charité Universitätsmedizin Berlin, Augustenburger Platz 1, 13353 Berlin, Germany
e-mail: marcus.czabanka@charite.de

A. Kowski
Department for Neurology, Charité Universitätsmedizin Berlin, Berlin, Germany

J. Vierecke · R. Hetzer
Department of Cardiothoracic and Vascular Surgery, Deutsches Herzzentrum Berlin DHZB, Berlin, Germany

C. Rosenthal
Department of Anaesthesiology and Intensive Care Medicine, Campus Charité Mitte and Campus Virchow-Klinikum, Charité–Universitätsmedizin Berlin, Berlin, Germany

Introduction

Intracranial hemorrhage represents a critical complication of mechanical circulatory support systems because anticoagulation may lead to large, space-occupying intraparenchymal hematomas imposing a decisive therapeutic dilemma [1–4]. The risk for developing intracerebral

hemorrhage under mechanical circulatory support ranges from 3 % to 11 % [5, 6]. While surgical hematoma evacuation may be indicated, associated anticoagulation represents a severe drawback to surgical intervention. With the introduction of the landmark REMATCH trial (Randomized Evaluation of Mechanical Assistance for the Treatment of Congestive Heart Failure), which demonstrated that patients with advanced heart failure have a survival benefit and increased quality of life under treatment with a left ventricular assist device, the use of mechanical supports systems is steadily increasing [1, 3]. This clinical success has changed treatment of end-stage left ventricular cardiac failure that consisted of medical support and ultimately heart transplantation to using mechanical circulatory support systems as a bridge to transplantation or long-term destination therapy [3]. Consequently, patients presenting with neurological complications resulting from mechanical cardiac assist systems, mostly left ventricular assist devices (LVADs), are becoming more frequent. However, clinical treatment experiences of intracranial hemorrhage in patients with mechanical circulatory support systems are scarce, and, therefore, there is a massive lack of knowledge regarding decisive treatment decisions like surgical patient selection, management of anticoagulation and early estimation of patient prognosis. It was the aim of our study to analyse patient outcome and the effects of surgical hematoma evacuation in patients with space-occupying intraparenchymal hematoma under mechanical circulatory support.

Materials

Study design

From January 1 2009 to January 1 2014, patients that required surgical therapy for the treatment of space-occupying supratentorial or infratentorial intracerebral hemorrhage due to mechanical circulatory support were included in our study. Clinical data were collected and analysed retrospectively. Data acquisition and analysis was performed in an anonymous fashion and was approved by the local Ethics Committee.

Patients required mechanical circulatory support due to underlying heart failure. All patients received a thorough clinical examination prior to surgery including a cranial computer tomography (CCT) scan prior as well as directly after surgery and 24 h after hematoma evacuation. CCT was used to analyse hematoma volume and localisation as described before [7]. All patients received standard intensive care medical treatment according to the underlying pathology and to current clinical guidelines. If necessary, further CCT scans were performed depending on the clinical obligation for further diagnostics. Detailed medical chart review focusing on coagulation parameters, antiplatelet therapy and anticoagulation therapy was performed. Patients were followed up until three months after surgery or until death occurred.

Outcome parameters

Two primary outcome parameters were defined in our study. The primary surgical parameter was the extent of hematoma evacuation. This parameter was defined as complete evacuation if in a postoperative CT scan (24 h after surgery) no remaining blood clots were visualized. Partial hematoma evacuation was defined as overall reduction of hematoma size with remaining blood clots. Ineffective hematoma evacuation was defined as no reduction of hematoma size after surgery. The second primary outcome parameter focused on clinical outcome of patients. For this purpose, the Modified Rankin Scale was assessed when patients were discharged from hospital [8].

Secondary outcome parameters included rate of recurrent hemorrhage (based on progressive size of intracranial hemorrhage in CT scans), rate of recurrent surgery and in-hospital mortality. Furthermore, we analysed the preoperative anticoagulation (International Normalized Ratio, platelet count, partial thromboplastin time (PTT)), antiplatelet therapy and postoperative anticoagulation regimen.

Results

Patient population

A total number of 12 patients (eight male, four female patients) were included in our study. Mean age of patients was 44±18 years with one paediatric patient (five years of age). In ten patients a LVAD with continuous flow, and in one patient a LVAD with pulsatile flow was used as mechanical circulatory support. In one patient extracorporeal membrane oxygenation was necessary due to septic respiratory decompensation. Dilative cardiomyopathy (DCM) was the underlying pathology causing heart failure in eight patients, restrictive cardiomyopathy (RCM) in one patient, massive virus-induced myocarditis and sepsis were the underlying pathology in the remaining patients. In the paediatric patient heart failure due to aortic stenosis and muscular stenosis of the left coronary artery was the cardiac pathology requiring mechanical circulatory support.

Initial GCS was 8 points (range from 3 to 14 points) with an interquartile range (IQR) of 7 points. Anisocoria was identified in two patients, whereas isocor pupils were assessed in nine patients. In nine patients intracerebral hemorrhage and in three patients intracerebellar hemorrhage occurred. Eleven patients received surgical hematoma evacuation using an osteoplastic supratentorial or infratentorial craniotomy. In one

patient decompressive hemicraniectomy was performed without hematoma evacuation because of the development of bilateral mydriasis in the operating theatre prior to craniotomy.

Anticoagulation

All patients were on therapeutic anticoagulation with warfarin with unfractionated heparin plus antiplatelet therapy before ictus. INR before surgery was 2,6±1,6 and PTT was 63,3± 40 s. All patients received substitution with red blood cell concentrate, platelets, fresh frozen plasma, fibrinogen or prothrombin complex prior to surgery as well as intraoperatively. Perioperative normalization of PTT (≤40 s.) and INR (≤1,2) were achieved in 50 % of patients (6/12), whereas 50 % of patients demonstrated only a moderate increase in PTT and INR (Tables 1 and 2).

Postoperative anticoagulation regimen aimed at achieving PTT of 60 s in eight patients using unfractionated heparin. Four of those patients died in the first 24 h after surgery; therefore, detailed analysis of postoperative anticoagulation was impossible (Table 2). Of the remaining four patients, only one patient survived with a mRS of 4 points at discharge from hospital. Due to fatal outcome, postoperative anticoagulation regime was changed to complete normalization of coagulation parameters in four patients. Obstruction of the left ventricular assist device was not observed. Out of this patient subpopulation, two patients (50 %) survived (mRS 5 and 4 points).

Surgical hematoma evacuation

The initial size of the supratentorial hematoma was 95± 41 cm^3 ,and the size of the infratentorial hematoma was 15± 28 cm^3. All hemorrhages were lobar hemorrhages. Localisation of hemorrhage was frontal (five patients), temporal (two patients), occipital (two patients) and cerebellar (three patients). Intraventricular involvement was observed in two patients.

Partial hematoma evacuation was achieved in 11 patients undergoing surgery. Complete or ineffective hematoma evacuation was not observed. In 75 % of patients recurrent hemorrhage was detected using repetitive CT scans. Three patients required resurgery aiming at improving hematoma removal. Resurgery was performed via the existing craniotomy without extending the surgical approach. In two patients undergoing recurrent surgery partial hematoma evacuation was achieved, whereas in one patient total hematoma removal was performed (Table 3).

Clinical outcome

Modified Rankin scale was six with an IQR of 0.5. Nine out of 12 patients died during the acute phase in hospital. Two survived in a vegetative state (mRS 5) and one with severe disability (mRS 4) (Table 3). Patients died either due to uncontrollable intracranial pressure or therapy restriction in the light of extensive parenchymal damage with extremely limited prognosis. Mean survival time was 55±48 h. Surviving patients were mRS 5 points (two patients) and 4 points (one patient) at discharge from hospital (Table 3).

Table 1 Patient characteristics

	Type of ICH		
	Supratentorial ICH	Infratentorial ICH	Entire cohort
Patient demographics			
No. of patients	9	3	12
Mean age years (SD)	35	52	44(18)
Sex			
Female	4	0	4
Male	5	3	8
LVAD continuous flow	8	2	10
LVAD pulsatile flow	1	0	1
ECMO	0	1	1
Underlying disease			
RCM	1	0	1
DCM	5	3	8
Septic heart failure	2	0	2
Aortic stenosis	1	0	1
GCS (IQR)	8 (5)	6 (3,5)	8 (7)
Hematoma size [cm^3] (SD)	95 (41)	15 (28)	n.a.
Hematoma localisation			
Frontal (ventricular)	5 (0)	n.a.	n.a.
Temporal (ventricular)	2 (0)	n.a.	n.a.
Occipital (ventricular)	2 (2)	n.a.	n.a.
Cerebellar (ventricular)	n.a.	3 (0)	n.a.
Coagulation parameters			
INR on admission (SD)	3,08 (1,56)	1,34 (0,07)	2,7 (1,6)
PTT on admission (SD)	71,8 (45,9)	61,7 (13,2)	63,3 (40,0)
Surgical procedure			
Evacuation	8	3	11
Hemicraniectomy	1	0	1

**LVAD* left ventricular assist device, *ECMO* extracorporeal membrane oxygenation, *RCM* restrictive cardiomyopathy, *DCM* dilatative cardiomyopathy, *IQR* interquartile range, *INR* international normalized ratio, *PTT* partial thromboplastin time, *SD* standard deviation, *ventricular* ventricular hemorrhage

Discussion

This series demonstrates reduced surgical and clinical outcome for patients requiring hematoma evacuation of supratentorial or infratentorial intraparenchymal hemorrhage

Table 2 Management of anticoagulation

	Type of ICH		
	Supratentorial ICH	Infratentorial ICH	Entire cohort
Preoperative anticoagulation			
Aspirin/Dipyridamole	9	3	12
Warfarin	7	1	8
Heparin	2	2	4
Substitution			
PRBC	6	2	8
Platelet concentrate	3	1	4
FFP	5	1	5
PCC	7	1	8
Fibrinogen	2	1	3
Intraoperative Coagulation			
PTT <40/INR <1.2	4	2	6
Postoperative Anticoagulation			
Normalized	2	2	4
Heparin (PTT >60)	7	1	8
Pump Failure	0	0	0

**PRBC* packed red blood cells, *FFP* fresh frozen plasma, *PCC* prothrombin complex, *PTT* partial thromboplastin time, *INR* international normalized ratio

under mechanical circulatory support. Preoperative and intraoperative substitution of coagulation factors and platelets did not protect sufficiently from recurrent hemorrhage. Postoperative normalization of coagulation parameters may support surgical therapy and suggests the potential to improve patient outcome without inducing obstruction of circulatory support systems.

Table 3 Outcome data

	Type of ICH		
	Supratentorial ICH	Infratentorial ICH	Entire cohort
Evacuation			
Complete	0	0	0
Partial	8	3	11
Insufficient	0	0	0
Recurrent hemorrhage (%)	7 (77 %)	2 (66 %)	9 (75 %)
Resurgery	2	1	3
mRS 6 (Mortality %)	6 (66 %)	3 (100 %)	9 (75 %)
mRS 5	2	0	2
mRS 4	1	0	1
mRS 1-3	0	0	0

**mRS* modified Rankin Scale

Treatment of intracerebral hemorrhage under mechanical circulatory support represents a major clinical challenge as patients face intracranial hemorrhage under anticoagulant and antiplatelet therapy. Treating physicians are forced to oppose the risk of recurrent hemorrhage or progressive hemorrhage versus the risk of assist device failure due to clotting and cerebrovascular embolic events if anticoagulation is discontinued. This treatment paradox is enforced if surgical hematoma evacuation becomes inevitable. Surgical treatment of intracranial intraparenchymal hemorrhage remains a matter of controversy. The Surgical Treatment for Intracerebral Hemorrhage I (STICH I) trial demonstrated no long-term benefit for surgery versus conservative management in intraparenchymal haemorrhage [9]. However, a benefit for superficial lobar hematomas was evaluated leading to the initiation of the Surgical Treatment for Intracerebral Hemorrhage II (STICH II) trial [10]. Recent data from this trial highlight a clinically relevant survival benefit for patients with superficial lobar intracerebral hematomas [11]. In our study we included patients with lobar superficial hematomas (in the case of supratentorial localisation) representing a patient population that might benefit from surgery. However, generalizing data from the STICH trials to our patients is flawed, because patients in our study were under enhanced anticoagulation and mechanical circulatory support. This difference is best shown by a very large hematoma volume in our patient population compared to STICH II patients and a reduced clinical state (median GCS 8 points, unilateral mydriasis in 2 and bilateral mydriasis in 1 patient) [11]. Therefore, hemorrhages were of the advanced, life-threatening stage in our study. Moreover, three patients were treated with cerebellar hemorrhages, which are not represented in the STICH trials. Current guidelines recommend surgical treatment of cerebellar hemorrhage in the case of neurological deterioration and if brainstem occlusion or hydrocephalus is present in the CT scan [12]. All of our patients fulfilled these criteria rendering strong indications for surgical hematoma removal.

One reason for the poor outcome of patients in our series was the fatal clinical situation before surgery. GCS of patients prior to surgery, anticoagulation, antiplatelet therapy, clinical signs of herniation and significant comorbidities represent clinically relevant risk factors that negatively influence surgical and clinical outcome. Unfortunately, there is hardly any evidence available helping in patient selection for surgical treatment of intraparenchymal hemorrhage under mechanical circulatory support. The largest case series include only very few patients with intracranial hemorrhage. Different conclusions result from these case series ranging from recommending the potential life saving effect of surgical hematoma removal to questioning surgical therapy [4, 13]. Mayer et al., and Wilson et al., demonstrate a lifesaving effect for the removal of subdural hematomas under LVAD therapy [2, 4]. However, in the case of intraparenchymal hemorrhage,

an 80 % 60-day mortality rate (four out of five patients) is reported [4]. Niebler et al., reported similar experiences in the treatment of paediatric patients with mechanical circulatory support [13]. One paediatric patient with a subdural hematoma was treated surgically resulting in survival of the patient with minimal neurological deficit. In the other patients (all presenting with intraparenchymal haemorrhage under a ventricular assist device) mortality rate was 75 % [13]. Based on these data, our study currently provides the largest systematic analysis of patients with intraparenchymal haemorrhage requiring surgery during mechanical circulatory support. Our study highlights the high rate of incomplete hematoma removal and the need for recurrent surgery in patients requiring mechanical circulatory support. Our series provides further insights into the role of postoperative management of anticoagulation. It is shown, that preoperative and intraoperative substitution of coagulation factors and platelets does correct laboratory coagulation values; however, the rate of recurrent haemorrhage remains high. In 75 % of patients (n=8), postoperative partial anticoagulation was performed (aiming at an aPTT of 60 s) in order to maintain patency of the mechanical circulatory support system and to reduce the risk for cerebral ischemia with only one out of eight patients surviving. Based on this fatal outcome, we changed postoperative management to normalizing coagulation parameters. In four patients complete normalization of coagulation parameters was maintained postoperatively without signs of assist device obstruction. Interestingly, 50 % of these patients survived intraparenchymal haemorrhage and were dismissed for rehabilitation. In this regard different reports demonstrate that medical anticoagulation may be withheld from patients with LVAD treatment for a restricted period of time without occlusion of LVAD [4, 13, 14]. These data support the hypothesis that postoperative maintenance of normal coagulation parameters may support the effects of surgical treatment and may improve clinical outcome.

Obviously, this series of patients is lacking quality standards that are applied to randomized controlled clinical trials. There is a selection bias because decision for surgery was not randomized but based on clinical arguments explaining the reduced GCS and large hematoma size of of the patients included. Therefore, data from this study cannot be generalized. It must be noted however, that surgical treatment in the herein described patients is usually withheld due to anticoagulation until surgery becomes inevitable due to a critical hematoma size. Our data provide important initial insights into hematoma management under critical clinical conditions and report the results of surgery in a selected group of patients. This knowledge may form the foundation for further systematic treatment evaluations in these difficult patients.

In conclusion, we report reduced surgical and clinical outcome in patients requiring surgical treatment for large intraparenchymal haemorrhage under mechanical circulatory support. Prolonged postoperative maintenance of normalized coagulation may not exalt the risk of LVAD malfunction but might be beneficial in these patients in order to improve outcome after surgical hematoma removal.

Acknowledgments This work was funded by NeuroCure Flexible Fund 2010, Universitätsmedizin Charité, Berlin and by "Friedrich C. Luft" Clinical Scientist Pilot Program (funded by Volkswagen Foundation and Charité Foundation).

The authors gratefully acknowledge Wolf Schmidt and Rodolfo Lopez for helping in data collection.

Conflicts of interest None.

References

1. Lazar RM, Shapiro PA, Jaski BE, Parides MK, Bourge RC, Watson JT, Damme L, Dembitsky W, Hosenpud JD, Gupta L, Tierney A, Kraus T, Naka Y (2004) Neurological events during long-term mechanical circulatory support for heart failure: the Randomized Evaluation of Mechanical Assistance for the Treatment of Congestive Heart Failure (REMATCH) experience. Circulation 109:2423–2427
2. Mayer RR, Hwang SW, Reddy GD, Morales DL, Whitehead WE, Curry DJ, Bollo RJ, Luerssen TG, Jea A (2012) Neurosurgical complications of left ventricular assist devices in children. J Neurosurg Pediatr 10:370–375
3. Rose EA, Gelijns AC, Moskowitz AJ, Heitjan DF, Stevenson LW, Dembitsky W, Long JW, Ascheim DD, Tierney AR, Levitan RG, Watson JT, Meier P, Ronan NS, Shapiro PA, Lazar RM, Miller LW, Gupta L, Frazier OH, Desvigne-Nickens P, Oz MC, Poirier VL (2001) Long-term use of a left ventricular assist device for end-stage heart failure. N Engl J Med 345:1435–1443
4. Wilson TJ, Stetler WR Jr, Al-Holou WN, Sullivan SE, Fletcher JJ (2013) Management of intracranial hemorrhage in patients with left ventricular assist devices. J Neurosurg 118:1063–1068
5. Miller LW, Pagani FD, Russell SD, John R, Boyle AJ, Aaronson KD, Conte JV, Naka Y, Mancini D, Delgado RM, MacGillivray TE, Farrar DJ, Frazier OH (2007) Use of a continuous-flow device in patients awaiting heart transplantation. N Engl J Med 357:885–896
6. Slaughter MS, Rogers JG, Milano CA, Russell SD, Conte JV, Feldman D, Sun B, Tatooles AJ, Delgado RM 3rd, Long JW, Wozniak TC, Ghumman W, Farrar DJ, Frazier OH (2009) Advanced heart failure treated with continuous-flow left ventricular assist device. N Engl J Med 361:2241–2251
7. Bhattathiri PS, Gregson B, Prasad KS, Mitchell P, Soh C, Mitra D, Gholkar A, Mendelow AD (2003) Reliability assessment of computerized tomography scanning measurements in intracerebral hematoma. Neurosurg Focus 15:E6
8. Rankin J (1957) Cerebral vascular accidents in patients over the age of 60. III. Diagnosis and treatment. Scott Med J 2:254–268
9. Mendelow AD, Gregson BA, Fernandes HM, Murray GD, Teasdale GM, Hope DT, Karimi A, Shaw MD, Barer DH (2005) Early surgery versus initial conservative treatment in patients with spontaneous supratentorial intracerebral haematomas in the International Surgical Trial in Intracerebral Haemorrhage (STICH): a randomised trial. Lancet 365:387–397
10. Mendelow AD, Gregson BA, Mitchell PM, Murray GD, Rowan EN, Gholkar AR (2011) Surgical Trial in Lobar Intracerebral Haemorrhage (STICH II) protocol. Trials 12:124

11. Mendelow AD, Gregson BA, Rowan EN, Murray GD, Gholkar A, Mitchell PM (2013) Early surgery versus initial conservative treatment in patients with spontaneous Supratentorial Lobar Intracerebral Haematomas (STICH II): a randomised trial. Lancet 382:397–408
12. Morgenstern LB, Hemphill JC 3rd, Anderson C, Becker K, Broderick JP, Connolly ES Jr, Greenberg SM, Huang JN, MacDonald RL, Messe SR, Mitchell PH, Selim M, Tamargo RJ (2010) Guidelines for the management of spontaneous intracerebral hemorrhage: a guideline for healthcare professionals from the American Heart Association/American Stroke Association. Stroke 41:2108–2129
13. Niebler RA, Lew SM, Zangwill SD, Woods RK, Mitchell ME, Tweddell JS, Ghanayem NS (2014) Incidence and outcome of pediatric patients with intracranial hemorrhage while supported on ventricular assist devices. Artif Organs 38:73–78
14. Pratt AK, Shah NS, Boyce SW (2014) Left ventricular assist device management in the ICU. Crit Care Med 42:158–168

JOURNAL OF NEUROTRAUMA 36:395–402 (January 15, 2019)

DOI: 10.1089/neu.2018.5657

Occurrence of Spontaneous Cortical Spreading Depression Is Increased by Blood Constituents and Impairs Neurological Recovery after Subdural Hematoma in Rats

Harald Krenzlin,[1,2] Daniel Jussen,[1,3] Michaela Plath,[1,4] Stephan J. Tretzel,[1] Tobias Krämer,[1] Oliver Kempski,[1] and Beat Alessandri[1]

Abstract

Acute subdural hemorrhage (ASDH) is common and associated with severe morbidity and mortality. To date, the role of spontaneous cortical spreading depression (sCSD) in exaggerating secondary injury after ASDH, is poorly understood. The present study contains two experimental groups: First, we investigated and characterized the occurrence of sCSD after subdural blood infusion (300 μL) via tissue impedance (IMP) measurement in a rat model. Second, we compared the occurrence and influence of sCSD on lesion growth and neurological deficit in the presence and absence of whole blood constituents. In the first experimental group, three IMP traits could be distinguished after ASDH: no sCSD, recurrent sCSD, and constant elevated IMP (anoxic depolarization [AD]). In the second experimental group, sCSD occurred more often after autologous blood, compared with paraffin oil infusion. Lesion volume 7 days post-ASDH was $27.3 \pm 6.8\,mm^3$ after blood and $3.4 \pm 2.1\,mm^3$ after paraffin oil infusion. Subgroup analysis showed larger lesion size in animals with sCSD, than in those without. Further, occurrence of sCSD led to worse neurological outcomes in both groups. sCSD occurs early after ASDH and does not depend on the presence of whole blood constituents. However, numbers and degree of sCSD are more frequent and severe after autologous blood infusion, compared with an inert volume substance. The occurrence of sCSD leads to lesion growth and worse neurological outcome. Thus, our data advocate close monitoring and targeted treatment of sCSD after ASDH evacuation.

Keywords: acute subdural hemorrhage; anoxic depolarization; secondary injury; spontaneous cortical spreading depression; tissue impedance

Introduction

In 1944, Leão discovered a cessation of electroencephalogram activity, which lasted for several minutes, while studying epilepsy in rabbits.[1] He later described the phenomenon as a loss of ion homeostasis spreading throughout the cortex, leading to spontaneous cortical spreading depression (sCSD) of electrical activity, after electrical or mechanical alteration.[1–3] sCSD has since been studied in various animal models and humans and was found to represent cortical excitations followed by a spreading loss of functioning neurons and astrocytes.[4] The wave-like depolarization is associated with changes in cerebral blood flow (CBF), perfusion, swollen neurons, and alterations in dendritic spines.[5,6]

Substances such as potassium, acetylcholine and glutamate, as well as conditions of hypoxia, hypoglycemia, ischemia, subarachnoid hemorrhage (SAH), traumatic brain injury (TBI), and seizures have been identified to cause sCSD.[7–10] Changes of the ionic homeostasis, the underlying mechanism of sCSD, leads to cellular swelling after influx of cations, declining extracellular space, and consecutive loss of membrane potentials.[9] These changes can be detected using tissue impedance (IMP) measurement as an indicator for swelling.[11] It has been shown that each CSD, either spontaneous or triggered by potassium chloride (KCl), leads to a transient increase in tissue impedance (average of 2 kOhm).[12] The restoration of the ion homeostasis is energy dependent and under physiological conditions the brain copes with hyperemia and

[1]Institute for Neurosurgical Pathophysiology, Johannes Gutenberg-University Mainz, Germany.
[2]Harvey Cushing Neurooncology Laboratories, Department of Neurosurgery, Brigham and Women's Hospital, Harvard Medical School, Boston, Massachusetts.
[3]Department of Neurosurgery, HELIOS Dr. Horst-Schmidt-Kliniken, Wiesbaden, Germany.
[4]Department of Otolaryngology–Head and Neck Surgery, Ruprecht-Karls-University, Heidelberg, Germany.

vasodilatation.[13,14] Increased energy demands are reflected in the form of decreased glucose, glycogen, and increased lactate concentrations. In sCSD under pathophysiological conditions (e.g., focal lesions), the surrounding microenvironment is acidic and high in potassium, which promotes vasoconstriction, leading to inverse hemodynamic reactions in regions with already compromised blood flow.[15] These intra-lesional conditions allow the persistent anoxic depolarization (AD) to become a transient depolarization spreading through the healthy, surrounding tissue.

Due to a poor neurovascular coupling, the raised energy demand in the wake of sCSD cannot be met; therefore, areas of watershed are at risk for becoming ischemic.[16] This undersupply may render more tissue susceptible to sCSD.[17,18] Consequently, ischemia and elevated energy demands lead to cell death in the peri-ischemic area and thus, secondary lesion growth.[18] The COSBID (Co-Operative Studies on Brain Injury Depolarizations) research group focuses on the causes and consequences of sCSD in lesion development under various pathological conditions (e.g., TBI, aneurysm/SAH and stroke).[19,20] Several COSBID studies demonstrate that electrocorticography (ECoG) depressions, identical to CSD in animal models, occur with a higher likelihood in patients with TBI and are estimated to be occur in as many as 56% of all patients with TBI.[21,22] Further, in clinical studies sCSD has repeatedly been proven by real-time monitoring of electrophysiology, blood flow, and cytotoxic edema to cause secondary damage.[23] It is reported that similar events might contribute to secondary lesion development after acute subdural hemorrhage (ASDH), an entity often associated with TBI, where extravasated blood causes elevated intracranial pressure (ICP) and consecutive ischemia.[24] It seems that factors other than merely volume mass lesions are important for cell death and lesion development, as subdural infusion of inert volume substances showed no substantial lesion formation despite similar ICP and CBF characteristics.[25] As ASDH pathophysiology comprises focal ischemia as well as the impact of blood constituents, sCSD may play a decisive role in secondary lesion progression and thus might be targeted by *N*-Methyl-D-aspartate (NMDA) antagonists (e.g., ketamine), anti-epileptic drugs (e.g., levetiracetam), NO donators, calcium channel blockers (e.g., nimodipine), or induced hypothermia.[7,26–28]

Our study was designed as a two-tailed approach to (1) characterize the occurrence of sCSD after ASDH and (2) to address whether sCSDs occurrence, lesion size, and neurological outcome depend on the presence of whole blood constituents rather than disturbances of ICP and CBF alone.

Methods

Experimental design

Experimental group 1. To investigate the occurrence and influence of sCSDs on the outcome after subdural hematoma, 300 μL autologous blood was injected subdurally in 20 male Sprague-Dawley rats. Monitoring of physiological parameters, ICP, and tissue IMP was performed starting 10 min prior to ASDH induction and continued for 180 min. All animals were then returned to their housing for 7 days. Ultimately, all animals were sacrificed and the lesion size was histologically determined.

Experimental group 2. To analyze the influence of whole blood constituents on sCSD occurrence, consecutive lesion size, and neurological outcome, paraffin oil was used as inert volume substance to form a subdural mass lesion lacking blood constituents. Twenty-eight male Sprague-Dawley rats were randomly assigned to sham, autologous blood, or paraffin oil infusion. Monitoring of vital parameters, as well as extended neuro-monitoring of ICP and tissue IMP was performed, starting 10 min prior to ASDH induction and continued for 180 min. All animals were then returned to their housing for 7 days and ultimately sacrificed for determination of the lesion volume.

Animal care and anesthesia

A total of 48 male Sprague-Dawley rats (Charles River, Germany) were used in all experiments. All animals were housed at room temperature of 22 ± 2°C and humidity >50%. Animals were anesthetized by intraperitoneal (i.p.) injection of chloral hydrate. The initial dose was 36 mg/ 100 g body weight. To keep the animals under anesthesia, the same dose was given hourly through a permanently placed i.p. catheter. The animals were intubated and mechanically ventilated and their body temperature was closely monitored and kept at 37.5°C throughout the operation using a heating pad and a rectal thermometer (Homeothermic Blanket Unit, Harvard, Kent, UK). All experimental procedures were approved by the local ethics committee and were in accordance with the German guidelines for animal use and care.

Surgical preparation for ASDH

The tail artery was cannulated for blood pressure measurement and sampling of blood for blood gas analysis (BGA). The volume needed for each BGA was 210 μL (ABL615/EML105, Radiometer, Copenhagen, DK). A catheter was placed in the jugular vein to obtain blood for subdural infusion. Animals were harnessed in a stereotaxic frame; a craniotomy with a diameter of 3 mm was made between the bregma and lambda suture on the left side as previously described.[29] Briefly, the dura was opened and a bent, L-shaped, blunt cannula (23G) was inserted and secured with tissue glue (Histoacryl; B Braun, Melsungen, Germany) and dental cement. Two further burr holes were drilled anterior to the bregma suture (anterior-posterior: 2 mm, midline: 2.5–3 mm) to insert the IMP electrodes (two stainless-steel wires covered in polyvinyl chloride for electrical insulation except for the sharp-pointed tips). IMP was measured at 1 kHz (10 mV, bias-free). Changes in tissue IMP were accompanied by direct current shifts during sCSD occurrence. ICP was measured intraventricularly through a 26G needle on the contralateral side. All probes and needles were also fixed with tissue glue. A laser Doppler probe was placed on the ipsilateral hemisphere frontal to the bregma (Vasamedics Laserflo BPM2, Vasamedics Fiber-Optic Probe 8*200 mm; St Paul, MN). All parameters were recorded continuously every minute during a 10-min baseline, subdural infusion of 300 μL autologous non-heparinized blood or paraffin oil at a flow rate of 50 μL/min (6-min period) and continued for 180 min after ASDH induction. After injection, the catheter was removed and the scalp was sutured; the animal could recover and was returned to regular housing. The sham-operated groups received no infusion.

Evaluation of behavioral and neurological deficits

Then, a Euroscore was compiled to quantify sensory and motor integrity by evaluating motor activity, orientation, and reaction to tactile, visual, and auditory stimuli.[30] To determine the Neuroscore, 10 items were assessed and scored separately, and then totaled to derive the overall Neuroscore. Each item was scored in a relatively binary fashion (present/absent, normal/abnormal) and assigned a score of 0 or 10 with 10 denoting an abnormal finding, and totaled to a maximum total Neuroscore of 100, with a higher Neuroscore denoting a more severe neurological deficit.

The neuro-status was assessed on the day before the experiment and on day 7. The beam-walk and beam-balance test were conducted in a quiet room in dim light on day 7 after ASDH induction. Before the operation, all animals were trained to walk along a beam

(diameter 1.8 cm, length 1 m, 2.5 cm between bars, 50 cm above ground) while the time to reach a black box was measured.[29]

Neuro-histological evaluation

The animals were transcardial-perfusion fixed with 0.9% saline and 4% paraformaldehyde (pH 7.4). Brains were carefully removed, post-fixed for 24 h, and embedded in paraffin wax. Sequential 3-μm thick coronal sections were cut 250 μm apart throughout the visible lesion space and stained with hematoxylin and eosin. The lesion on each section was quantified using Optimas 6.1 software combined with a CCD Super Color CV950 camera (Denmark) mounted on a Zeiss Axiopod 2Plus. From the measured area (A_n [mm^2]) on each section and the distance (d = 0.25 mm) between the consecutive sections the entire are of damage was calculated and expressed as the lesion volume (V, mm^3) by the following equation:

$$V = \sum (A_n \times d).$$

Statistical analysis

Data are expressed as mean ± stand error of the mean (SEM). Comparison of the different groups was performed using a one-way analysis of variance (ANOVA) or standard *t* test (Sigma-Plot 11.0, Systat, CA). Differences were considered statistically significant at $p < 0.05$. Subgroup analysis was performed comparing animals with and without sCSDs.

Results

ASDH elicits sCSDs (Experimental group 1)

To investigate the occurrence and influence of sCSDs on the outcome after ASHD, 300 μL autologous blood was subdurally injected and the physiological parameters, ICP, and tissue IMP were monitored starting 10 min prior to ASDH induction and were continued for 180 min. Arterial blood gases taken before and after infusion of blood remained stable with physiological boundaries over the course of the experiment.

Mean arterial blood pressure (MAP) showed peak values 10 min after ASDH induction (80.9 ± 3.44 mm Hg, $p = 0.017$) and recovered within 60 min to baseline levels of 61.08 ± 5.5 mm Hg (Fig. 1). No MAP increase was observed in sham operated animals. The ICP increased during ASDH induction with peak values of 47.14 ± 13.32 mm Hg at the end of the infusion (Fig. 1). Thereafter, it dropped to values twice as high as baseline and remained elevated during the entire monitoring period. As the ICP increased during ASDH induction, MAP showed a slightly shifted sinusoidal course as manifestation of the Cushing reflex (Fig. 1).

After ASDH induction, all animals displayed an initial increase of the tissue IMP, whereas no increased IMP was detectable in sham operated animals (Fig. 2A). The cerebral perfusion pressure (CPP) was inversely correlated to the IMP (Fig. 2B). Overall, three different traits of IMP were observed: (1) no sCSDs ($n = 7$), (2) detectable sCSDs ($n = 8$), and (3) continuous IMP elevation as equivalent of AD ($n = 5$) (Fig. 2C). IMP recordings were calibrated to 2254.44 ± 61.50 Ω as baseline readings and normalized to 100%. Subdural blood infusion initiated a collinear increase of IMP and ICP. No statistically significant difference in the initial IMP increment ($p = 0.685$) or duration ($p = 0.084$) was detected between animals with and without further sCSDs. Peak value of 172.55 ± 17.60% of baseline was reached at the end of infusion and IMP decreased within 30 min after ASDH induction. First sCSDs occurred 53.86 ± 1.73 min after ASDH in eight animals, whereas no

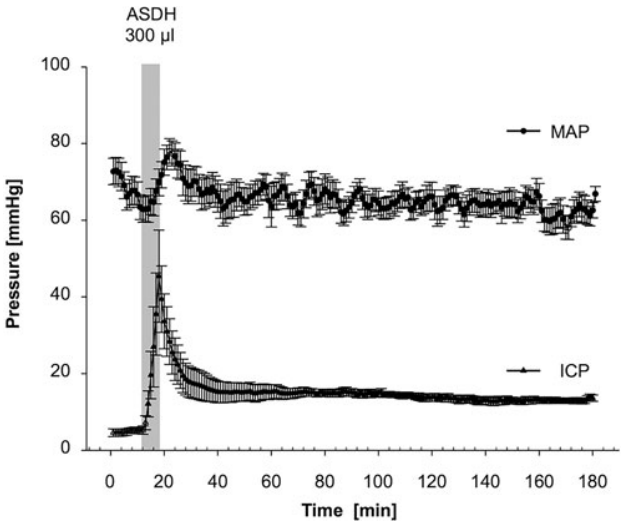

FIG. 1. Measurment of ICP and MAP during ASDH induction. MAP and ICP were measured starting 10 min prior to the subdural injection of 300 μL autologous blood and continued for 180 min ($n = 20$). The MAP showed peak values 10 min after ASDH induction (80.9 ± 3.44 mm Hg, $p = 0.017$) and recovered within 60 min to baseline levels. No MAP increase was observed in sham operated animals ($n = 3$). ICP increased during ASDH induction with peak values at the end of the infusion (47.14 ± 13.32 mm Hg). ICP and MAP showed slightly shifted sinusoidal curves as manifestation of the Cushing reflex. ASDH, acute subdural hemorrhage; ICP, intracranial pressure; MAP, mean arterial blood pressure.

sCSDs were observed in seven animals. On average 6 ± 0.58 sCSDs were observed. In five animals a continuous IMP elevation with peak values of 166.67 ± 21.01% of baseline was observed. Three of these animals died within 24 h after ASDH. All recorded sCSDs revealed similar traits. Each lasted 2.66 ± 0.31 min, whereas the first one lasted longest (3.43 ± 0.34 min) and the last one shortest (2.47 ± 0.28 min). The mean elevation of baseline was 15 ± 0.02 % and was consistent for each animal.

To evaluate the overall lesion volume, sequential coronal sections were cut throughout the visible lesion and stained with hematoxylin and eosin. The overall lesion volume for all animals was 46.2 ± 17.1 mm^3. If sCSDs had been detected, the lesion size was found to be larger by a statistical significance (56.7 ± 10.7 mm^3), compared with those without initial sCSDs (27.7 ± 10.4 mm^3; $p = 0.01$) (Fig. 3). Two animals classified as AD had a mean lesion size of 55.8 ± 3.7 mm^3.

sCSDs are more frequent and severe after autologous blood infusion leading to increased lesions and worse neurological outcomes (Experimental group 2)

In the second experimental group, paraffin oil was used as an inert volume substance to form a subdural mass lesion lacking blood constituents. Within this group the influence of whole blood constituents on sCSD occurrence, consecutive lesion size, and neurological outcome was analyzed. Twenty-eight animals were randomly assigned for autologous blood ($n = 13$), paraffin oil ($n = 12$), or sham ($n = 3$) operation. All peri-procedural parameters were measured comparable to the first experimental group.

MAP rose from 64.8 ± 3.1 mm Hg to peak values of 80.1 ± 7.3 mm Hg 6 min after the end of the infusion in the blood-infused animals. During paraffin oil infusion, MAP increased from 76.4 ± 2

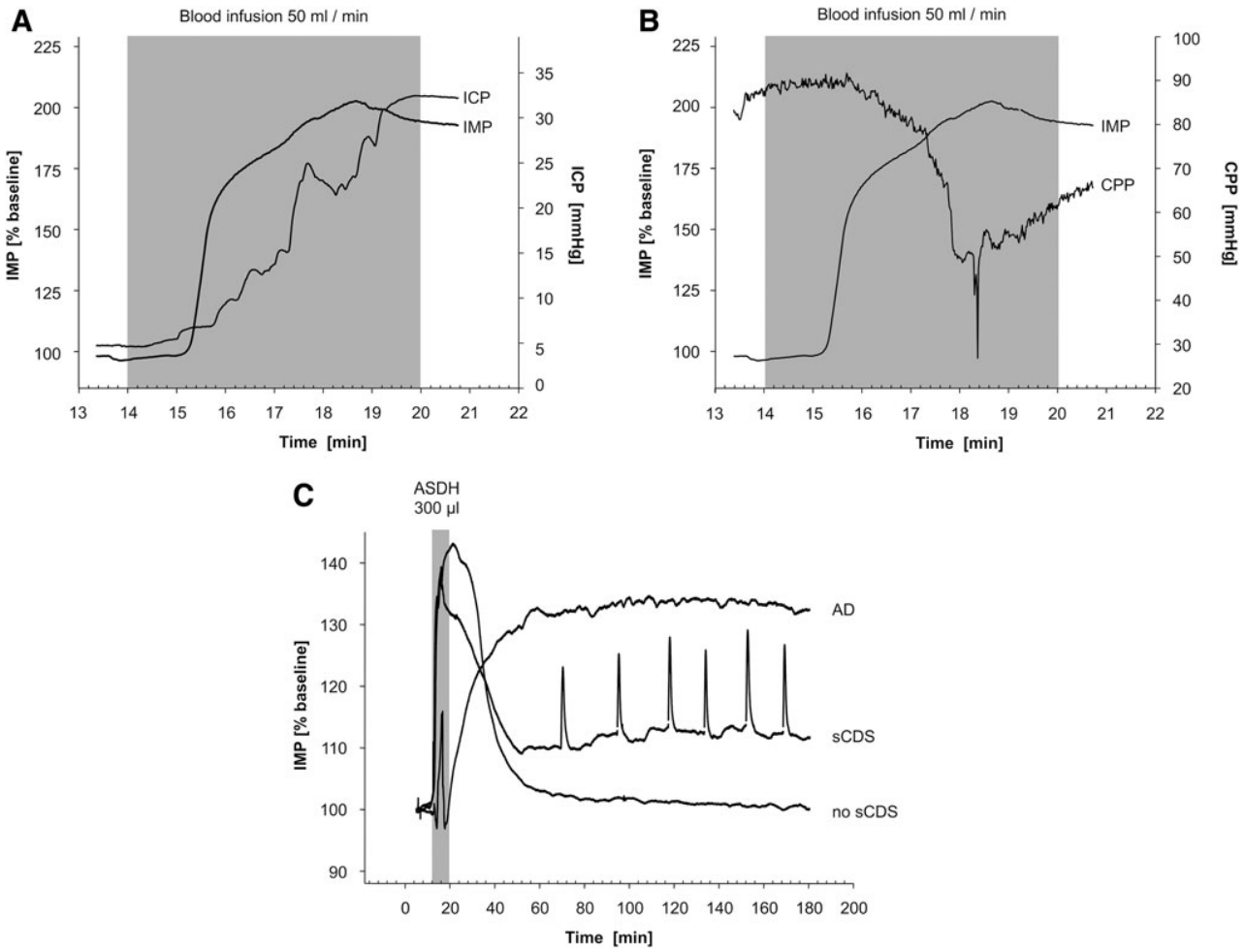

FIG. 2. IMP and ICP changes during and after subdural blood infusion. Depicted are the tissue IMP measurements in % of baseline. **(A)** IMP and ICP increased linearly in all animals during the subdural blood infusion and returned to elevated baseline levels within 30 min. **(B)** A CPP decrease was observed, while the IMP increased. **(C)** During the monitoring period, animals either exhibited continuous slightly elevated baseline IMP (no sCSD, $n=8$), intermittent sharp IMP elevations (sCSDs, $n=8$), or continuous high elevated IMP recordings (AD, $n=4$). AD, anoxic depolarization; ICP, intracranial pressure; IMP, impedance; sCSD, spontaneous cortical spreading depression.

to 80.6 ± 4.7 mm Hg showing no differences between both groups. ICP increased similarly during blood and paraffin injection and peaked at the end of the infusion (sham: 9 ± 2 mm Hg; blood: 52 ± 6 mm Hg; paraffin: 41 ± 6 mm Hg). CBF dropped in both treatment groups, reaching minimum values at the end of the infusion (blood: 26.9 ± 7.7% of baseline; paraffin: 35.4 ± 6.8% of baseline) (Fig. 4). During the observational period CBF temporarily exceed the baseline level after 15 min, before flattening of below baseline (blood: 74.1 ± 9.3 %; paraffin: 62.9 ± 4.3% after 180 min post ASDH induction). All CBF changes were of statistical significance within each group compared with baseline ($p<0.001$), whereas there was no significant difference between blood and paraffin oil infusion. Further, subgroup analysis revealed no significant difference in CBF between animals with and without sCSD.

Measurement of tissue IMP confirmed the classification of different IMP traits as observed in the first experimental group. Animals displaying no sCSDs, sCSDs, or AD were observed equally after autologous blood (no sCSDs, $n=4$; sCSDs, $n=4$; AD, $n=5$) or paraffin oil infusion (no sCSDs, $n=4$; sCSDs, $n=3$; AD, $n=5$). IMP recordings ranged from 1487 to 3023 Ω (2229 ± 358 Ω). All values were normalized to each individual baseline (100%). In those animals receiving autologous blood, an initial IMP increase of 149.8 ± 12.8% ($p=0.008$) compared with baseline levels was registered. Peak values were recorded 8.8 ± 1.6 min after the start of the infusion. In those animals receiving paraffin oil, peak values were registered after 5 min and reached 128.5 ± 10.6% of baseline levels. IMP remained elevated during the time of monitoring (blood: 106.09 ± 1.8 % [$p=0.015$]; paraffin: 108.0 ± 2.2% [$p=0.008$]). sCSDs were detected in both groups (blood, $n=4$; paraffin oil, $n=3$). After paraffin oil infusion, the first sCSD occurred after 14.9 ± 6.9 min (peak 118.2 ± 5.9%). An average number of 1.7 sCSD, which lasted for 11.2 ± 1.9 min, were detected in this group. In contrast, after blood infusion the first sCSD occurred after 91.11 ± 26.36 min (peak 114.8 ± 2.7%). In this group, an average of 6.8 sCSD, with a mean duration of 5.84 ± 0.69 min were detected. No sCSD occurred in sham operated controls. AD occurred after blood ($n=5$) and paraffin infusion ($n=5$). All AD animals died either intraoperatively or before the primary end-point of our study, and were therefore excluded.

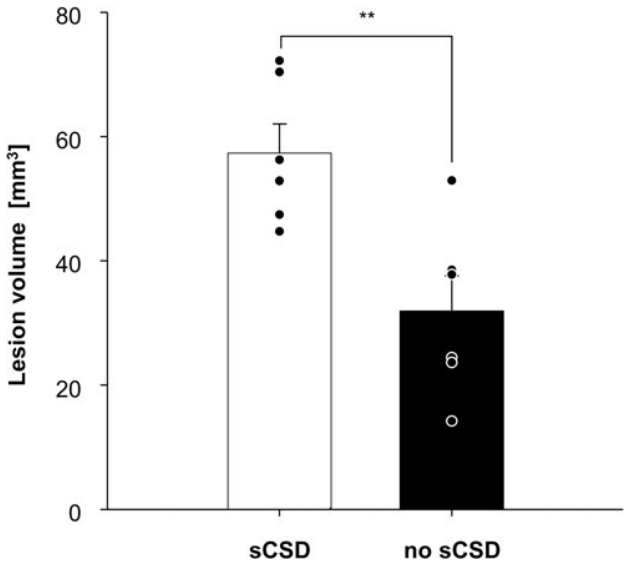

FIG. 3. Lesion size differs with the occurrence of sCSD. Lesion size of animals with sCSD showed significantly ($p=0.01$) larger cortical lesions 7 days after ASDH induction compared with animals without sCSD. ASDH, acute subdural hemorrhage; sCSD, spontaneous cortical spreading depression.

Lesion volumes were significantly larger after blood infusion ($27.3\pm6.8\,mm^3$) compared with paraffin infusion ($3.4\pm2.1\,mm^3$) ($p=0.004$) (Fig. 5A). A subgroup analysis showed that the lesion volumes largely differed within both groups between animals with sCSD (blood: $43.2\pm5.8\,mm^3$; paraffin: $4.4\pm2.4\,mm^3$) and those with no sCSD (blood: $11.5\pm3.5\,mm^3$; paraffin: $2.4\pm0.8\,mm^3$). Although the differences within the blood group reached statistical significance ($p=0.003$), the differences within the paraffin infusion group did not (Fig. 5B).

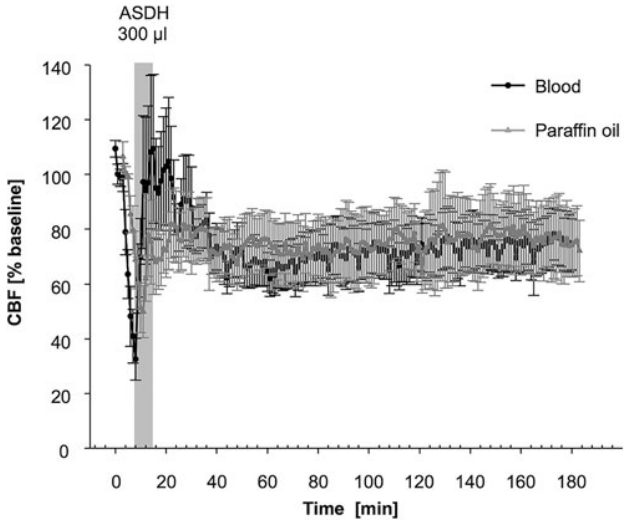

FIG. 4. Comparison of CBF in blood and paraffin oil treatment groups. The CBF was measured starting 5 min prior to the subdural injection of 300 μL autologous blood ($n=13$) or paraffin oil ($n=12$) and continued for 180 min. Measurment of CBF shows no significant variations between blood and paraffin oil treatment groups. CBF, cerebral blood flow.

A Neuroscore assessment was used to evaluate motor and behavioral deficits in relation to the subsequent analyzed lesion size. In both groups, animals with large lesions scored higher 7 days after ASDH, compared with those with smaller lesions (blood: $p<0.001$, $r^2=0.95$; paraffin: $p=0.014$, $r^2=0.59$), representing more severe deficits (Fig. 6A). Subgroup analysis revealed a linear association of sCSD and poorer scoring values ($p<0.001$, $r^2=0.96$), however not in the no sCSD group ($p=0.12$, $r^2=0.35$) (Fig. 6B). Animals needed significantly longer to solve the beam-walk test after autologous blood infusion (53.4 ± 2.6 sec), compared with those with paraffin lesions (30.4 ± 3.0 sec) ($p<0.001$). Additionally, all subgroups showed a significant correlation between a shorter beam-walk time and a larger lesion size (blood: $p=0.0068$, $r^2=0.73$, paraffin: $p=0.025$, $r^2=0.66$; sCSD: $p=0.0034$, $r^2=0.85$; no sCSD: $p=0.0019$, $r^2=0.82$). Finally, the beam-balance test revealed significant deficits in correlation to the lesion size in both treatment groups and the subgroup analysis (blood: $p=0.0003$, $r^2=0.91$; paraffin: $p=0.0013$, $r^2=0.89$; sCSD: $p=0.006$, $r^2=0.88$; no sCSD: $p=0.045$, $r^2=0.52$). A further subgroup analysis revealed that animals with sCSD balanced for a shorter time, compared with those without sCSDs (sCSD: 17.6 ± 3.6 sec; no sCSD 44.4 ± 4.4 sec; $p=0.005$) confirming that animals with sCSD have more severe neurological defects than these animals without sCSD.

Discussion

Our experiments demonstrate that sCSD occur in the wake of ASDH in rats. These sCSDs are more often, but not exclusively, observed in the presence of whole blood constituents. Although the appearance of sCSDs was in all cases associated with a larger lesion volume and more severe neurological deficits, statistical significance was only reached in those animals receiving subdural infusion of autologous blood. AD was associated with pre-term death of the animal.

sCSDs is an electrophysiological phenomenon with little impact on healthy tissue. However, cerebral ischemia seems to trigger sCSDs under various pathological conditions, leading to a supply-demand mismatch that creates a vicious circle propagating the delayed cerebral ischemia syndrome.[31] In compromised microvasculature, the attempted vasodilatation often fails, leading to a vasoconstriction and depolarization in this region instead.[20] If the spreading depolarization-induced perfusion deficit is so severe that it delays the energy-dependent recovery from sCSD, it leads to a prolonged change of the cortical slow potential indicating prolonged neuronal calcium overload.[13,20,32] This inverse hemodynamic response to spreading depolarization locally converts a harmless short-lasting depolarization into a harmful intermediate or even terminal depolarization.[20] The resulting perfusion deficit aggravates the need for energy substrates and increases the tissue at risk.[21] Under pathological conditions such as cerebral ischemia, TBI, or SAH, sCSD are known to increase O_2 consumption, resulting in neuronal swelling and contributing to neuronal injury.[5,7,33] The swollen neurons become acidic and lose their hyperpolarization, leading to the release of glutamate among other neurotransmitters and thus causing excitotoxicity of the surrounding tissue while propagating the spread.[10] sCSDs can last from several minutes to hours and cause vasoconstriction and consecutive lesion growth.[34–36] Additionally, the accumulation of hemolysis products hemoglobin and potassium after SAH can induce spreading ischemia, an inverse hemodynamic response to sCSD in tissue at risk, thus expanding cortical infarction.[37] In our experiments, the largest lesion size in the no sCSDs group was comparable to the smallest lesion in the sCSD

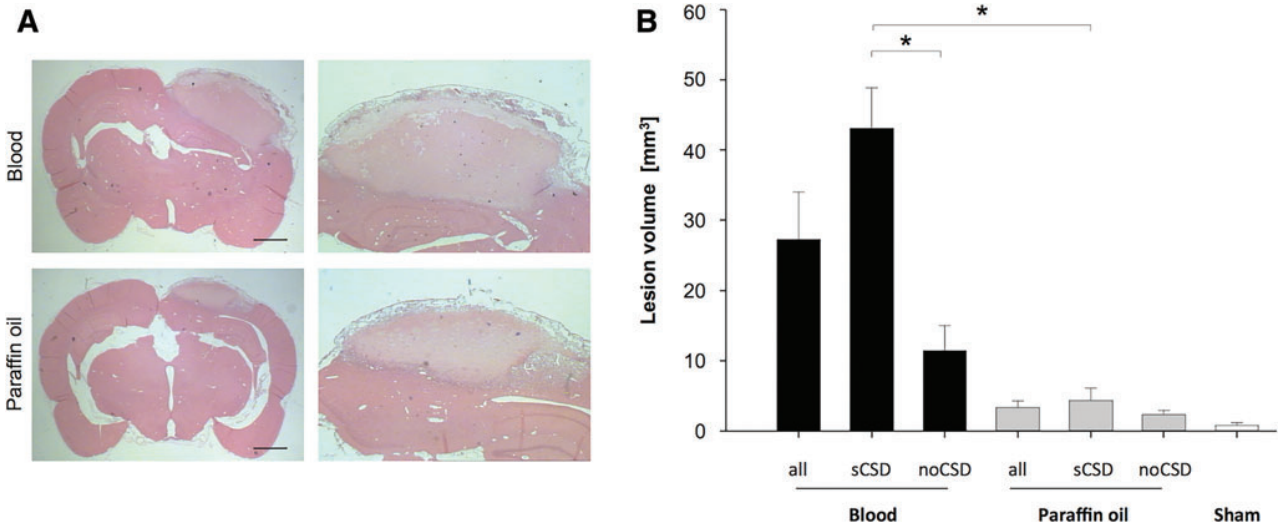

FIG. 5. Lesion size is larger after the occurrence of sCSDs. Lesion volume differed between autologous blood and paraffin oil injection and within the subgroups sCSD and no sCSD. **(A)** Representative paraffin section of cortical lesions stained in hematoxylin and eosin after blood and paraffin oil infusion. **(B)** Animals in the blood group showed larger lesions compared with paraffin oil, whereas subgroup analysis showed that lesion size was increased after the occurrence of sCSD (blood, $p = 0.003$; paraffin oil, $p = 0.956$). sCSD, spontaneous cortical spreading depression. Color image is available online at www.liebertpub.com/neu

group. Thus, the initial lesion size is not solely responsible for the occurrence of sCSDs and other contributory factors, such as blood constituents, are necessary to trigger their occurrence. Artificial induction of sCSDs after SAH, using cortical KCl, lead to significantly larger lesions in rats.[3] In 13 patients with SAH, hypoperfusion was coupled to the clustered occurrence of sCSD, resulting in local development of ischemic stroke.[38] These observations advocate a driving role of sCSD in lesion growth after TBI and SAH, rather than being an epiphenomenon of more severe brain damage. This observation is reinforced by another COSBID study, where spreading depolarization was found to cycle around an ischemic lesion and contribute to its perpetual enlargement.[39] In our experimental groups, increased numbers of sCSDs likewise coincided with larger lesions and more severe neurological deficits.

Similar predisposing factors as described for the occurrence of sCSD after SAH, can also be observed after ASDH. We could demonstrate that ASDH elicits sCSDs, which occur more often in the presence of blood constituents, rather than in the presence of

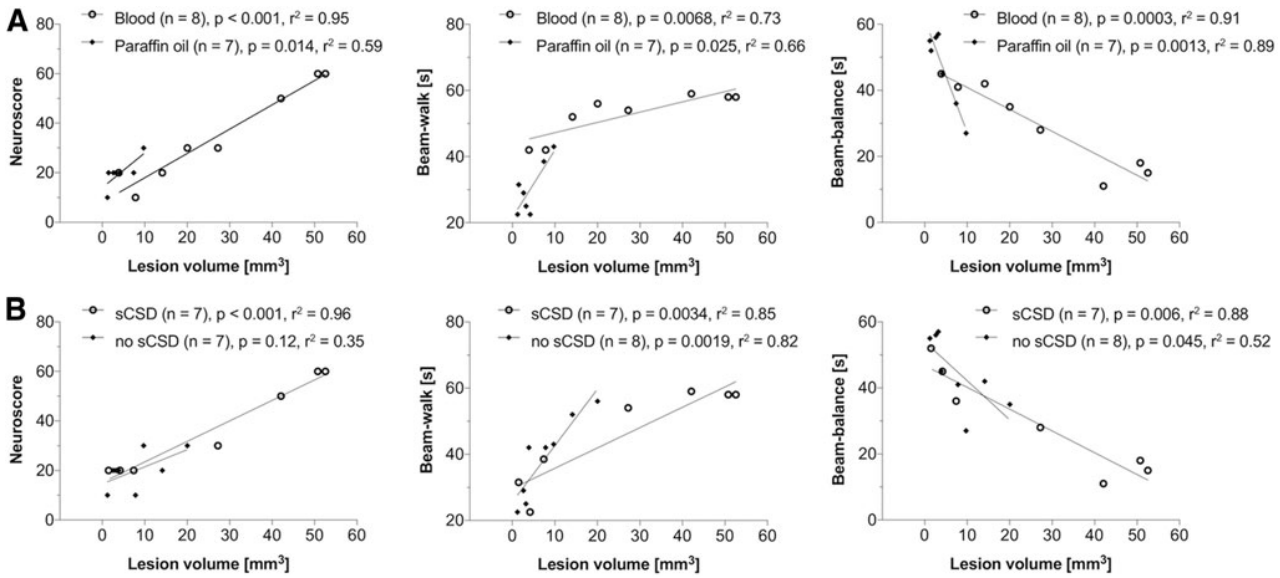

FIG. 6. Linear correlation between Neuroscore, beam-walk, and beam-balance test with the lesion volume 7 days post-operation. The association was analyzed between autologous blood and paraffin oil injection **(A)** and between the subgroups sCSD and no sCSD **(B)**. The Neuroscore does correlate with the lesion size in blood and the sCSD subgroups, not in the absence of sCSD. The beam-walk test and the beam-balance showed a significant correlation with the lesion volume in all subgroups. sCSD, spontaneous cortical spreading depression.

paraffin oil. Further, sCSD occurred independently of changes in CBF or ICP. In our study, lesion size and neurological deficit correlate more closely with the occurrence of sCSD in the presence of autologous blood and, subsequently, blood hemolysis products, than in the presence of paraffin oil. Number, frequency, and duration of sCSD were higher in animals injected with whole blood, underlining a possible interrelation of hemolysis products and sCSD pathogenesis. Nevertheless, neither the occurrence nor the number of sCSDs was a sole predictor of larger lesion volumes and neurological deficits in the absence of blood constituents. We demonstrated that larger lesion size does not necessarily lead to sCSD occurrence but rather is shaped by those spreading depressions. These results fall in line with the recent literature while broadening the scope by introducing ASDH as disease influenced by the occurrence of sCSD.[3,39]

It has long been thought that increased ICP was the main cause for the damage development underneath the blood clot. Recently, it became more evident, that this expansion is not solely due to elevated ICP, generated by a subdural volume, but a result of the interplay of ICP, CBF, and blood-derived products in the acute phase of hemorrhage.[40] MAP and ICP has been previously shown to follow similar traits after subdural infusion of blood or paraffin oil, although difference in lesion size is eveident.[41] Lesion volume, development of neurological deficits, and the occurrence of sCSD seem dependent on the presence of whole blood constituents such as thrombin, complement, and other blood-derived products. In contrast, direct intra-parenchymal thrombin injection, subdural infusion of lysed blood, or cortex superfusion with a mixture of hemoglobin and potassium caused a slow CBF decrease and sCSD.[36,42,43] sCSD elicitation by KCl injection causes a similar expansion of focal venous ischemic injury.[12] In our study, animals receiving paraffin oil instead of autologous blood as subdural volume substance, not only had smaller lesion volumes, but also performed better in neurological outcome assessments. sCSD occurred more seldom in the absence of blood constituents but still correlated with a poorer neurological outcome. It was recently shown that a combination of acute ICP increase, local CBF reduction, and the presence of blood constituents are critical for the damage caused by ASDH.[41] We detected no dependency of sCSD occurrence from CBF or ICP. On the contrary, it has recently been shown that each sCSDs increases the peri-infarct area where the CBF is reduced by 19%.[30,34] Pharmacological prevention of these periodical CBF drops leads to decreased lesion volumes 24 h after onset.[34] Thus, the occurrence of sCSDs represents an influencing factor, which might also determine the lesion size and neurological outcome after ASDH. It is noteworthy that no interrelation of sCSD and lesion size has been detected after controlled cortical impact, where no subdural blood collection was present.[44]

Results from a recent multi-center approach by the COSBID research group demonstrated that sCSD is a critical factor for outcome in patients with various traumatic and spontaneous pathologies.[19] Our presented data argue in a likewise fashion and emphasize that the largely excepted paradigm of sCSD contribution to secondary lesion development also applies to ASDH. In the light of these findings, clinical decision-making should consider a combination of blood removal to prevent the negative influence of blood constituents released by its degradation and monitoring of sCSD using ECoG. The invasive nature of monitoring sCSD over a prolonged period of time does currently hamper a broader usage.[19] Nevertheless, recognition and monitoring of sCSD might lead to a paradigm shift in our understanding of the pathophysiology of several brain injuries and thus pave the way for targeted anti-sCSD therapies including weak NMDA antagonists such as ketamine, NO donors, or nimodipine.[19]

In conclusion, we provide evidence that the accumulation of autologous blood increases the likelihood of sCSD occurrence in a rat ASDH model. sCSDs correlate with compromised neurological outcome in the pre- and absence of whole blood. Lesion growth was increased by sCSDs in animals receiving subdural autologous blood, whereas it only remained a trend in the animals receiving paraffin oil. We postulate that sCSDs are a contributing factor, but not the sole driver of lesion development and neurological deficit after ASDH.

Acknowledgments

We thank A. Ehlert, F. Kafai, L. Kopacz, and M. Malzahn for their technical and secretarial support during the experiments.

Author Disclosure Statement

No competing financial interests exist.

References

1. Leão, A.A.P. (1951). The slow voltage variation of cortical spreading depression of activity. Electroencephalogr. Clin. Neurophysiol. 3, 315–321.
2. Somjen, G.G. (2005). Aristides Leão's discovery of cortical spreading depression. J. of Neurophysiol. 94, 2–4.
3. Hamming, A.M., Wermer, M.J., Umesh Rudrapatna, S., Lanier, C., van Os, H.J., van den Bergh, W.M., Ferrari, M.D., van der Toorn, A., van den Maagdenberg, A.M., Stowe, A.M., and Dijkhuizen, R.M. (2016). Spreading depolarizations increase delayed brain injury in a rat model of subarachnoid hemorrhage. J. Cereb. Blood Flow Metab. 36, 1224–1231.
4. Kraig, R.P., and Nicholson, C. (1978). Extracellular ionic variations during spreading depression. Neuroscience 3, 1045–1059.
5. Takano, K., Latour, L.L., Formato, J.E., Carano, R.A., Helmer, K.G., Hasegawa, Y., Sotak, C.H., and Fisher, M. (1996). The role of spreading depression in focal ischemia evaluated by diffusion mapping. Ann. Neurol. 39, 308–318.
6. Zhou, N., Gordon, G.R., Feighan, D., and MacVicar, B.A. (2010). Transient swelling, acidification, and mitochondrial depolarization occurs in neurons but not astrocytes during spreading depression. Cereb. Cortex 20, 2614–2624.
7. Hartings, J.A., Bullock, M.R., Okonkwo, D.O., Murray, L.S., Murray, G.D., Fabricius, M., Maas, A.I., Woitzik, J., Sakowitz, O., Mathern, B., Roozenbeek, B., Lingsma, H., Dreier, J.P., Puccio, A.M., Shutter, L.A., Pahl, C., and Strong, A.J. (2011). Spreading depolarisations and outcome after traumatic brain injury: a prospective observational study. Lancet Neurol. 10, 1058–1064.
8. Dohmen, C., Sakowitz, O.W., Fabricius, M., Bosche, B., Reithmeier, T., Ernestus, R.I., Brinker, G., Dreier, J.P., Woitzik, J., Strong, A.J., and Graf, R. (2008). Spreading depolarizations occur in human ischemic stroke with high incidence. Ann. Neurol. 63, 720–728.
9. Dreier, J.P., Drenckhahn, C., Woitzik, J., Major, S., Offenhauser, N., Weber-Carstens, S., Wolf, S., Strong, A.J., Vajkoczy, P., and Hartings, J.A. (2013). Spreading ischemia after aneurysmal subarachnoid hemorrhage. Acta Neurochir. Suppl. 115, 125–129.
10. Kramer, D.R., Fujii, T., Ohiorhenuan, I., and Liu, C.Y. (2016). Cortical spreading depolarization: pathophysiology, implications, and future directions. J. Clin. Neuroscience 24, 22–27.
11. Tamaki, R., Orie, S.I., Alessandri, B., Kempski, O., and Heimann, A. (2017). Spreading depression and focal venous cerebral ischemia enhance cortical neurogenesis. Neural Regen. Res. 12, 1278–1286.
12. Otsuka, H., Ueda, K., Heimann, A., and Kempski, O. (2000). Effects of cortical spreading depression on cortical blood flow, impedance, DC potential, and infarct size in a rat venous infarct model. Exp. Neurol. 162, 201–214.
13. Lauritzen, M., Hansen, A.J., Kronborg, D.. and Wieloch, T. (1990). Cortical spreading depression is associated with arachidonic acid accumulation and preservation of energy charge. J. Cereb. Blood Flow Metab. 10, 115–122.

14. Leão, A.A.P. (1944). Pial circulation and spreading depression of activity in the cerebral cortex. J. Neurophysiol. 7, 391–396.
15. Windmuller, O., Lindauer, U., Foddis, M., Einhaupl, K.M., Dirnagl, U., Heinemann, U., and Dreier, J.P. (2005). Ion changes in spreading ischaemia induce rat middle cerebral artery constriction in the absence of NO. Brain 128, 2042–2051.
16. Hartings, J.A., Watanabe, T., Bullock, M.R., Okonkwo, D.O., Fabricius, M., Woitzik, J., Dreier, J.P., Puccio, A., Shutter, L.A., Pahl, C., Strong, A.J.; andthe Co-Operative Study on Brain Injury Depolarizations. (2011). Spreading depolarizations have prolonged direct current shifts and are associated with poor outcome in brain trauma. Brain 134, 1529–1540.
17. Piilgaard, H., and Lauritzen, M. (2009). Persistent increase in oxygen consumption and impaired neurovascular coupling after spreading depression in rat neocortex. J. Cereb. Blood Flow Metab. 29, 1517–1527.
18. Sukhotinsky, I., Dilekoz, E., Moskowitz, M.A., and Ayata, C. (2008). Hypoxia and hypotension transform the blood flow response to cortical spreading depression from hyperemia into hypoperfusion in the rat. J. Cereb. Blood Flow Metabolism 28, 1369–1376.
19. Lauritzen, M., Dreier, J.P., Fabricius, M., Hartings, J.A., Graf, R., and Strong, A.J. (2011). Clinical relevance of cortical spreading depression in neurological disorders: migraine, malignant stroke, subarachnoid and intracranial hemorrhage, and traumatic brain injury. J. Cereb. Blood Flow Metab. 31, 17–35.
20. Dreier, J.P. (2011). The role of spreading depression, spreading depolarization and spreading ischemia in neurological disease. Nature Med. 17, 439–447.
21. Fabricius, M., Fuhr, S., Bhatia, R., Boutelle, M., Hashemi, P., Strong, A.J., and Lauritzen, M. (2006). Cortical spreading depression and peri-infarct depolarization in acutely injured human cerebral cortex. Brain 129, 778–790.
22. Strong, A.J., Fabricius, M., Boutelle, M.G., Hibbins, S.J., Hopwood, S.E., Jones, R., Parkin, M.C., and Lauritzen, M. (2002). Spreading and synchronous depressions of cortical activity in acutely injured human brain. Stroke 33, 2738–2743.
23. Hartings, J.A., Shuttleworth, C.W., Kirov, S.A., Ayata, C., Hinzman, J.M., Foreman, B., Andrew, R.D., Boutelle, M.G., Brennan, K.C., Carlson, A.P., Dahlem, M.A., Drenckhahn, C., Dohmen, C., Fabricius, M., Farkas, E., Feuerstein, D., Graf, R., Helbok, R., Lauritzen, M., Major, S., Oliveira-Ferreira, A.I., Richter, F., Rosenthal, E.S., Sakowitz, O.W., Sanchez-Porras, R., Santos, E., Scholl, M., Strong, A.J., Urbach, A., Westover, M.B., Winkler, M.K., Witte, O.W., Woitzik, J., and Dreier, J.P. (2017). The continuum of spreading depolarizations in acute cortical lesion development: examining Leao's legacy. J. Cereb. Blood Flow Metab. 37, 1571–1594.
24. Kuroda, Y., and Bullock, R. (1992). Local cerebral blood flow mapping before and after removal of acute subdural hematoma in the rat. Neurosurgery 30, 687–691.
25. Jussen, D., Krenzlin, H., Papaioannou, C., Ens, S., Kempski, O., and Alessandri, B. (2017). Blood aggravates histological and functional damage after acute subdural hematoma in rats. J. Neurotrauma. 34, 906–913.
26. Hertle, D.N., Dreier, J.P., Woitzik, J., Hartings, J.A., Bullock, R., Okonkwo, D.O., Shutter, L.A., Vidgeon, S., Strong, A.J., Kowoll, C., Dohmen, C., Diedler, J., Veltkamp, R., Bruckner, T., Unterberg, A.W., and Sakowitz, O.W. (2012). Effect of analgesics and sedatives on the occurrence of spreading depolarizations accompanying acute brain injury. Brain 135, 2390–2398.
27. Hartings, J.A., Tortella, F.C., Strong, A.J., Bhatia, R., Bullock, M.R., Fabricius, M., Vo, H.A., Bell, R.S., Armonda, R.A., Ecklund, J.M. and Dreier, J.P. (2006). Spreading Depolarizations of Cerebral Cortex After Brain Injury: Mechanism of Injury Progression and Relevance to Military Neurotrauma. Walter Reed Army Institute of Research: Silver Springs, MD. Poster presentation at Army Science Conference.
28. Wang, Y.F., Yen, J.C., Kao, L.S., Fuh, J.L., and Wang, S.J. (2014). EHMTI-0140. The potential role of levetiracetam in migraine treatment: an animal study. J. Headache Pain 15, Suppl. 1, F30–F30.
29. Alessandri, B., Nishioka, T., Heimann, A., Bullock, R.M., and Kempski, O. (2006). Caspase-dependent cell death involved in brain damage after acute subdural hematoma in rats. Brain Res. 1111, 196–202.
30. Nedelmann, M., Wilhelm-Schwenkmezger, T., Alessandri, B., Heimann, A., Schneider, F., Eicke, B.M., Dieterich, M., and Kempski, O. (2007). Cerebral embolic ischemia in rats: correlation of stroke severity and functional deficit as important outcome parameter. Brain Res. 1130, 188–196.
31. Oka, F., Hoffmann, U., Lee, J.H., Shin, H.K., Chung, D.Y., Yuzawa, I., Chen, S.P., Atalay, Y.B., Nozari, A., Hopson, K.P., Qin, T., and Ayata, C. (2017). Requisite ischemia for spreading depolarization occurrence after subarachnoid hemorrhage in rodents. J. Cereb. Blood Flow Metab. 37, 1829–1840.
32. Windmüller, O., Lindauer, U., Foddis, M., Einhäupl, K.M., Dirnagl, U., Heinemann, U., and Dreier, J.P. (2005). Ion changes in spreading ischaemia induce rat middle cerebral artery constriction in the absence of NO. Brain 128, 2042–2051.
33. Bosche, B., Graf, R., Ernestus, R.I., Dohmen, C., Reithmeier, T., Brinker, G., Strong, A.J., Dreier, J.P., and Woitzik, J. (2010). Recurrent spreading depolarizations after subarachnoid hemorrhage decreases oxygen availability in human cerebral cortex. Ann. Neurol. 67, 607–617.
34. Shin, H.K., Dunn, A.K., Jones, P.B., Boas, D.A., Moskowitz, M.A., and Ayata, C. (2006). Vasoconstrictive neurovascular coupling during focal ischemic depolarizations. J. Cereb. Blood Flow Metab. 26, 1018–1030.
35. Strong, A.J., Anderson, P.J., Watts, H.R., Virley, D.J., Lloyd, A., Irving, E.A., Nagafuji, T., Ninomiya, M., Nakamura, H., Dunn, A.K., and Graf, R. (2007). Peri-infarct depolarizations lead to loss of perfusion in ischaemic gyrencephalic cerebral cortex. Brain 130, 995–1008.
36. Dreier, J.P., Ebert, N., Priller, J., Megow, D., Lindauer, U., Klee, R., Reuter, U., Imai, Y., Einhaupl, K.M., Victorov, I., and Dirnagl, U. (2000). Products of hemolysis in the subarachnoid space inducing spreading ischemia in the cortex and focal necrosis in rats: a model for delayed ischemic neurological deficits after subarachnoid hemorrhage? J. Neurosurg. 93, 658–666.
37. Dreier, J.P., Woitzik, J., Fabricius, M., Bhatia, R., Major, S., Drenckhahn, C., Lehmann, T.N., Sarrafzadeh, A., Willumsen, L., Hartings, J.A., Sakowitz, O.W., Seemann, J.H., Thieme, A., Lauritzen, M., and Strong, A.J. (2006). Delayed ischaemic neurological deficits after subarachnoid haemorrhage are associated with clusters of spreading depolarizations. Brain 129, 3224–3237.
38. Dreier, J.P., Major, S., Manning, A., Woitzik, J., Drenckhahn, C., Steinbrink, J., Tolias, C., Oliveira-Ferreira, A.I., Fabricius, M., Hartings, J.A., Vajkoczy, P., Lauritzen, M., Dirnagl, U., Bohner, G., and Strong, A.J. (2009). Cortical spreading ischaemia is a novel process involved in ischaemic damage in patients with aneurysmal subarachnoid haemorrhage. Brain y132, 1866–1881.
39. Nakamura, H., Strong, A.J., Dohmen, C., Sakowitz, O.W., Vollmar, S., Sue, M., Kracht, L., Hashemi, P., Bhatia, R., Yoshimine, T., Dreier, J.P., Dunn, A.K., and Graf, R. (2010). Spreading depolarizations cycle around and enlarge focal ischaemic brain lesions. Brain 133, 1994–2006.
40. Baechli, H., Behzad, M., Schreckenberger, M., Buchholz, H.G., Heimann, A., Kempski, O., and Alessandri, B. (2009). Blood-induced brain edema, tissue death and depression of glucose metabolism in rat cortex after acute subdural hematoma is larger than after identical volumes of inert paraffin oil. J. Cereb. Blood Flow Metab. 30, 576–585.
41. Jussen, D., Krenzlin, H., Papaioannou, C., Ens, S., Kempski, O., and Alessandri, B. (2017). Blood aggravates histological and functional damage after acute subdural hematoma in rats. J. Neurotrauma 34, 906–913.
42. Fujimoto, S., Katsuki, H., Ohnishi, M., Takagi, M., Kume, T., and Akaike, A. (2007). Thrombin induces striatal neurotoxicity depending on mitogen-activated protein kinase pathways in vivo. Neuroscience 144, 694–701.
43. Gao, B.B., Clermont, A., Rook, S., Fonda, S.J., Srinivasan, V.J., Wojtkowski, M., Fujimoto, J.G., Avery, R.L., Arrigg, P.G., Bursell, S.E., Aiello, L.P., and Feener, E.P. (2007). Extracellular carbonic anhydrase mediates hemorrhagic retinal and cerebral vascular permeability through prekallikrein activation. Nature Med. 13, 181–188.
44. von Baumgarten, L., Trabold, R., Thal, S., Back, T., and Plesnila, N. (2008). Role of cortical spreading depressions for secondary brain damage after traumatic brain injury in mice. J. Cereb. Blood Flow Metab. 28, 1353–1360.

Address correspondence to:
Harald Krenzlin, MD
Institute for Neurosurgical Pathophysiology
Johannes Gutenberg-University Mainz, Germany
Langenbeckstrasse 1
55101 Mainz
Germany

E-mail: h.krenzlin@t-online.de

Cytomegalovirus promotes murine glioblastoma growth via pericyte recruitment and angiogenesis

Harald Krenzlin,[1] Prajna Behera,[1] Viola Lorenz,[2] Carmela Passaro,[1] Mykola Zdioruk,[1] Michal O. Nowicki,[1] Korneel Grauwet,[1] Hong Zhang,[1] Magdalena Skubal,[1] Hirotaka Ito,[1] Rachel Zane,[1] Michael Gutknecht,[3] Marion B. Griessl,[3] Franz Ricklefs,[4] Lai Ding,[5] Sharon Peled,[6] Arun Rooj,[1] C. David James,[7] Charles S. Cobbs,[8] Charles H. Cook,[3] E. Antonio Chiocca,[1] and Sean E. Lawler[1]

[1]Department of Neurosurgery, Brigham and Women's Hospital, [2]Division of Newborn Medicine, Boston Children's Hospital, and [3]Department of Surgery, Beth Israel Deaconess Medical Center, Harvard Medical School, Boston, Massachusetts, USA. [4]Department of Neurosurgery, University Medical Center Hamburg-Eppendorf, Hamburg, Germany. [5]Program for Interdisciplinary Neuroscience, NeuroTechnology Studio, Brigham and Women's Hospital, Boston, Massachusetts, USA. [6]Department of Radiology, Brigham and Women's Hospital, Harvard Medical School, Boston, Massachusetts, USA. [7]Department of Neurosurgery, Feinberg School of Medicine, Northwestern University, Chicago, Illinois, USA. [8]Swedish Neuroscience Institute, Ben and Catherine Ivy Center for Advanced Brain Tumor Treatment, Seattle, Washington, USA.

Cytomegalovirus (CMV) has been implicated in glioblastoma (GBM); however, a mechanistic connection in vivo has not been established. The purpose of this study is to characterize the effects of murine CMV (MCMV) on GBM growth in murine models. Syngeneic GBM models were established in mice perinatally infected with MCMV. We found that tumor growth was markedly enhanced in MCMV$^+$ mice, with a significant reduction in overall survival compared with that of controls ($P < 0.001$). We observed increased angiogenesis and tumor blood flow in MCMV$^+$ mice. MCMV reactivation was observed in intratumoral perivascular pericytes and tumor cells in mouse and human GBM specimens, and pericyte coverage of tumor vasculature was strikingly augmented in MCMV$^+$ mice. We identified PDGF-D as a CMV-induced factor essential for pericyte recruitment, angiogenesis, and tumor growth. The antiviral drug cidofovir improved survival in MCMV$^+$ mice, inhibiting MCMV reactivation, PDGF-D expression, pericyte recruitment, and tumor angiogenesis. These data show that MCMV potentiates GBM growth in vivo by increased pericyte recruitment and angiogenesis due to alterations in the secretome of CMV-infected cells. Our model provides evidence for a role of CMV in GBM growth and supports the application of antiviral approaches for GBM therapy.

Introduction

Glioblastoma (GBM) is the most common malignant brain tumor, with approximately 10,000 new cases per year in the US. There is no effective treatment, and patient survival remains dismal (1, 2). The standard-of-care treatment combining maximal surgical resection, irradiation, and temozolomide has a median survival of 14.6 months (3), and 5-year survival rates are below 10% (4). Despite remarkable progress in our understanding of the genetics and cell biology of GBM (1, 2), little progress has been made in improving patient survival. Major clinical challenges include tumor invasiveness and the delivery of drugs across the blood-brain barrier as well as inter- and intratumoral heterogeneity and drug resistance. Recent work has suggested a potential role for human cytomegalovirus (HCMV) in GBM growth, although this is not well understood at present.

HCMV is highly prevalent in human populations, and following resolution of primary infection, persists for the lifetime of its host in a latent state, periodically reactivating during periods of stress and immunocompromise (5). Interestingly, HCMV proteins and nucleic acids have been identified in up to 90% of GBM specimens (6–10) as well as in some other cancers (11, 12). Accumulating clinical data support the relevance of HCMV in GBM (13–19), with some encouraging responses reported with HCMV-targeted immunotherapies (14–18). Vaccination with DCs pulsed with tumor lysates led to expansion of mostly anti-CMV T cells in 1 responder (14), and CMV pp65 mRNA–pulsed autologous DCs showed promising long-term survival data in GBM (15–17). Ex vivo expansion of anti-CMV T cells and their administration in combination with temozolomide led to increased long-term progression-free survival (18). Data from primary GBM patients suggested that the antiviral drug valganciclovir could prolong median overall survival (19).

Although various HCMV proteins increase GBM cell proliferation, invasion, and angiogenesis (20, 21), a mechanistic link between HCMV and cancer in vivo has not been established, and the role of HCMV in GBM remains a subject of debate, with some groups unable to detect the presence of CMV in tumor specimens (22, 23). The use of mouse models to investigate the role of CMV in tumor growth would therefore be helpful in understanding the potential importance of CMV in GBM as well as providing an opportunity to rationally investigate antiviral therapeutic approaches. Using a genetically engineered GBM mouse model, we previously showed that systemic murine CMV (MCMV) infection accelerates malignant glioma progression (24), but no mechanism was established. To address this question, here we developed and characterized an MCMV GBM mouse model based on

Conflict of interest: The authors have declared that no conflict of interest exists.

Submitted: July 16, 2018; **Accepted:** February 5, 2019.
Reference information: *J Clin Invest*. 2019;129(4):1671–1683.
https://doi.org/10.1172/JCI123375.

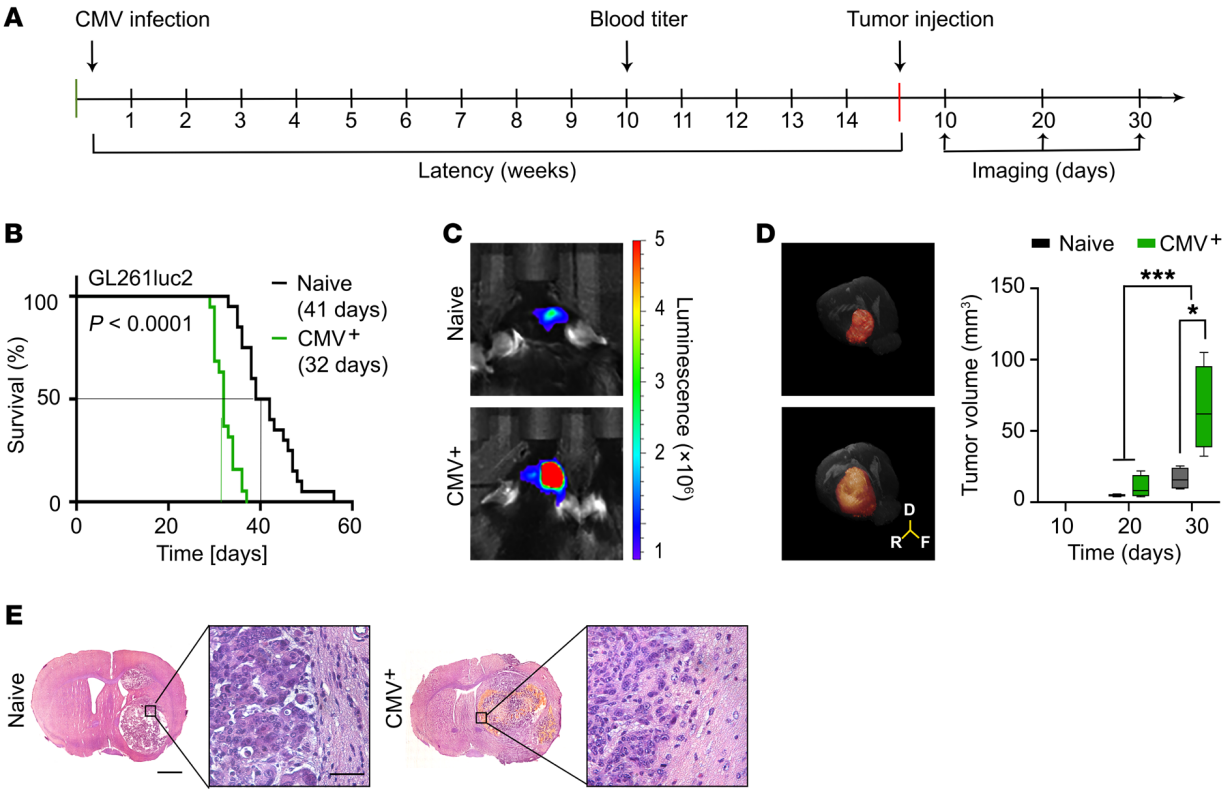

Figure 1. MCMV infection accelerates GBM growth in mice. (**A**) Experimental overview. (**B**) Kaplan-Meier curves of GL261Luc2 tumor-bearing mice. Uninfected, $n = 20$; MCMV$^+$, $n = 19$. $P < 0.0001$, log-rank test. Median survival is indicated on plot and shown in parentheses. (**C**) BLI and (**D**) MRI analysis of tumor-bearing MCMV$^+$ and control animals 30 days after tumor implantation. (**D**) Tumor volume rendering from MRI images (left), tumor volume over time (right). $n = 3$. Box extends from the 25th to 75th percentile, and the median is indicated by a horizontal line. The whiskers represent the maximum and minimum values. Statistical analysis was performed by 2-way ANOVA with Bonferroni's correction. $^*P < 0.05$; $^{***}P < 0.005$. (**E**) H&E staining of GL261Luc2 tumors at end points. Scale bars: 1 mm (left panels); 50 μm (right panels).

orthotopically injected murine GBMs in a syngeneic background. Our data demonstrate that tumor growth is significantly faster in the presence of MCMV and that angiogenesis is significantly ($P < 0.005$)elevated in these tumors, with a striking increase in pericyte coverage of tumor-associated blood vessels. We identified PDGF-D as an essential mediator of these effects. The angiogenic phenotype was reversed by the antiviral drug cidofovir. These data support a role for CMV in accelerating GBM growth via a proangiogenic mechanism and provide a rationale for the use of antiviral therapies in CMV-associated tumors, such as GBM.

Results

CMV accelerates GBM growth in a mouse model. To investigate the role of CMV in GBM in vivo, C57BL/6 mice were infected at P2 with Δm157 Smith strain MCMV (MCMV$^+$) and allowed to resolve over at least 15 weeks (24) (Figure 1A). We stereotactically implanted luciferase-expressing murine GL261Luc2 GBM cells intracranially in MCMV$^+$ and naive control mice. MCMV$^+$ mice had significantly shorter survival than controls ($P < 0.001$) (Figure 1B) and earlier onset of clinical signs of deterioration, including weight loss (Supplemental Figure 1A; supplemental material available online with this article; https://doi.org/10.1172/JCI123375DS1). Bioluminescence imaging (BLI) revealed significantly faster tumor growth in MCMV$^+$ mice compared with controls (Figure 1C and Supplemental Figure 1B). This was confirmed by T2-weighted MRI, which showed significantly larger tumor volumes in MCMV$^+$ mice (Figure 1D and Supplemental Figure 1C). Histologic analysis showed increased hemorrhage and poorly defined tumor margins in MCMV$^+$ mice compared with controls (Figure 1E).

Increased angiogenesis in MCMV$^+$ murine GBM. Further histological examination showed a pronounced increase in Ki67 and CD31 staining in MCMV$^+$ mice, suggesting enhanced cell proliferation and tumor angiogenesis (Figure 2, A and B). Consistent with this, image analysis (25) showed that total blood vessel length, total area of vessel coverage, and vessel branching were significantly increased in MCMV$^+$ mouse tumors (Figure 2B). We confirmed this MCMV-associated phenotype using a second murine GBM cell line, CT-2A (26), which also displayed significantly shorter survival and increased blood vessel parameters in MCMV$^+$ mice compared with controls (Figure 2, C and D). Accordingly, increased intratumoral blood flow was observed in MCMV$^+$ mice compared with controls by arterial spin-labeling–functional MRI (ASL-fMRI) (Figure 2E). Thus, our data show that the presence of preexisting MCMV infection is associated with increased angiogenesis, elevated intratumoral blood flow, and faster tumor growth in a mouse GBM model.

Detection of CMV in pericytes and tumor cells in both mouse and human GBM. HCMV immediate early 1 (IE1) and pp65 gene products have been detected in human GBM (6–10). Similarly, we detected MCMV expression by immunofluorescence microscopy

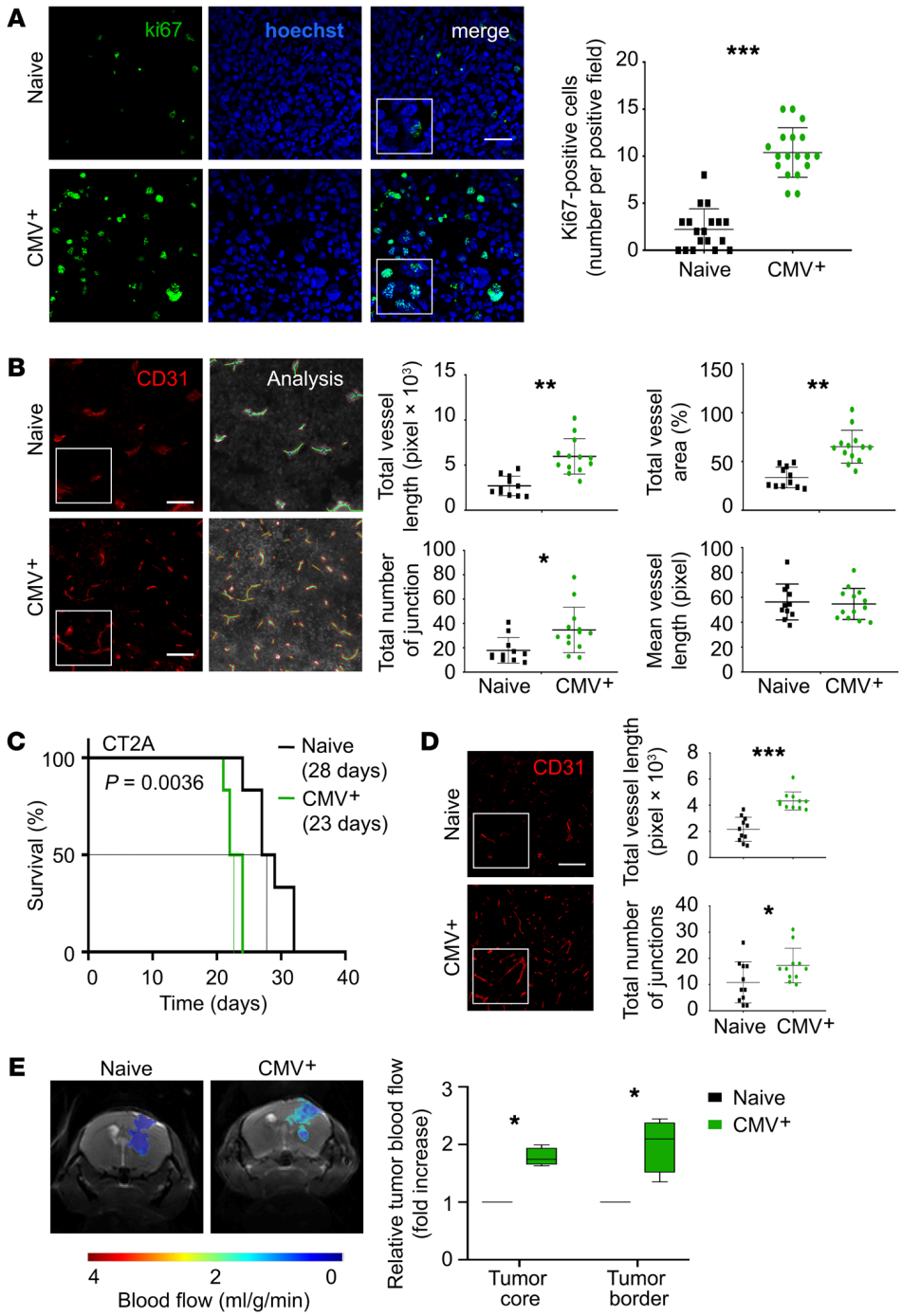

Figure 2. MCMV infection accelerates GBM blood vessel formation in mice. (**A**) Ki67 (green) immunofluorescence in brain sections taken from animals at the end point of survival studies. DAPI-stained nuclei are shown in blue. Scale bar: 50 μm. Graph shows Ki67-positive nuclei counts from 12 independent fields in 3 tumor samples. ***$P < 0.005$, Student's t test. (**B**) CD31 (red) immunofluorescence in sections from GL261Luc2 tumors at survival end points (left panels). Scale bars: 100 μm. AngioTool analysis (right panels). Graphs show data for vascular parameters. Images are from 12 independent fields for each condition. $n = 4$. *$P < 0.05$; **$P < 0.01$ Student's t test. (**C**) Kaplan-Meier survival curve of mice intracranially implanted with the murine CT-2A GBM cell line. Uninfected ($n = 6$) vs. MCMV$^+$ ($n = 6$). $P < 0.01$, log-rank test. Median survival is indicated on plot and shown in parentheses. (**D**) Left panels show CD31 immunofluorescence staining (red) of tumor vasculature in 20 μm sections from CT-2A tumors in control and MCMV$^+$ animals at survival end points. Scale bar: 100 μm. Graphs show representations of the data for vascular parameters based on analysis of angiogenesis and vessel morphology. Images are from 12 independent fields and 3 tumor specimens for each condition. *$P < 0.05$; ***$P < 0.005$, Student's t test. (**E**) ASL-fMRI showing T2 coronal sections with ASL heatmap overlay. Quantitative analysis of both groups at corresponding ROIs. $n = 3$. Box extends from the 25th to 75th percentile, and the median is indicated by a horizontal line. Whiskers represent the maximum and minimum values. *$P < 0.05$, Student's t test.

in GBMs from MCMV$^+$ but not control mice (Figure 3A and Supplemental Figure 2A) and observed a time-dependent increase of the MCMV IE1 homolog m123 mRNA by quantitative reverse-transcriptase PCR (qRT-PCR) after tumor implantation (Figure 3B). MCMV immunostaining was mostly localized in tumors and was heterogeneous. Extratumoral MCMV immunostaining was confined to the choroid plexus and ventricular regions and was otherwise absent from normal brain tissue, consistent with previous observations (24, 27) (Supplemental Figure 2B). No MCMV reactivation was detected in lung tissue from MCMV$^+$ tumor-bearing mice (Supplemental Figure 2C). Costaining of tumors from MCMV$^+$ mice for the endothelial cell marker CD31 localized MCMV in the perivascular niche (Figure 3C). MCMV is known to infect pericytes (28), and immunostaining also colocalized with the pericyte marker NG2 in close proximity to tumor-associated blood vessels (Figure 3C). Additionally, MCMV colocalized with tumor cell markers CD133 and luciferase (Supplemental Figure 2D). Thus, MCMV is present in both tumor cells and the perivascular niche of GBMs in MCMV$^+$ mice.

Immunostaining for NG2 revealed striking differences between MCMV$^+$ mice and controls, with extensive coverage of tumor vasculature with NG2$^+$ cells in MCMV$^+$ mice only (Figure 3D). Immunostaining and flow cytometry showed a marked increase (up to 400%) of intratumoral NG2$^+$ cells in MCMV$^+$ mice

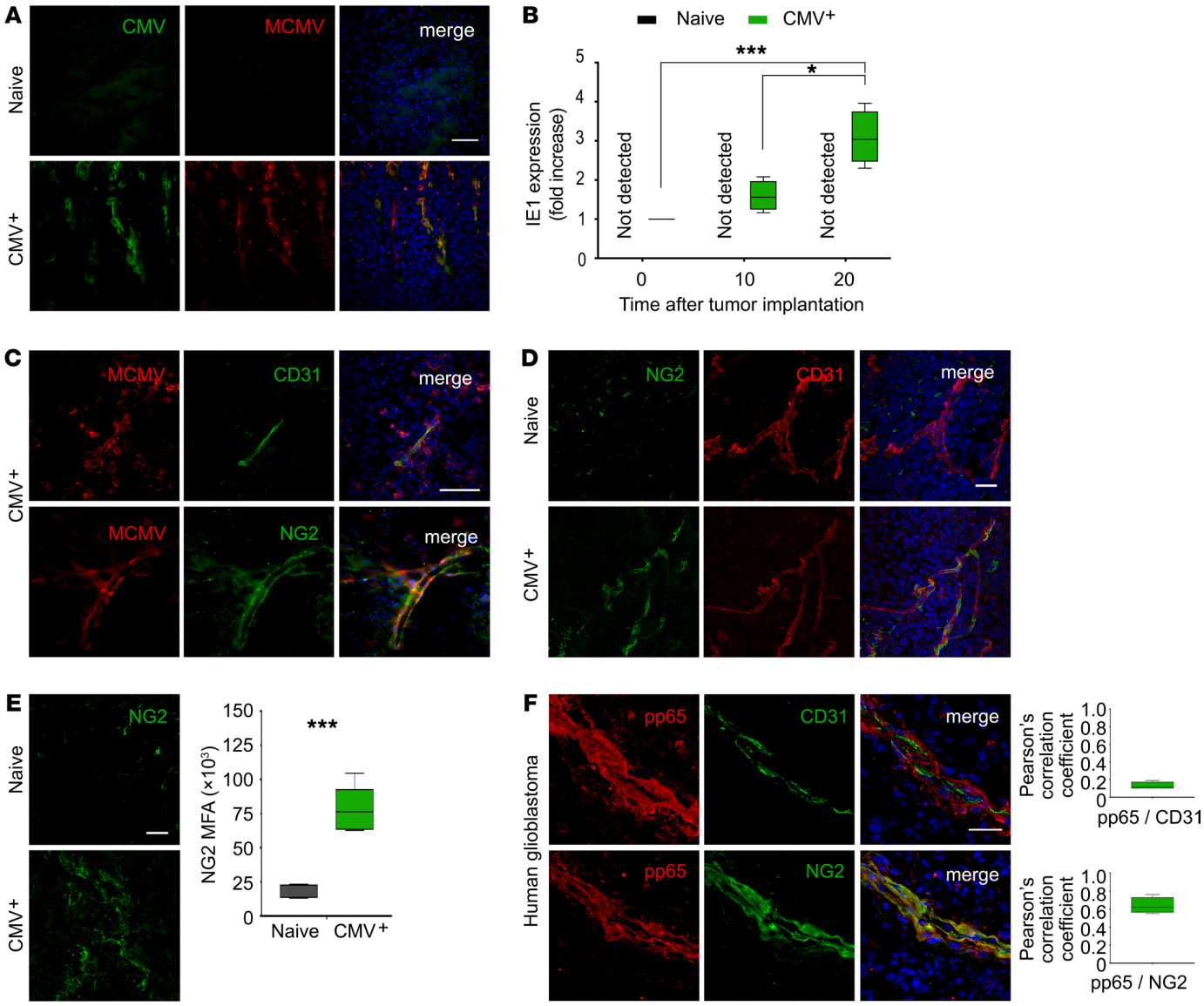

Figure 3. CMV associates with vascular pericytes in GBM. (**A**) CMV (green, Virusys CA150-1 antibody; red, Virusys CA003-100 antibody) immunofluorescence staining in brain sections from animals at the end point of survival studies. DAPI-stained nuclei are shown in blue. Scale bar: 50 μm. (**B**) Real-time qPCR analysis of MCMV IE1/m123 mRNA levels in GL261Luc2 tumors from MCMV⁺ and naive mice. $n = 3$. Box extends from 25th to 75th percentile, and median is indicated by horizontal line. Whiskers represent maximum and minimum values. $^*P < 0.05$; $^{***}P < 0.005$, Holm-Šídák test. (**C**) CMV (red, Virusys CA003-100), CD31 (green), and NG2 (green) immunofluorescence in tumor sections from MCMV⁺ mice. DAPI-stained nuclei are shown in blue. Scale bar: 50 μm. (**D**) CD31 (red), NG2 (green), and nuclei (blue) immunofluorescence in tumors from MCMV⁺ mice. Scale bar: 50 μm. (**E**) NG2 fluorescence intensity in 12 independent fields of view from murine GBMs. $n = 3$. Box extends from 25th to 75th percentile, and median is indicated by horizontal line. Whiskers represent maximum and minimum values. Scale bar: 50 μm. $^{***}P < 0.005$, Student's t test. (**F**) CMV (red, Virusys CA003-100), CD31 (green), and NG2 (green) immunostaining immunofluorescence in human GBM. Scale bar: 50 μm. Pearson's rank colocalization. $n = 3$. Box extends from 25th to 75th percentile, and median is indicated by horizontal line. Whiskers represent maximum and minimum values.

(Figure 3E and Supplemental Figure 2E). NG2 staining in MCMV⁺ animals strongly colocalized with the pericyte marker PDGFR-β, whereas no colocalization was observed with Olig2, a classic marker of NG2-positive glial cells (28), confirming that these MCMV/NG2-positive cells are pericytes and not glial cells (Supplemental Figure 2F). Together, these data show MCMV-associated accumulation of pericytes in GBM vasculature and suggest that these pericytes can harbor CMV in vivo.

To confirm our findings in human GBM, we immunohistochemically visualized HCMV (Figure 3F and Supplemental Figure 3, A and B). HCMV pp65 and IE1 were not detected in normal human brain by immunofluorescence (Supplemental Figure 3C). In human tumor specimens, HCMV colocalized with GBM markers CD133, Olig2, and vimentin (Supplemental Figure 3, D and E). Also, strong colocalization of HCMV with perivascular NG2⁺ cells, but not CD31⁺ endothelial cells (Figure 3F and Supplemental Figure 3D), was observed in human GBM, a finding consistent with HCMV association with pericytes. Furthermore, IE1 was detected in 17 out of 18 GBM samples and absent in pooled cortical control RNA (Supplemental Figure 3F). In summary, our data show wide-

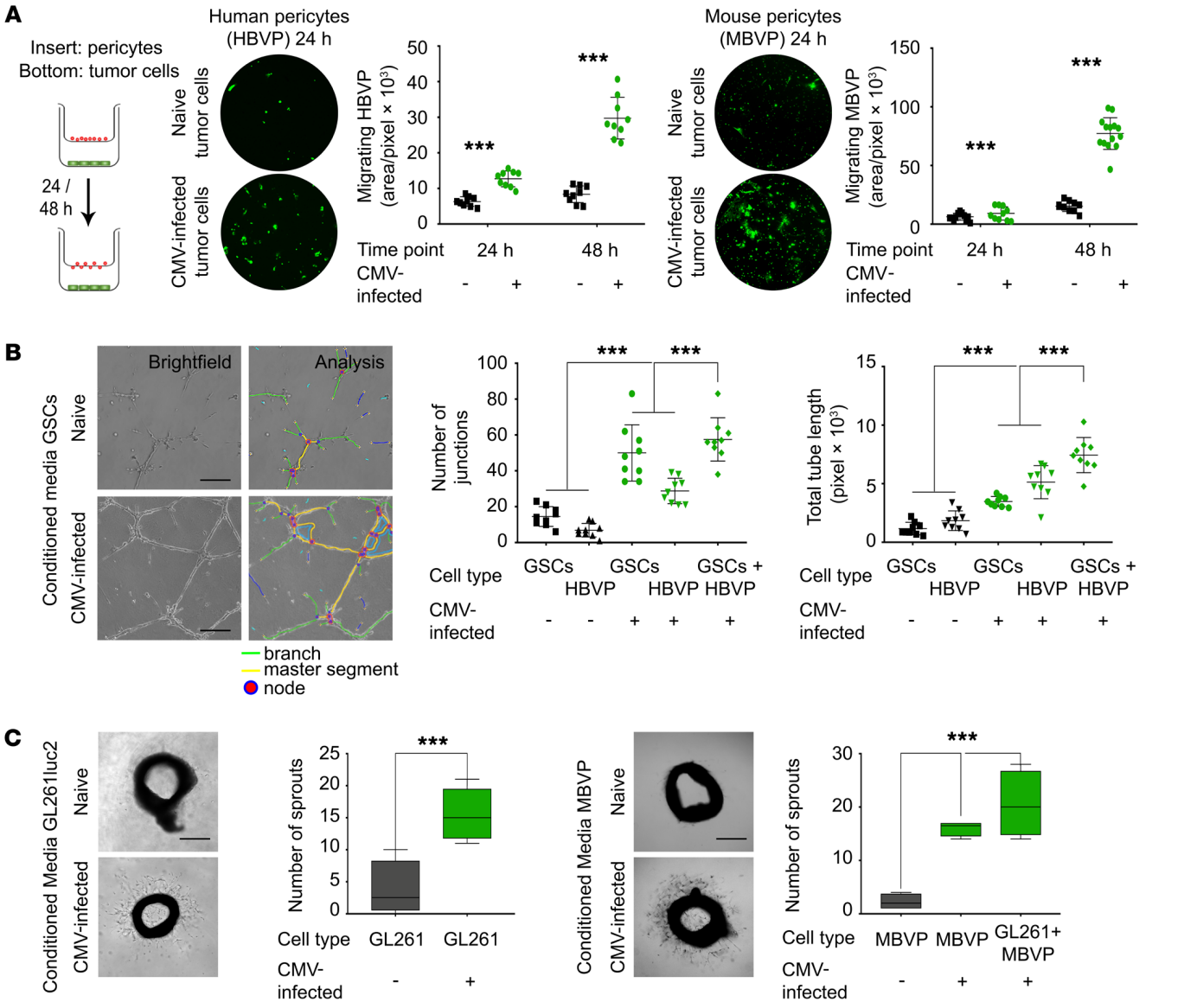

Figure 4. Conditioned medium from CMV-infected GBM cells increases pericyte migration and endothelial cell tube formation. (**A**) Transwell migration of HBVPs and MBVPs. Data are presented as mean ± SD. ***$P < 0.005$, Holm-Šídák test. (**B**) HBMEC tube formation on Matrigel performed in the presence of conditioned media from HCMV-infected human GSCs or HBVPs. Data are presented as mean ± SD. ***$P < 0.005$, Holm-Šídák test. (**C**) Aortic ring assay performed using conditioned media from uninfected and CMV-infected GL261Luc2 cells or MBVPs. Graphical representation shows number of sprouting vessels. Data are presented as box and whisker plot. Box extends from 25th to 75th percentile, and median is indicated by horizontal line. Whiskers represent maximum and minimum values. ***$P < 0.005$, 2-way ANOVA. Scale bars: 50 μM (**B**); 1 mm for (**C**).

spread detection of HCMV in GBM, and while the perivascular niche seems to be a major site of CMV infection, infected cells are observed throughout the tumor tissue in all specimens ($n = 5$) analyzed. Colocalization of NG2 and pp65 was estimated as very high (86.2% ± 11.1%). Thus, in human GBM, HCMV staining patterns are similar to those observed in the MCMV⁺ mouse GBM model.

The CMV-infected cell secretome increases pericyte migration and angiogenesis in vitro. Pericytes have been implicated in GBM and are known to participate in angiogenesis, vessel stabilization, and regulation of cerebral blood flow (29–32). We therefore studied how CMV might mechanistically enhance pericyte accumulation and angiogenesis in GBM. Because CMV is readily detectable in both human and murine tumor cells, we hypothesized that CMV-infected tumor cells might attract pericytes. Using Transwell coculture assays, we confirmed that brain vascular pericytes migrate faster toward CMV-infected tumor cells compared with uninfected controls in both human and murine contexts (Figure 4A). To further investigate the effects of CMV infection of pericytes and GBM cells on angiogenesis, we cultured human brain microvascular endothelial cells (HBMECs) with conditioned media from HCMV-infected patient-derived GBM stem-like cells (GSCs) or human brain vascular pericytes (HBVPs). Both media induced significant increases in tube formation compared with control media, and when conditioned media from HCMV-infected GSCs and HBVPs were combined, tube formation was further enhanced (Figure 4B).

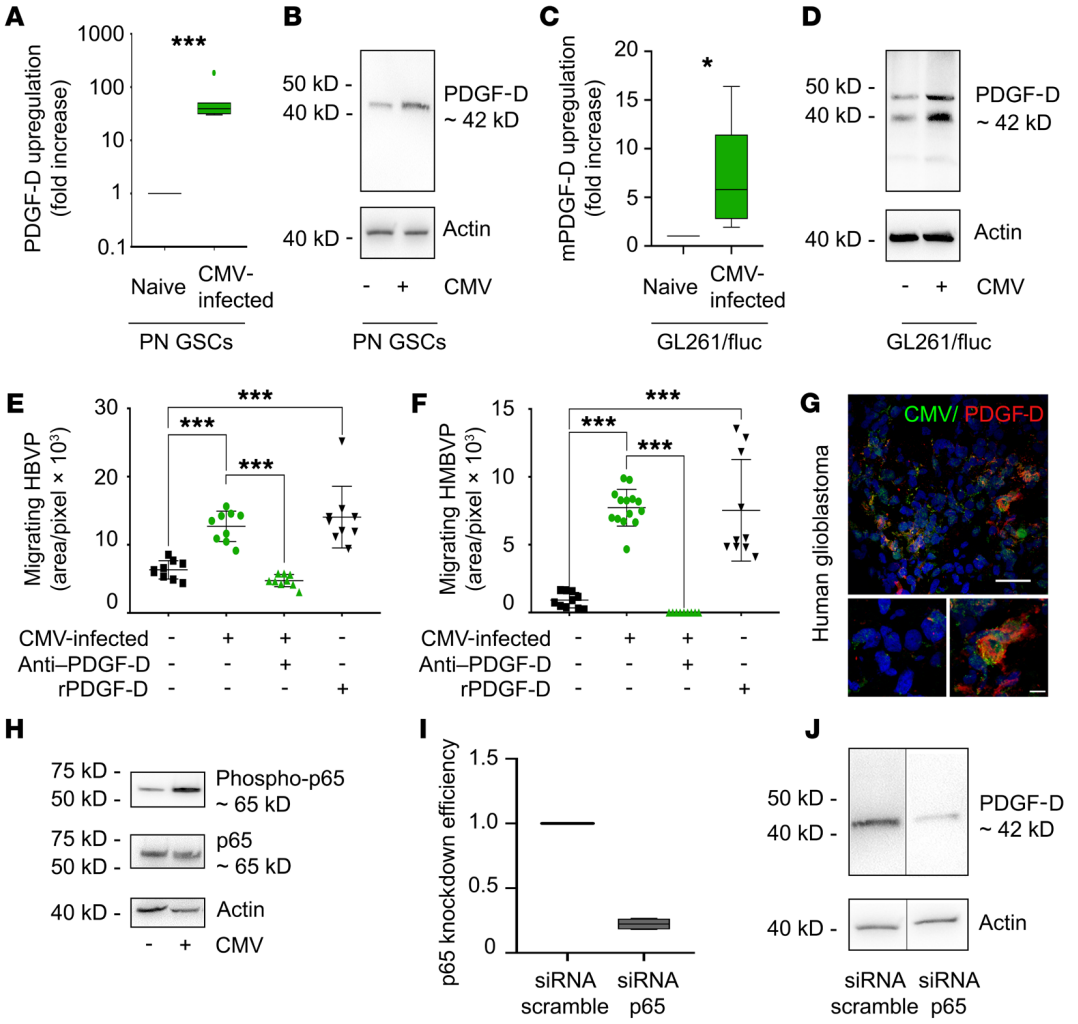

Figure 5. PDGF-D upregulation by CMV in GBM. (**A**) qRT-PCR for PDGF-D in GSCs after HCMV infection. Box extends from 25th to 75th percentile, and median is indicated by horizontal line. Whiskers represent the maximum and minimum values. Outlier is shown by a green circle. (**B**) Western blot for PDGF-D in GSCs after HCMV infection. (**C**) qRT-PCR for PDGF-D in GL261Luc2 cells after MCMV infection. Box extends from 25th to 75th percentile, and median is indicated by horizontal line. Whiskers represent maximum and minimum values. (**D**) Western blot for PDGF-D in GL261Luc2 cells after MCMV infection. qRT-PCR data are represented as mean ± SD. $^{*}P < 0.05$; $^{***}P < 0.005$, Student's *t* test (**A** and **C**). (**E** and **F**) Transwell migration of HBVP and MBVP in the presence and absence of PDGF-D–neutralizing antibodies, or recombinant PDGF-D (rPDGF-D), as indicated. CMV-infected GBM cells and controls were grown on the bottom of a 12-well plate, as shown. Data are represented as mean ± SD. $^{***}P < 0.005$, Holm-Šídák test. (**G**) PDGF-D (red) and CMV (green) immunofluorescence showing areas of high CMV (lower right) and low CMV (lower left) in human GBM. DAPI-stained nuclei are shown in blue. Scale bar: 50 μm (upper images) 10 μm (lower images). (**H**) Increased phosphorylation of NF-κB p65 subunit RelA in G44 GSCs 24 hours after infection with HCMV Towne strain. (**I**) siRNA-mediated knockdown of RelA in G44 GSCs 48 hours after transfection. Box extends from 25th to 75th percentile, and median is indicated by horizontal line. Whiskers represent maximum and minimum values. (**J**) PDGF-D downregulation in response to HCMV infection after RelA knockdown in G44 GSCs.

When explanted mouse aortic rings were exposed to media from MCMV-infected GL261Luc2 cells or infected mouse brain vascular pericytes (MBVPs), there was increased endothelial cell sprouting, with the combination of both media showing the greatest effect (Figure 4C). Taken together, these data suggest a model in which CMV infection of GBM cells and/or pericytes induces a proangiogenic secretome.

CMV-induced PDGF-D regulates pericyte recruitment and angiogenesis in vitro. Consistent with the effects of CMV-conditioned medium on angiogenesis, RNA-Seq of human GSCs after HCMV infection showed angiogenesis as a prominent Gene Ontology (GO) term. To prioritize genes further, we compared upregulated genes after HCMV infection of G44 GSCs with a curated list of secreted proangiogenic proteins. This identified 6 mRNAs with potential proangiogenic roles upregulated in HCMV-infected GSCs: BMP4 (33), CCL2 (34), CXCL8 (35), LIF (36), WNT4 (37), and PDGFD, as shown in Supplemental Table 1. Of these, PDGF-D, a known regulator of pericyte function (38–40), has not been studied in GBM. Because of the pronounced effect on pericytes in our mouse model, we further investigated the potential role of PDGF-D in mediating the observed phenotypes. Independent validation confirmed that PDGF-D was upregulated in GSCs after HCMV infection at both the mRNA and protein levels, and this upregulation persisted over time in human GSCs after HCMV infection (Figure 5, A and B, and Supplemental Figure 4, A and B). *Pdgfd* mRNA and protein upregulation were also observed in MCMV-infected murine GL261Luc2 cells (Figure 5, C and D). Functional studies showed that migration of both human and

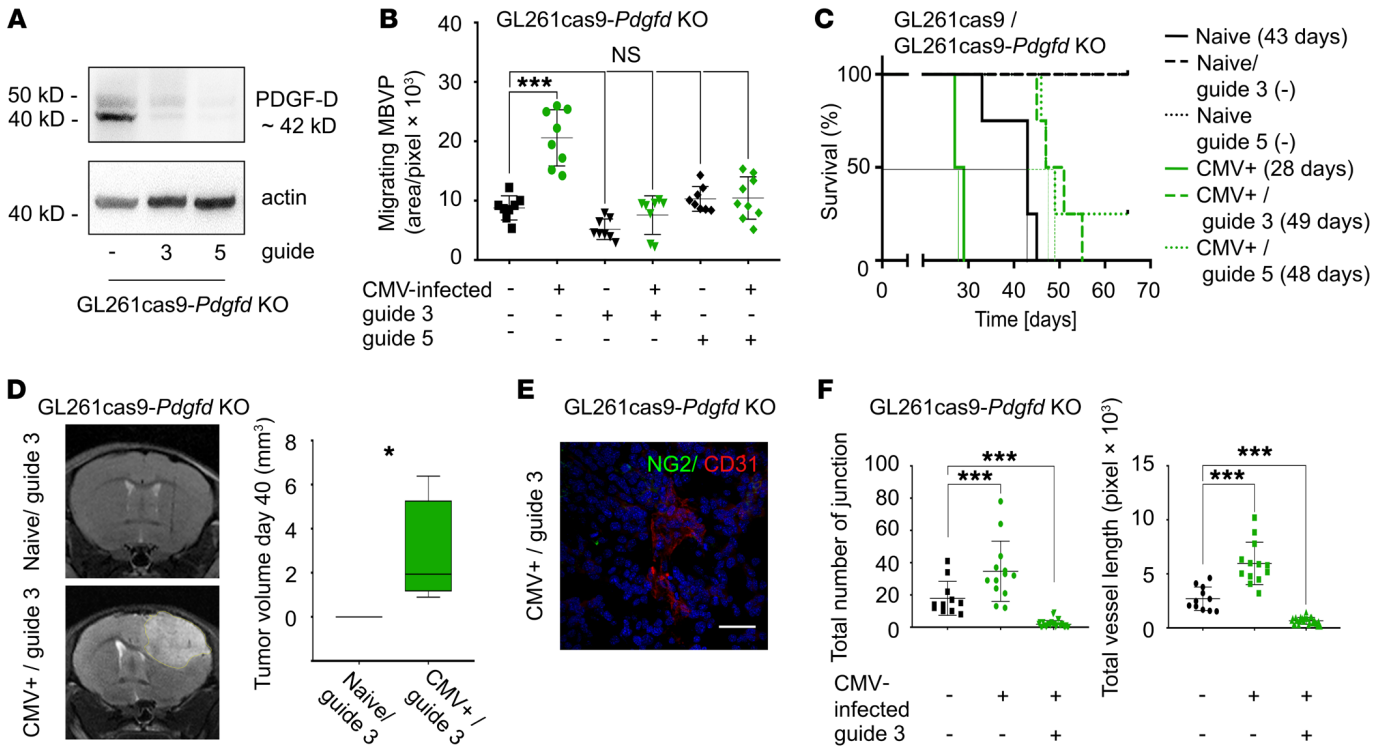

Figure 6. PDGF-D mediates the effects of MCMV in murine GBM. (**A**) Western blot for PDGF-D in GL261cas9-*Pdgfd*-KO cells. (**B**) Transwell migration assay of MBVPs toward GL261cas9-*PDGFD*-KO cells. Data are represented as mean ± SD. ***$P < 0.005$, 2-way ANOVA. (**C**) Kaplan-Meier curves of naive and MCMV$^+$ mice intracranially implanted with GL261Cas9 ($n = 4$), GL261cas9-*Pdgfd*-KO (guide 3) ($n = 4$), or GL261cas9-*Pdgfd*-KO guide 5 ($n = 4$). Median survival is indicated on plot and shown in parentheses. (**D**) T2-weighted MRI at day 30. Box extends from 25th to 75th percentile, and median is indicated by horizontal line. Whiskers represent the maximum and minimum values. *$P < 0.05$, 2-way ANOVA. (**E**) CD31 (red), NG2 (green), and nuclei (blue) immunofluorescence in GL261*Pdgfd*-KO tumors at end points. Scale bar: 50 μm. (**F**) Quantitative analysis of angiogenesis and vessel morphology in tumor sections. Data are represented as mean ± SD. **$P < 0.01$; ***$P < 0.005$, 2-way ANOVA.

murine pericytes toward CMV-infected GBM cells was abolished by a PDGF-D–neutralizing antibody, while recombinant PDGF-D induced vigorous pericyte migration (Figure 5, E and F). In addition, endothelial tube formation by HCMV-infected GSC-conditioned medium was partially blocked by PDGF-D–neutralizing antibodies, and recombinant human PDGF-D induced tube formation, although to a lesser extent than CMV-infected cell-conditioned medium (Supplemental Figure 4C). Immunofluorescence showed that PDGF-D was widespread in MCMV$^+$ GL261Luc2 tumors and in human GBM specimens, where it partially colocalized with HCMV pp65 staining (Figure 5G and Supplemental Figure 4D). In contrast, intratumoral PDGF-D was barely detectable in MCMV-naive controls (Supplemental Figure 4D), and in normal human brain, PDGF-D staining was confined only to vasculature (Supplemental Figure 4E). Taken together, these data suggest that CMV-induced PDGF-D expression may play an important role in GBM biology.

To further investigate the upregulation of PDGF-D expression after CMV infection, we examined the potential signaling pathways involved. It has been previously reported that CMV infection leads to activation of the NF-κB–signaling pathway (41, 42). It has also been reported in ChIP-Seq studies that PDGF-D expression may be NF-κB regulated (43); therefore, we investigated this pathway in our GSCs. Western blotting against the phosphorylated p65/RELA subunit of NF-κB 24 hours after infection of G44 GSCs with HCMV indicated that the pathway was activated (Figure 5H). Treatment of G44 GSCs with siRNA against RELA/p65 efficiently knocked down RELA (Figure 5I) and ablated upregulation of PDGF-D in response to HCMV infection, as shown by Western blotting (Figure 5J). Thus, NF-κB is involved in PDGF-D upregulation by HCMV in GSCs.

Pdgfd knockdown impairs GBM growth in vivo. To further investigate the role of PDGF-D in CMV-induced GBM growth, *Pdgfd* was knocked out (*Pdgfd*-KO) in GL261 cells using CRISPR/cas9 technology (Figure 6A). Loss of PDGF-D expression was verified by Western blotting (Figure 6A). CMV infection did not restore PDGF-D expression in *Pdgfd*-KO cells (Supplemental Figure 5A). *Pdgfd*-KO cells showed growth kinetics and MCMV infection similar to those of control cells in vitro (Supplemental Figure 5B), but showed impaired pericyte attraction compared with control cells after MCMV infection (Figure 6B). Consistent with our model, orthotopically implanted PDGF-D–competent GL261Cas9 cells grew as tumors, with mortality significantly enhanced in MCMV$^+$ mice compared with naive mice (Figure 6C). In contrast, MCMV-naive mice receiving *Pdgfd*-KO tumor cells all survived more than 60 days (Figure 6C), suggesting a critical role for PDGF-D in GBM progression. Interestingly, lethality was restored when *Pdgfd*-KO tumors were implanted in MCMV$^+$ mice, albeit it was significantly delayed compared with what occurred with PDGF-D–competent tumors (Fig-

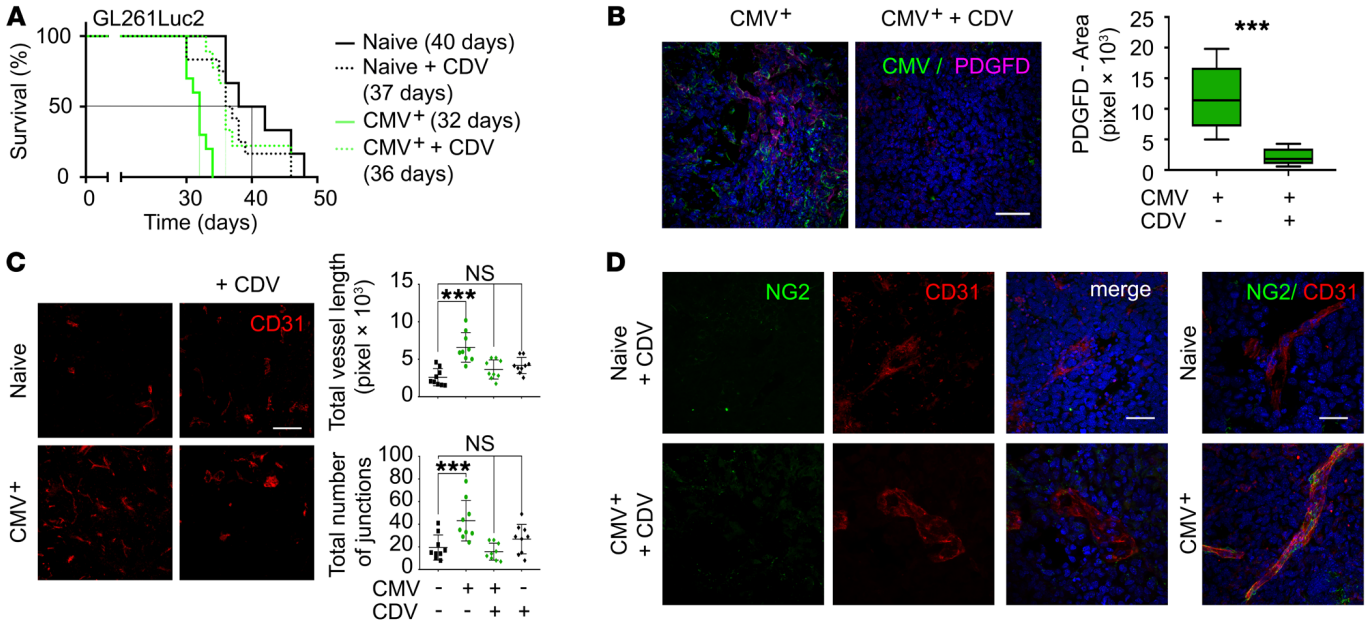

Figure 7. Cidofovir reverses CMV-induced proangiogenic phenotype in MCMV⁺ GBM mice. (**A**) Kaplan-Meier survival curve of naive and MCMV⁺ GL261Luc2 tumor-bearing mice treated with cidofovir (CDV). Median survival is indicated on plot and shown in parentheses. (**B**) CMV (green, Virusys CA150-1 antibody) and PDGF-D (magenta) immunofluorescence of tumor sections from CDV-treated mice. DAPI-stained nuclei are shown in blue. Scale bar: 100 μm. Box plot shows quantitation of PDGF-D fluorescence intensity (n = 3). Box extends from 25th to 75th percentile, and median is indicated by horizontal line. Whiskers represent maximum and minimum values. ***P < 0.005, Student's t test. Error bars indicate SD. (**C**) Quantitative analysis of angiogenesis and vessel morphology after CDV treatment. Scale bar: 100 μm. ***P < 0.005, 2-way ANOVA. Error bars indicate SD. Scale bar: 50 μm. (**D**) CD31 (red), NG2 (green), and nuclei (blue) immunofluorescence in tumor sections at survival end points after CDV treatment.

ure 6C). MRI performed at day 40 confirmed *Pdgfd*-KO tumor establishment only in MCMV⁺ animals (Figure 6D). *Pdgfd*-KO tumors showed reduced accumulation of pericytes and reduced vessel coverage (Figure 6E), with fewer vessels and branch junctions compared with PDGF-D–competent controls, consistent with impaired angiogenesis (Figure 6F). Together, these results demonstrate an essential role for PDGF-D in GBM growth that can be rescued by MCMV.

The antiviral drug cidofovir reverses the growth-promoting effects of MCMV in the mouse GBM model. The presence of elevated MCMV mRNA and protein after tumor implantation suggested importance of viral activity in our tumor-progression phenotype. To confirm this, MCMV⁺ mice were treated with the viral DNA synthesis inhibitor cidofovir (44) after tumor implantation. Whereas cidofovir treatment had no effect on the survival of naive GL261Luc2 tumor-bearing mice, it significantly improved survival in MCMV⁺ mice compared with untreated controls (Figure 7A). These observations suggest that, under these treatment conditions, cidofovir does not have direct antitumor effects, as tumor growth in MCMV-naive mice was unchanged. Consistent with a direct antiviral effect, MCMV immunostaining was markedly decreased in cidofovir-treated MCMV⁺ mice, and this was associated with dramatically decreased PDGF-D staining and reduction of tumor vascularization to CMV-naive levels (Figure 7, B and C). Finally, cidofovir treatment led to the reversal of MCMV-induced vascular pericyte accumulation (Figure 7D). Together, these results suggest that CMV acts as a critical potentiator of tumor progression by stimulating PDGF-D expression, pericyte accumulation, and GBM angiogenesis.

Discussion

Here, we provide what we believe is the first report of an in vivo mechanism underlying the promotion of GBM growth by CMV. We have shown that MCMV infection clearly potentiates tumor growth in implantable intracranial murine GBM models. We identified PDGF-D as an essential factor for intracranial GBM growth whose expression is induced by CMV infection of GSCs and stimulates both pericyte attraction and angiogenesis. Importantly, CMV-stimulated tumor growth is reversed by treatment with cidofovir, an FDA-approved antiviral agent (44). Together, these data provide support for the potential clinical importance of CMV in GBM progression and suggest both CMV and PDGF-D as targets in GBM therapy.

Proangiogenic effects of CMV. The most striking effects in CMV⁺ mice were on angiogenesis. We observed (a) increased intratumoral blood vessel length and branching, (b) increased pericyte coverage of intratumoral blood vessels, (c) increased intratumoral blood flow, (d) a proangiogenic secretome in CMV-infected pericytes, and (e) a proangiogenic and pericyte-attracting secretome in CMV-infected GBM cells. These observations support the concept that a CMV-mediated increase in vessel number and maturity is likely to be a major factor in the increased tumor growth in the context of the MCMV⁺ mice. Indeed, it has been established that CMV has proangiogenic effects in nontumoral settings (45–47), and a role in tumor angiogenesis has been previously speculated, although never established (48). One of our most striking observations was the striking increase in pericyte coverage of the tumor vasculature in MCMV⁺ animals. Pericytes are permissive for CMV infection (28), and indeed, these tumor-associated pericytes strongly stain for MCMV in both our model and in human tumors.

Pericytes are essential for fully functional brain vasculature (49), and a direct correlation between pericyte coverage of tumor vasculature and diminished survival in patients with GBM has been reported, highlighting the relevance of this observation (31). Overall, we examined tumor samples from 5 patients using immunofluorescence and 18 using RT-PCR (Figure 3 and Supplemental Figure 3). Of those, all 5 immunostained samples were positive for HCMV pp65 and only 1 sample from the PCR study was negative for CMV. Although CMV reactivity was predominantly found in the perivascular niche, single cells remained positive throughout the tumor. Further studies on an extended panel of tumors are warranted.

CMV reactivation in the mouse model. As reported in human specimens, MCMV reactivation could be detected in our mouse model. We observed (a) a time-dependent increase of MCMV IE1/m123 levels as tumors grew and (b) the presence of CMV in intratumoral pericytes as well as tumor cells by immunostaining in both the mouse model and in human GBM specimens.

This is the first report, to our knowledge, to show that CMV is reactivated in perivascular intratumoral pericytes, suggesting potentially important biological mechanisms. We speculate that CMV reactivation occurs within the tumor microenvironment due to local immunosuppression that prevents control of CMV reactivation by the adaptive immune system. Based on our observations, we also speculate that at least one source of intratumoral CMV may be pericytes recruited from the circulation and are currently investigating this hypothesis. Indeed, pericytes are known to be permissive for CMV infection and may play a role in CMV retinitis (28). Our data so far suggest that CMV reactivation is specific to the immunosuppressive tumor microenvironment. We were unable to see any symptoms of systemic CMV reactivation or detect its presence in lung tissue from MCMV-infected tumor-bearing animals. However, this does not discount the possibility that CMV may be reactivated in other tissues or specific cell types during tumor growth. Also, there are many additional CMV-encoded transcripts we could search for. This is an area of current investigation.

One of the challenges in this field of study is to relate changes seen in vitro under acute infection conditions, to those seen in vivo when the virus is undergoing long term reactivation in multiple cell types within the tumor microenvironment. Our mouse model will allow highly detailed studies of viral gene reactivation and other molecular changes temporally and by cell type enabling a detailed understanding of the dynamics of the process. Measurement of MCMV transcript levels showed a 10-fold lower expression of IE1/m123 in vivo compared with in vitro by qRT-PCR. On a cellular level, this difference is likely smaller, due to the lower numbers of cells infected in vivo versus in vitro. Initial comparisons of CMV IE1/m123 levels between the murine model and human GBM specimens suggest that levels of CMV activation may be slightly higher in the murine model (data not shown). However, this does not account for the variable of numbers of cells infected per specimen and changes in CMV activation over tumor evolution. Further detailed studies are therefore needed to survey multiple genes and specimens in each system.

PDGF-D as a mediator of the effects of CMV on pericyte recruitment and angiogenesis. In our system, CMV infection of GSCs promotes the secretion of a wide array of different proangiogenic cytokines, a phenotype previously observed in other cell types (45–48). Comparison of our RNA-Seq data with GO terms for secreted angiogenic molecules revealed several upregulated mRNAs encoding secreted proteins involved in the promotion of angiogenesis in GBM by CMV, as shown in Supplemental Table 1, suggesting that promotion of angiogenesis is multifactorial. Interestingly, our RNA-Seq data scored highly for PDGF-D, which is known to be involved in the control of pericyte migration (50), but has not been studied in the context of GBM. Similarly to PDGF-B, PDGF-D is a ligand of PDGFR-β, and null mouse mutants of either PDGFR-β or PDGF-B are lethal in utero due to hemorrhage caused by abnormal, pericyte-lacking vasculature (51). Additionally, PDGF-D is known to be involved in pericyte, macrophage, and monocyte chemotaxis as well as the induction of angiogenesis in vitro (52, 53).

Our in vitro data suggest that PDGF-D is responsible for pericyte accumulation in GBM in CMV^+ mice and also contributes to angiogenesis. We showed by qRT-PCR and Western blotting that PDGF-D is clearly upregulated in human GSCs and mouse GBM cells after infection with CMV, and we confirmed that PDGF-D alone can stimulate pericyte migration in both mouse and human systems. Depletion of PDGF-D by blocking antibodies or CRISPR-mediated gene editing completely blocks pericyte migration in vitro. Most compelling is the observation that GBM cells lacking PDGF-D cannot grow in CMV-naive hosts, showing lack of both pericyte influx and angiogenesis. However, when these same KO cells are introduced into $MCMV^+$ mice, tumor growth and lethality are restored, although more slowly than in WT controls, suggesting that extratumoral factors provided by MCMV in the model may overcome the lack of PDGF-D in tumor cells. Whether CMV is providing PDGF-D or a different compensatory factor is a subject of current investigation. Our data suggest the importance of PDGF-D as a potential therapeutic target in vivo.

Regulation of PDGF-D expression by NF-κB. We showed that PDGF-D upregulation is at least in part regulated by CMV activation of NF-κB signaling (Figure 5, H–J). It has been previously shown that, after HCMV infection, cells show a virus-regulated induction of NF-κB signaling (41). Purified viral glycoproteins were shown to induce NF-κB activity (41, 42). In this study, we showed that in human GSCs, infection with CMV results in the activation of NF-κB signaling via p65 phosphorylation. Because NF-κB has also been associated with PDGF-D in ChIP-Seq studies (43), we hypothesized that NF-κB activation might also lead to PDGF-D upregulation. This was confirmed by siRNA-mediated inhibition of NF-κB signaling. As the induction of PDGF-D expression by CMV was only partially inhibited, other mechanisms, such as Sp-1 induction upon CMV infection, might also be involved in PDGF-D upregulation (54, 55).

Effects of antiviral therapy in CMV GBM models. In recent years, clinical approaches targeting CMV have led to encouraging clinical results (13–18). These approaches include CMV-targeted immunotherapies and the antiviral drug valganciclovir, which is a substrate of CMV thymidine kinase (TK), rendering infected cells exquisitely sensitive to its effects by accumulation of toxic metabolites catalyzed by viral TK activity. However, MCMV does not have a homolog of the HCMV TK gene and is not sensitive to valganciclovir. Therefore, in the current report, we tested the effects of cidofovir, an FDA-approved antiviral drug that inhibits viral DNA polymerase and blocks MCMV

replication. Treatment of MCMV$^+$ GL261 tumor-bearing mice with cidofovir caused reversal of the MCMV-induced phenotype, with a reduction of tumor-infiltrating pericytes, decreased tumor vasculature, and improved survival, consistent with these clinical observations. Previous work has suggested that cidofovir has antitumor potential both in vitro and in vivo in combination with irradiation (56). The use of cidofovir as an anticancer drug is not restricted to GBM and has been shown to be effective in HPV-associated cervical cancer (57), although with some toxicity (58). Thus, the current report suggests that cidofovir might improve survival in hosts with CMV, but it is not clear that CMV-naive hosts would show such a benefit. Our observation that cidofovir treatment could reverse the effects of CMV on GBM growth provides at least proof of principle supporting the potential use of antiviral treatments in brain tumors. Importantly, others have shown potentially favorable data on the use of valganciclovir in patients (19) and have also shown that cidofovir can sensitize cells to irradiation (56). This suggests that incorporating irradiation into our model would show further enhancement of animal survival and would strongly support clinical application. Studies are currently underway with additional antiviral drugs in combination with other therapies to assess the translational relevance of this approach.

Limitations. This study was performed in mouse GBM models, and MCMV has many differences from HCMV. The lack of TK in MCMV limits our ability to test valganciclovir in this model; however, an engineered MCMV with a copy of HCMV TK has been created (59), and we will investigate this in order to model the effects of valganciclovir. CMV and its relationship with GBM and cancer remains a controversial area, with some groups unable to detect CMV in human specimens (22, 23). At present, there are no reports of next-generation sequencing data from human tumor specimens containing CMV sequences, which may be explainable by low levels of CMV in tumors as well as a high level of natural genetic variation in CMV. Also, until this study, there was no mechanistic explanation, to our knowledge, of how CMV could influence tumor growth. Our observations therefore add to the weight of evidence that CMV can play a role in tumor growth and may be therapeutically very important.

Summary and perspective. Our observations provide insights into how CMV infection affects GBM growth in vivo and are supported by observations in human patient specimens. These data strengthen the argument for a role of CMV in GBM growth and a rationale for antiviral therapy in overcoming treatment limitations in current GBM therapy. Finally, in identifying PDGF-D as a contributor to the CMV-induced phenotype, we have identified a target for potentiating current GBM therapy regimens, augmenting immunotherapeutic approaches, and ultimately, developing new approaches to treating GBM.

Methods

Cell culture and virus propagation. NIH3T3 mouse fibroblasts and MRC-5 cells were purchased from ATCC and cultured in DMEM with 10% FBS (Sigma-Aldrich), penicillin (100 U/ml), and streptomycin (10 mg/ml) (Thermo Fisher). MCMV lacking the m157 gene (24) was provided by Ulrich Koszinowski (Ludwig-Maximilians-Universitat, Munich, Germany), and HCMV-GFP Towne strain was provided by Bill Britt (University of Alabama, Birmingham, Alabama, USA). MCMV and HCMV strains were cultured in NIH3T3 and MRC-5 cells, respectively, and viral titer was measured as previously described (24). GL261Luc2 murine glioma cells were purchased from PerkinElmer. CT-2A murine glioma cells were a gift from Thomas Seyfried (Boston College, Boston, Massachusetts, USA). HBMEC cells were purchased from ScienCell Research Laboratories and grown according to the manufacturer's recommendations. Primary human GSCs (G34, G35, G44, G157) were obtained by dissociation of gross tumor samples and cultivated in neurosphere media, as previously described (60). Mycoplasma testing was routinely done by PCR. GBM subtype classification was done by gene-expression profiling as previously described (60).

CMV infection in vitro. For CMV infection in vitro, we seeded up to 10^6 cells in 6-well plates and treated with CMV or mock infection (purified extract from uninfected fibroblasts) the next day. We infected GL261Luc2 neurospheres with MCMV (MOI of 1) or patient-derived human GSCs with HCMV (MOI of 1) for 2 hours. Cells were then rinsed with Dulbecco's PBS (DPBS) (Thermo Fisher) and covered with fresh culture medium.

Transwell cell migration assay. Cells were seeded in a 24-well culture plate, infected with CMV (MOI of 1), and cultured for 72 hours. Light transmission blocking Transwell inserts (FluoroBlock, Corning) with a pore size of 8 μm were used. 1×10^6 Cells were trypsinized and stained with Vybrant DiO Cell-Labeling Solution (Thermo Fisher). Cells were added to the Transwell compartment and incubated at 37°C. Images were taken after 24 hours and 48 hours. For each assay, 15 images from 3 separate wells were analyzed. Each assay was repeated 3 times.

Flow cytometry. Flow cytometry was performed on a FACS LSR II or Fortessa (BD Biosciences). Cells were gated by forward scatter/side scatter while excluding duplets by forward scatter area/forward scatter height. Subsequently, CD45$^+$ (BioLegend, catalog 103101) cells were gated, with further classification by their expression of NG2 (Stratech, catalog bs-4800R-FITC) and PDGFR-β (BioLegend, catalog 136007).

qRT-PCR. Total RNA was extracted using TRIzol and treated with RNase-free DNase (QIAGEN). mRNA expression analysis was carried out using Power SYBR Green (Applied Biosystems). RNA concentration was quantified using a Nanodrop RNA 6000 (Thermo Fisher) and analyzed using the Applied Biosystems StepOnePlus PCR machine (Thermo Fisher). See Supplemental Table 2 for primer sequences.

Generation of knockdown cell lines using siRNA. Human RELA was knocked down using siRNA technology. Briefly, GSCs were transfected using siRNA oligonucleotides against p65/RELA (QIAGEN) or nontargeting controls at 100 pmol/5×10^5 cells and validated at the mRNA and protein levels. Cells were processed 48 hours after transfection. All transfections were performed with Lipofectamine 2000 (Life Technologies) following the manufacturer's recommendations. Antibodies used were as follows: NF-κB p65 XP rabbit mAb (clone D14E12, catalog 8242), phospho–NF-κB p65 (Ser536) mouse mAb (clone E1Z1T, catalog 13346) (Cell Signaling Technology).

In vivo studies. Six-week-old male and female C57BL/6 mice were purchased from The Jackson Laboratory and mated once. The f1 generation was inoculated with a nonlethal dose of Δ157 MCMV Smith strain at P2 (10^3 PFU) by i.p. injection, as previously described (24). After 14 weeks, 1000 cells (GL261Luc2, GL261Cas9, GL261*PDGF*KO,

and CT-2A) in 3 μl normal saline were injected intracranially to establish mouse brain tumors (2 mm right lateral, 1 mm frontal to the bregma, and 3 mm deep). Infection was confirmed in serum samples using the commercial pathology service provided by Charles River (anti-MCMV Multiplexed Fluorometric ImmunoAssay). Cidofovir treatment was performed by i.p. injection (100 mg/kg) 3 times per week for 2 weeks. DMSO and sterile saline were used as vehicle.

Imaging methods. MRI data were acquired using a Bruker 7 Tesla scanner (Bruker Biospin). Animals were kept under isoflurane narcosis throughout the scan. Respiration and heart rate were monitored. Body temperature was maintained using a homeothermic blanket. ASL was performed as previously described (61). Briefly, the animal was carefully positioned with the labeling coil located at the neck to allow labeling of blood flowing through the carotid arteries. For ASL, single-shot, gradient-echo, echo-planar imaging (EPI) acquisition was used. Paired images were acquired alternately — one with ASL (labeled image) and the other without (control). Tumor blood flow was analyzed by comparing specified regions of interest (ROIs) with their anatomical parallel in the contralateral hemisphere. The average difference in ROIs was compared between different animals and translated into relative fold-change difference. T2-weighted images were acquired using the RARE pulse sequence. The resulting segmentations were reviewed manually to ensure accuracy.

Generation of KO cell lines using CRISPR/Cas9. The murine *Pdgfd* gene was knocked out using CRISPR/Cas9 technology. Briefly, GL261 cells were lentivirally transduced with the Cas9 gene. Stable Cas9-expressing clones were then transduced with a lentivirus expressing a gRNA specifically designed to target the murine *Pdgfd* gene (designated as guide 3 and guide 5). The plasmid constructs used to make the lentivirus vectors, pLentiCAS9Blast and pLentiGuide (guide 3 targets exon 2 of the gene: 5′-GGGTAGCTGTTCGGGAAGCG-3′; guide 5 targets exon 3 of the gene: 5′-TTTGTTCTTGACGTTATCCT-3′) were purchased from GenScript. Cells successfully transfected with the gRNA were positively selected using puromycin resistance, and single clones were isolated via serial dilution. Only clones testing negative for PDGF-D expression by Western blot analysis were used.

RNA-Seq. Triplicates of proneural GSCs (G44) were infected with HCMV at an MOI of 0.1. Cells were then kept in culture for 3 days. Uninfected cells served as controls. Equal quantities of total RNA were isolated using the TRIzol reagent (Thermo Fisher) according to the manufacturer's protocol. RNA degradation and contamination were monitored on 1% agarose gels, and RNA integrity was assessed with the RNA Nano 6000 Assay Kit and a Bioanalyzer 2100 system (Agilent Technologies). Sequencing libraries were generated using the Illumina paired-end indexing protocol. Corresponding RNA-Seq paired-end reads were processed using the TopHat suite with Cufflinks. Raw reads in fastq format were mapped to the reference organism using STAR software. Clean data were obtained by removing reads containing adapter sequences, reads containing poly-N, and low-quality reads from raw data. The Q20, Q30, GC-content, and sequence duplication levels of the clean data were calculated. All downstream analyses were based on high-quality clean data. All RNAseq data were deposited in the EMBL-EBI's ArrayExpress database (E-MTAB-7613).

Analysis was performed using the Kyoto Encyclopedia of Genes and Genomes (KEGG) for pathway enrichment analyses and Protein ANalysis THrough Evolutionary Relationships (PANTHER) for GO.

Immunoblotting. Cells were lysed using RIPA buffer containing 1% protease inhibitor cocktail (Merck Millipore) and 5% phosphatase inhibitor cocktail (Roche). Total protein concentration was measured using the Bradford protein assay. Primary antibodies used were against HCMV (Virusys Corporation, catalog CA150-1; 1:1000), HCMV pp65 (Virusys, catalog CA003-100; 1:1000), anti-human PDGF-D (Thermo Fisher, catalog 40-2100; 1:1000), and β-actin (Cell Signaling Technology, catalog 4967; 1:1000).

Immunohistochemistry. Mice were euthanized using CO_2 inhalation and subsequently perfused with 4% neutral-buffered formalin (Sigma-Aldrich) for fixation. Cryoprotection was performed using 30% sucrose. All mouse brain slides were obtained from 30 μm frozen sections. Permeabilization was done using 1% Triton X-100 (Sigma-Aldrich) in PBS (Thermo Fisher) for 10 minutes. Slides were then incubated with the primary antibody (1:100 in normal serum) overnight at 4°C. For detection of the primary antibody, species-matched fluorophore-coupled antibodies were incubated for 1 hour at room temperature. Slides were then covered with antifade mounting medium (Vectashield, Vector Laboratories) and coverslipped. All fluorescent and bright-field microscopy-based assays were observed using a Nikon Eclipse Ti microscope (Nikon). High-resolution confocal fluorescent microscopy was performed using a Zeiss LSM 710 confocal microscope system and visualized using ZEN Zeiss Imaging software. For human specimens, IHC staining was performed as previously described (6). Briefly, tissue specimens were incubated with antibodies against CMV (Virusys Corp.), followed by H&E counterstaining. We first validated the MCMV immunostaining conditions in vitro by staining of MCMV-infected and noninfected GL261 cells. Additional controls used for antibody specificity were brain and tumors from noninfected control animals, brain subventricular zone staining in infected animals, and the absence of any background staining with secondary antibodies alone. For colocalization, images were imported into the *Fiji* version of the free image-processing software ImageJ (NIH). The preinstalled plugin for colocalization analysis *coloc2*, which uses a pixel intensity correlation measurement, was used to calculate colocalization parameters (Pearson's coefficient and Spearman's rank correlation). For immunofluorescence studies, the following antibodies were used: anti-mouse, CD31 (Bio-Rad, catalog TLD-3A12, 1:100), PDGF-D (Thermo Fisher, catalog 40-2100, 1:100), and PDGFRβ (BioLegend, 323605, 1:100); anti-human, PDGF-D (R&D, catalog AF1159, 1:100), CD133 (BioLegend, catalog S16016B, 1:100), Vimentin (SP20, Thermo Fisher, catalog MA5-16409, 1:100), and CD31 (Bio-Rad, catalog MCA1738, 1:100); anti-human mouse Ki67 (Abcam, catalog ab15580, 1:100), NG2 (EMD Millipore, 1:100), and Olig2 (Merck, catalog MABN50, 1:100); anti-CMV (Virusys Corp., catalog CA150-1, 1:1000) and HCMV pp65 (Virusys, catalog CA003-100, 1:1000).

Quantification of tumor vasculature in frozen sections. Immunofluorescence staining using anti-CD31 antibodies (Bio-Rad, catalog MCA2388GA) was performed in coronal frozen brain sections. An ImageJ algorithm (provided by Institute for the Neurosciences, Neuro Technology Studio, Brigham and Women's Hospital) was used to automate vessel detection and characterization for length, area, and branching points (25).

Statistics. All microscope-based assays were edited/quantified using ImageJ, including the Analyze Particles function of binary images with automatic threshold. Data are expressed as mean ± SD. Unpaired 2-tailed Student's *t* test was used for comparison between

2 groups. Each group was tested for Gaussian distribution, if 1-way ANOVA was passed, followed by Bonferroni's test. If this failed, the Kruskal-Wallis test followed by Dunn's correction was conducted to test for significance among multiple groups. Pearson's correlation with nonlinear regression analysis was performed to compute Pearson's *r*, R2, and *P* values. The Holm-Šídák test was used for some experiments, as indicated in the figure legends. Statistical analyses were performed using Microsoft Office Excel 2011 or Graph Pad Prism 6 software. $P < 0.05$ was considered statistically significant.

Study approval. Tumor samples were obtained using a protocol approved by the Dana-Farber Cancer Institute IRB. Written, informed consent was received from all participants prior to inclusion in the study. Animal studies were approved by the Brigham and Women's Hospital Center for Comparative Medicine IACUC.

Author contributions

HK designed the study, acquired and analyzed data, and participated in manuscript writing. PB, VL, CP, MZ, MON, KG, HZ, MS, HI, MG, MBG, FR, LD, RZ, AR, and SP assisted in experimental design, execution, and data analysis. CDJ and CSC assisted in experimental design and interpretation of data. CHC provided reagents. CHC and EAC assisted in experimental design and interpretation and participated in manuscript writing. SEL designed the study, analyzed data, and wrote the paper. All authors discussed the results and commented on the manuscript.

Acknowledgments

This work was funded in part by the following: NIH grants NCI RO1 CA195532 (to EAC) and NCI R01 CA184283 (to CSC) and an American Brain Tumor Association postdoctoral research fellowship (to CP). We thank James Zoldak for critical reading of the manuscript.

Address correspondence to: Sean E. Lawler, Harvey Cushing Neurooncology Laboratories, Department of Neurosurgery, Brigham and Women's Hospital, Hale Building for Transformative Medicine, 60 Fenwood Road, Boston, Massachusetts 02115, USA. Phone: 1.617.525.5650; Email: slawler@bwh.harvard.edu.

HK's present address is: Department of Neurosurgery, University Medical Center Mainz, Germany.

1. Alexander BM, Cloughesy TF. Adult glioblastoma. *J Clin Oncol*. 2017;35(21):2402–2409.
2. Louis DN, et al. The 2016 World Health Organization Classification of Tumors of the Central Nervous System: a summary. *Acta Neuropathol*. 2016;131(6):803–820.
3. Stupp R, et al. Radiotherapy plus concomitant and adjuvant temozolomide for glioblastoma. *N Engl J Med*. 2005;352(10):987–996.
4. Stupp R, et al. Effects of radiotherapy with concomitant and adjuvant temozolomide versus radiotherapy alone on survival in glioblastoma in a randomised phase III study: 5-year analysis of the EORTC-NCIC trial. *Lancet Oncol*. 2009;10(5):459–466.
5. Mocarski E, et al. Cytomegaloviruses. In: Knipe DM, Howley PM, eds. *Fields Virology*. 6th ed. Philadelphia, Pennsylvania, USA: Wolters, Kluwer, Lippincott, Williams & Wilkins; 2013:1960-2014.
6. Cobbs CS, et al. Human cytomegalovirus infection and expression in human malignant glioma. *Cancer Res*. 2002;62(12):3347–3350.
7. Dziurzynski K, et al. Glioma-associated cytomegalovirus mediates subversion of the monocyte lineage to a tumor propagating phenotype. *Clin Cancer Res*. 2011;17(14):4642–4649.
8. Rahbar A, et al. Human cytomegalovirus infection levels in glioblastoma multiforme are of prognostic value for survival. *J Clin Virol*. 2013;57(1):36–42.
9. Bhattacharjee B, Renzette N, Kowalik TF. Genetic analysis of cytomegalovirus in malignant gliomas. *J Virol*. 2012;86(12):6815–6824.
10. Lucas KG, Bao L, Bruggeman R, Dunham K, Specht C. The detection of CMV pp65 and IE1 in glioblastoma multiforme. *J Neurooncol*. 2011;103(2):231–238.
11. Harkins LE, et al. Detection of human cytomegalovirus in normal and neoplastic breast epithelium. *Herpesviridae*. 2010;1(1):8.
12. Chen HP, et al. Human cytomegalovirus preferentially infects the neoplastic epithelium of colorectal cancer: a quantitative and histological analysis. *J Clin Virol*. 2012;54(3):240–244.
13. Nair SK, Sampson JH, Mitchell DA. Immunological targeting of cytomegalovirus for glioblastoma therapy. *Oncoimmunology*. 2014;3:e29289.
14. Prins RM, Cloughesy TF, Liau LM. Cytomegalovirus immunity after vaccination with autologous glioblastoma lysate. *N Engl J Med*. 2008;359(5):539–541.
15. Mitchell DA, et al. Tetanus toxoid and CCL3 improve dendritic cell vaccines in mice and glioblastoma patients. *Nature*. 2015;519(7543):366–369.
16. Batich KA, et al. Long-term survival in glioblastoma with cytomegalovirus pp65-targeted vaccination. *Clin Cancer Res*. 2017;23(8):1898–1909.
17. Reap EA, et al. Dendritic cells enhance polyfunctionality of adoptively transferred T cells that target cytomegalovirus in glioblastoma. *Cancer Res*. 2018;78(1):256–264.
18. Schuessler A, et al. Autologous T-cell therapy for cytomegalovirus as a consolidative treatment for recurrent glioblastoma. *Cancer Res*. 2014;74(13):3466–3476.
19. Stragliotto G, et al. Effects of valganciclovir as an add-on therapy in patients with cytomegalovirus-positive glioblastoma: a randomized, double-blind, hypothesis-generating study. *Int J Cancer*. 2013;133(5):1204–1213.
20. MacManiman JD, et al. Human cytomegalovirus-encoded pUL7 is a novel CEACAM1-like molecule responsible for promotion of angiogenesis. *MBio*. 2014;5(6):e02035.
21. Soroceanu L, et al. Cytomegalovirus immediate-early proteins promote stemness properties in glioblastoma. *Cancer Res*. 2015;75(15):3065–3076.
22. Lawler SE. Cytomegalovirus and glioblastoma; controversies and opportunities. *J Neurooncol*. 2015;123(3):465–471.
23. Holdhoff M, et al. Absence of cytomegalovirus in glioblastoma and other high-grade gliomas by real-time PCR, immunohistochemistry, and in situ hybridization. *Clin Cancer Res*. 2017;23(12):3150–3157.
24. Price RL, et al. Cytomegalovirus contributes to glioblastoma in the context of tumor suppressor mutations. *Cancer Res*. 2013;73(11):3441–3450.
25. Zudaire E, Gambardella L, Kurcz C, Vermeren S. A computational tool for quantitative analysis of vascular networks. *PLoS ONE*. 2011;6(11):e27385.
26. Garg AD, et al. Dendritic cell vaccines based on immunogenic cell death elicit danger signals and T cell-driven rejection of high-grade glioma. *Sci Transl Med*. 2016;8(328):328ra27.
27. Shanley JD, Jordan MC, Cook ML, Stevens JG. Pathogenesis of reactivated latent murine cytomegalovirus infection. *Am J Pathol*. 1979;95(1):67–80.
28. Alcendor DJ, Charest AM, Zhu WQ, Vigil HE, Knobel SM. Infection and upregulation of proinflammatory cytokines in human brain vascular pericytes by human cytomegalovirus. *J Neuroinflammation*. 2012;9:95.
29. Nakano M, et al. NG2 glial cells regulate neuroimmunological responses to maintain neuronal function and survival. *Sci Rep*. 2017;7:42041.
30. Hall CN, et al. Capillary pericytes regulate cerebral blood flow in health and disease. *Nature*. 2014;508(7494):55–60.
31. Caspani EM, Crossley PH, Redondo-Garcia C, Martinez S. Glioblastoma: a pathogenic crosstalk between tumor cells and pericytes. *PLoS ONE*. 2014;9(7):e101402.
32. Zhou W, et al. Targeting glioma stem cell-derived pericytes disrupts the blood-tumor barrier and improves chemotherapeutic efficacy. *Cell Stem Cell*. 2017;21(5):591–603.e4.
33. Piccirillo SG, et al. Bone morphogenetic proteins inhibit the tumorigenic potential of human brain tumour-initiating cells. *Nature*. 2006;444(7120):761–765.
34. Chang AL, et al. CCL2 produced by the glioma microenvironment is essential for the recruitment of regulatory T cells and myeloid-derived suppres-

sor cells. *Cancer Res*. 2016;76(19):5671–5682.
35. Brat DJ, Bellail AC, Van Meir EG. The role of interleukin-8 and its receptors in gliomagenesis and tumoral angiogenesis. *Neuro-oncology*. 2005;7(2):122–133.
36. Peñuelas S, et al. TGF-beta increases glioma-initiating cell self-renewal through the induction of LIF in human glioblastoma. *Cancer Cell*. 2009;15(4):315–327.
37. Daneman R, Agalliu D, Zhou L, Kuhnert F, Kuo CJ, Barres BA. Wnt/beta-catenin signaling is required for CNS, but not non-CNS, angiogenesis. *Proc Natl Acad Sci U S A*. 2009;106(2):641–646.
38. Kumar A, et al. Platelet-derived growth factor-DD targeting arrests pathological angiogenesis by modulating glycogen synthase kinase-3beta phosphorylation. *J Biol Chem*. 2010;285(20):15500–15510.
39. Gladh H, et al. Mice lacking platelet-derived growth factor D display a mild vascular phenotype. *PLoS ONE*. 2016;11(3):e0152276.
40. Furuhashi M, et al. Platelet-derived growth factor production by B16 melanoma cells leads to increased pericyte abundance in tumors and an associated increase in tumor growth rate. *Cancer Res*. 2004;64(8):2725–2733.
41. Yurochko AD, Kowalik TF, Huong SM, Huang ES. Human cytomegalovirus upregulates NF-kappa B activity by transactivating the NF-kappa B p105/p50 and p65 promoters. *J Virol*. 1995;69(9):5391–5400.
42. Yurochko AD, Hwang ES, Rasmussen L, Keay S, Pereira L, Huang ES. The human cytomegalovirus UL55 (gB) and UL75 (gH) glycoprotein ligands initiate the rapid activation of Sp1 and NF-kappaB during infection. *J Virol*. 1997;71(7):5051–5059.
43. Satoh J. Molecular network of ChIP-Seq-based NF-κB p65 target genes involves diverse immune functions relevant to the immunopathogenesis of multiple sclerosis. *Mult Scler Relat Disord*. 2014;3(1):94–106.
44. Chakrabarti S, Collingham KE, Osman H, Fegan CD, Milligan DW. Cidofovir as primary pre-emptive therapy for post-transplant cytomegalovirus infections. *Bone Marrow Transplant*. 2001;28(9):879–881.
45. Botto S, et al. IL-6 in human cytomegalovirus secretome promotes angiogenesis and survival of endothelial cells through the stimulation of survivin. *Blood*. 2011;117(1):352–361.
46. Dumortier J, et al. Human cytomegalovirus secretome contains factors that induce angiogenesis and wound healing. *J Virol*. 2008;82(13):6524–6535.
47. Streblow DN, Dumortier J, Moses AV, Orloff SL, Nelson JA. Mechanisms of cytomegalovirus-accelerated vascular disease: induction of paracrine factors that promote angiogenesis and wound healing. *Curr Top Microbiol Immunol*. 2008;325:397–415.
48. Caposio P, Orloff SL, Streblow DN. The role of cytomegalovirus in angiogenesis. *Virus Res*. 2011;157(2):204–211.
49. Sweeney MD, Ayyadurai S, Zlokovic BV. Pericytes of the neurovascular unit: key functions and signaling pathways. *Nat Neurosci*. 2016;19(6):771–783.
50. Rajkumar VS, et al. Platelet-derived growth factor-beta receptor activation is essential for fibroblast and pericyte recruitment during cutaneous wound healing. *Am J Pathol*. 2006;169(6):2254–2265.
51. Hellström M, Kalén M, Lindahl P, Abramsson A, Betsholtz C. Role of PDGF-B and PDGFR-beta in recruitment of vascular smooth muscle cells and pericytes during embryonic blood vessel formation in the mouse. *Development*. 1999;126(14):3047–3055.
52. Bergsten E, et al. PDGF-D is a specific, protease-activated ligand for the PDGF beta-receptor. *Nat Cell Biol*. 2001;3(5):512–516.
53. Uutela M, et al. PDGF-D induces macrophage recruitment, increased interstitial pressure, and blood vessel maturation during angiogenesis. *Blood*. 2004;104(10):3198–3204.
54. Liu MY, Eyries M, Zhang C, Santiago FS, Khachigian LM. Inducible platelet-derived growth factor D-chain expression by angiotensin II and hydrogen peroxide involves transcriptional regulation by Ets-1 and Sp1. *Blood*. 2006;107(6):2322–2329.
55. Yurochko AD, Mayo MW, Poma EE, Baldwin AS, Huang ES. Induction of the transcription factor Sp1 during human cytomegalovirus infection mediates upregulation of the p65 and p105/p50 NF-kappaB promoters. *J Virol*. 1997;71(6):4638–4648.
56. Hadaczek P, et al. Cidofovir: a novel antitumor agent for glioblastoma. *Clin Cancer Res*. 2013;19(23):6473–6483.
57. De Schutter T, et al. Cidofovir treatment improves the pathology caused by the growth of human papillomavirus-positive cervical carcinoma xenografts in athymic nude mice. *Cancer Lett*. 2013;329(2):137–145.
58. Deutsch E, et al. Phase I trial evaluating the antiviral agent Cidofovir in combination with chemoradiation in cervical cancer patients. *Oncotarget*. 2016;7(18):25549–25557.
59. Snyder CM, Cho KS, Bonnett EL, Allan JE, Hill AB. Sustained CD8+ T cell memory inflation after infection with a single-cycle cytomegalovirus. *PLoS Pathog*. 2011;7(10):e1002295.
60. Ricklefs F, et al. Extracellular vesicles from high-grade glioma exchange diverse pro-oncogenic signals that maintain intratumoral heterogeneity. *Cancer Res*. 2016;76(10):2876–2881.
61. Muir ER. Preclinical arterial spin labeling measurement of cerebral blood flow. *Methods Mol Biol*. 2018;1718:59–70.